



HAL
open science

Contributions au traitement des signaux ultrasonores pour des mesures instantanées en écoulements transitoires

Irina Murgan

► **To cite this version:**

Irina Murgan. Contributions au traitement des signaux ultrasonores pour des mesures instantanées en écoulements transitoires. Traitement du signal et de l'image [eess.SP]. Université Grenoble Alpes, 2017. Français. NNT : 2017GREAT120 . tel-02127133

HAL Id: tel-02127133

<https://theses.hal.science/tel-02127133>

Submitted on 13 May 2019

HAL is a multi-disciplinary open access archive for the deposit and dissemination of scientific research documents, whether they are published or not. The documents may come from teaching and research institutions in France or abroad, or from public or private research centers.

L'archive ouverte pluridisciplinaire **HAL**, est destinée au dépôt et à la diffusion de documents scientifiques de niveau recherche, publiés ou non, émanant des établissements d'enseignement et de recherche français ou étrangers, des laboratoires publics ou privés.

THÈSE

Pour obtenir le grade de

DOCTEUR DE LA COMMUNAUTE UNIVERSITE GRENOBLE ALPES

Spécialité : **Signal, Image Parole, Télécoms**

Arrêté ministériel : 25 mai 2016

Présentée par

Irina Alexandra MURGAN

Thèse dirigée par **Cornel IOANA** codirigée par **Gabriel VASILE** et **Stéphane BARRE**, préparée au sein du **Grenoble Images Parole Signal Automatique (GIPSA-Lab)** dans l'Ecole Doctorale d'électronique, électrotechnique, automatique et traitement du signal (EEATS)

Contributions au traitement des signaux ultrasonores pour des mesures instantanées en écoulements transitoires

Thèse soutenue publiquement le **23 Novembre 2017**,
devant le jury composé de :

Mme. Henda DJERIDI

Président du jury, Professeur, Institut National Polytechnique Grenoble

Mme. Marie CHABERT

Rapporteur du jury, Professeur, Institut National Polytechnique Toulouse

M. Romeo SUSAN-RESIGA

Rapporteur du jury, Professeur, Université Politehnica Timisoara

M. Alexandru ȘERBĂNESCU

Membre du jury, Professeur, Académie Technique Militaire de Bucarest

M. Ljubisa STANKOVIC

Membre du jury, Professeur, Université du Monténégro

M. Cornel IOANA

Directeur, Maître de conférences, Institut Polytechnique de Grenoble

Mme. Diana Maria BUCUR

Membre invité, Professeur, Université Politehnica Bucarest

M. Stéphane BARRE

Membre invité, Chargé de recherche CNRS, LEGI, France

M. Gabriel VASILE

Membre invité, Chargé de recherche CNRS, Gipsa-Lab, France



THESIS

Ultrasound signal processing contributions for instantaneous transitory flow measurements

Presented and defended by

Irina Alexandra MURGAN

for jointly obtaining the

DOCTORATE DEGREE

of University of Grenoble

*Doctoral School for Electronics, Power Systems, Automatic Control and Signal Processing
Specialization: Signal, Image, Speech, Telecommunications*

Thesis directed by **Cornel IOANA**, **Gabriel VASILE** and **Stéphane BARRE**.
Prepared in the Grenoble Image Parole Signal Automatique laboratory (GIPSA-lab).

Defended in Grenoble, on 23th November 2017, in front of the jury:

Reviewers : **Mrs. Marie CHABERT**
Professor, INP-ENSEEIH Toulouse, France

Mr. Romeo SUSAN-RESIGA
Professor, University POLITEHNICA of Timisoara, Romania

Examiners : **Mrs. Henda DJERIDI**
Professor, Grenoble INP, France

Mr. Alexandru ȘERBĂNESCU
Professeur, Military Technical Academy, Romania

Mr. Ljubisa STANKOVIC
Professeur, University of Montenegro

Mr. Cornel IOANA
Associate Professor, Grenoble INP, France

Invited: **Mrs. Diana Maria BUCUR**
Associate Professor, University POLITEHNICA of Bucharest

Mr. Stéphane BARRE
CNRS Researcher, LEGI, France

Mr. Gabriel VASILE
CNRS Researcher, GIPSA-lab, France

Acknowledgements

Firstly, I would like to express my sincere gratitude to my supervisors Dr. Cornel IOANA, Dr. Gabriel VASILE and Dr. Stéphane BARRE for their continuous support of my Ph.D study and related research, for their patience, motivation, and immense knowledge. Their guidance helped me in all the time of research and writing of this thesis.

Besides my supervisors, I would like to thank my thesis committee: Prof. Henda DJERIDI, Prof. Marie CHABERT, Prof. Romeo SUSAN-RESIGA, Prof. Alexandru SERBANESCU and Prof. Ljubisa STANKOVIC, for given me a great honor in agreeing to evaluate my work. Thank you for all insightful comments and encouragement, but also for the hard questions which incited me to widen my future research from various perspectives.

My sincere thanks also goes to Dr. Florentina BUNEA, Prof. Diana Maria BUCUR and Prof. Gabriel CIOCAN who provided me an opportunity to join their team as intern, and who gave us access to the laboratory and research facilities. Without their precious support it would not be possible to conduct this research. In particular, I am grateful to Prof. CIOCAN for enlightening me the first glance of research.

My thanks go also to my formers Prof. Catalin Pana and Prof. Ana-Maria Arisanu for their guidance, for sharing their knowledge, for their hard work and dedication.

I thank my fellow labmates and friends Ion, Teodor, Costin, Saloua, Francesca and Karina for the stimulating discussions and for all the time that we have had in the last three years. Also, I like to express my thanks to my friends Cristina Dinescu, George Buzea, Mirela Ion, Sorin Popa, Oana Rosioru, Carmen si Catalin Badina, Ileana Ciocan, Georgia si Mircea Cablea, Andrei Popescu, Laurentiu Trifan for all the great moments that we have spent together during my stay in Grenoble.

I am especially grateful to my family for being beside me all the time, for their support, encouragements and love. Especially thank you, Mihai, for being part of my life, for motivating me and for guiding me through new adventures. Thank you very much to all of you!

Contents

Table of acronyms and abbreviations	vii
Introduction	9
Hydraulic phenomena in non-stationary state	11
1.1 Introduction	12
1.2 Transient flows	13
1.3 Cavitation.....	15
1.4 Summary.....	16
Ultrasound flow monitoring	17
2.1 Acoustic flow monitoring principle.....	18
2.2 Measurement issues	21
2.3 Summary.....	23
Single path ultrasound processing	25
3.1 Wide band signals.....	26
3.2 Matched filtering for <i>TOA</i> estimation.....	27
3.3 Compressive sensing based signal reconstruction.....	28
3.4 Numerical example.....	33
3.5 Summary.....	39
Active and passive multi-sensor sensing.....	41
4.1 Active multi-sensor sensing.....	42
4.2 Passive multi-sensor sensing	50
4.3 Summary.....	55
Results in applicative contexts	57
5.1 Transducers position offset compensation	58
5.2 Asymmetric velocity profile construction	61
5.3 Acoustic flow metering	65
5.4 Cavitation vortex detection.....	70
Conclusion & Perspectives	75
Appendix A Statistical moments of a joint pdf function.....	77
Appendix B Résumé étendu	79
Bibliography	89

List of Figures

Figure 1.1 Laminar and turbulent flow velocity profiles	12
Figure 1.2. a) Contracted flow pipe streamlines and b) the corresponding velocity profile	14
Figure 1.3. Cavitation phase diagram. Source [Fra05 pp.2]	15
Figure 1.4. Bubbles cavitation a) and attached foil cavitation b). Source [FM85]	15
Figure 1.5. Vortex cavitation development downstream a Francis turbine. Source [ICA08]..	16
Figure 2.1. Ultrasonic transducer principle	18
Figure 2.2. Ultrasonic flow monitoring principles	18
Figure 2.3. a) Passive ultrasonic method uses one or more transducers to record acoustic waves generated by the flow; b) The active ultrasonic method uses at least one emitter (E) to generate an acoustic wave to propagate through the flow, and at least one receiver (R) to record the travelling acoustic wave.	19
Figure 2.4. Propagation time difference estimation: $\Delta t = t_{BA} - t_{AB}$, where d is the distance between the emitter and the receiver	20
Figure 2.5. Circular pipe cross section: a) Fully developed velocity flow profile; b) Disturbed velocity flow profile. Source: [Tuv16].....	21
Figure 2.6. The “flow blow” effect	22
Figure 3.1. LFM signals with different slopes, used for simultaneous emission in the direction of the flow and in the opposite direction.	26
Figure 3.2. The diagram of the received signal processing using matched filtering technique	28
Figure 3.3. Warping transform and L-statistics purpose in signal pre-processing before the compressive sensing reconstruction	32
Figure 3.4. a) Emitted and received signals in the case of perfectly aligned transducers and b) misaligned transducers.	34
Figure 3.5. a) Emitted/received spectrums in the case of perfectly aligned transducers and b) emitted/received spectrums, in the case of misaligned transducers.	35
Figure 3.6. a) Spectral content of the emitted signal and b) of the received one. The received signal spectral information are sparse compared to the one of the emitted signal.....	35
Figure 3.7. Estimated warping function that stationaries the signal’s time-frequency content and the warped signal spectrogram.	36

Figure 3.8. The spectrogram of the recovered signal in the warped domain	36
Figure 3.9. The spectrum of the emitted signal $s(t)$, of the received signal $x_2(t)$ and of the CS-based recovered one $x_2'(t)$	36
Figure 3.10. The recovered signal's spectrogram in the original time axis domain	37
Figure 3.11. a) Classical TOA procedure estimation and b) TOA estimation based on compressive sensing reconstruction before matched filtering.	37
Figure 3.12. Matched filter responses for TOA estimation using a) the corrupted signal and b) the reconstructed signal.	38
Figure 3.13. Variation of the TOA error estimation with the SNR of the received signal.	39
Figure 4.1. Diagram of 2D sensing array with $M \times N$ transducers. dx and dy are the distances between elements along x -axis, respectively along y -axis. θ is the angle of observation normal to the array and ϕ is the angle with the x -axis.	42
Figure 4.2. Parameters definition for a sensing array of 2×2 transducers.	44
Figure 4.3. Directivity diagram for a 2×2 sensing array that doesn't satisfy the spatial sampling theorem.	45
Figure 4.4. Directivity diagram for a non-intrusive 2×2 sensing array that follows the rule imposed by the spatial sampling theorem, considering the propagation first in the steel.	45
Figure 4.5. The beamforming algorithm diagram.	46
Figure 4.6. The beamforming algorithm principle.	47
Figure 4.7. Principe of adaptive beam-forming in the case of two element receiver.....	49
Figure 4.8. 3D rotation of a circle with angle φ , around the y -direction.	51
Figure 4.9. Probability density function of the X transform of a Gaussian noise $\sim N(2.5, 0.5)$ has the mean=0.15 and the variance=0.01 if it is computed using (7), and it has the mean=0.17 and the variance=0.3 if it is numerical estimated.	53
Figure 4.10. SNR level test.	54
Figure 5.1. An example of the application principle representation.	58
Figure 5.2. Misaligned transducers. R1 is the misaligned receiver that is supposed to record the reflected acoustic wave, while the receiver R2 is positioned where the acoustic wave is actually reflected.	58
Figure 5.3. Emitted and received wave forms for the ideal and real cases.	59
Figure 5.4. The result of the matched filter applied on the emitted signal and the received signal in the case of misaligned transducers.	60
Figure 5.5. The spectrums of the: reference received signal in the proper configuration, E-R2, (in black line); received signal in the case of misaligned transducers, E-R1 (in blue line); the recovered signal (in red line).	60

Figure 5.6. The matched filter response for the recovered signal.	61
Figure 5.7. Experimental facility used for velocity profile estimation.	62
Figure 5.8. Experimental configuration for the symmetric velocity profile estimation: a) the two “V” paths [E1-R1] and [E2-R2] correspond to emitted signal in the flow direction (the red continuous line), respectively in the opposite direction (the red dotted line); b) The transducers clamp-on open-channel side.....	63
Figure 5.9. Experimental configuration for the asymmetric velocity profile estimation: a) each three set of “V” paths [E1-R3, E1-E2, E1-R4] and [E2-R1 , E2-E1, E2-R2] correspond to emitted signal in the flow direction (the red continuous line), respectively in the opposite direction (the red dotted line); b) The transducers clamp-on open-channel side.	63
Figure 5.10. Symmetric flow velocity profile measured with Pitot tube (the blue curve) and estimated with acoustic time of flight meter (the red curve).....	64
Figure 5.11 Asymmetric flow velocity profile measured with Pitot tube (the blue curve) and estimated with acoustic time of flight meter (the red curve).....	64
Figure 5.12. a) The transducers displacement in ‘V’ configuration and b) the equipment used for the experimental tests.	66
Figure 5.13. The emitted signals on CH1 and CH2 with their corresponding time-frequency content.	66
Figure 5.14.a. Signal processing results, for one emission period, at 5 m/s.	67
Figure 5.15. The mean flow velocity estimation using matched filtering and matched filter with adapted beamforming techniques.....	69
Figure 5.16. The error variation for flow velocity estimation using the matched filter and the matched filter with adaptive beamforming	69
Figure 5.17. The extensometer placement on the alternator bearing.	70
Figure 5.18. Measured data processing method.....	71
Figure 5.19 Statistical moments variation as a function of the gate opening.....	72
Figure 5.20. 3D interpretation of the vortex cavitation appearance during a Francis turbine operation. Q_i , with $i = 1,18$ denotes the flow rate.	73
Figure 5.21. 3D interpretation of the vortex cavitation appearance.	74
Figure B.1. Organisation globale des axes de recherché: a) la configuration mono-capteur et b) la configuration multi-capteurs.	81
Figure B.2. Les signaux de type MLFs de pentes différentes utilisés pour l’émission simultanée dans le sens et en contre sens de l’écoulement.	81
Figure B.3. Illustration du principe de mesure de vitesse d’écoulement par différence de temps de transit.	82

Figure B.4. Les ondes émises et reçues a) dans le cas des capteurs parfaitement alignés et b) dans le cas des capteurs désalignés.	83
Figure B.5. Le déplacement du diagramme de directivité vue à la réception.	84
Figure B.6. Le résultat du filtrage adapté pour le signal reçu dans a) la configuration des capteurs désalignés et b) pour le signal reconstruit par le compressive sensing.	84
Figure B.7. Le spectre du signal émis, du signal reçu et du signal après la reconstruction.	85
Figure B.8. La variation de l'erreur pour l'estimation de la vitesse d'écoulement en utilisant le filtrage adapté et la technique basée sur la formation de voie.	86
Figure B.9 Profil des vitesses symétrique mesuré avec le tube Pitot (la courbe bleu) et estimé avec les cordes acoustiques (la courbe rouge)	86

Table of acronyms and abbreviations

CERG	Centre d'Etude et de Recherche de Grenoble
CS	Compressive Sensing
EDF	Electricité de France
ICPE	National Institute for R&D in Electrical Engineering
IFL	Instantaneous Frequency Law
LDA	Laser Doppler Anemometry
LFM	Linear Frequency Modulation
Pdf	Probability density function
PIV	Particle Image Velocimetry
SNR	Signal to Noise Ratio
STFT	Short Time Fourier Transform
TOA	Time of Arrival
UPV	Ultrasonic Velocity Profile

Introduction

Transitory flows are always encountered in real-life applications and their instantaneous non-intrusive monitoring is a topic of interest of great challenge. In the hydraulic equipment management, the velocity profile represents a fundamental parameter that provides data for flow analysis and characterization. Flow velocity profile shows not only the velocity magnitude, but also information about the fluid's behavior through the domain of interest.

There are two types of transitory flows that make the subject of our study, which are presented in the first chapter: partially obstructed flows and the transitory high flow rates. Also the cavitation vortex is included in our research for non-intrusive and passive hydraulic systems monitoring.

Non-intrusive acoustic methods, discussed in Chapter 2, are among the current techniques used in dynamic flow measurements. In contrast to conventional methods, where the measurement instrument interfere directly with the flow domain, the flow velocity profiling using non-intrusive methods allows the estimation of velocity profile as a two variables function: space and time, keeping constants the measuring configuration coordinates. Well known methods as ultrasonic pulse Doppler or laser Doppler anemometry are efficient, but limited in terms of measured velocity range imposed by the emitted wave's frequency. The velocity range encountered in most hydraulic applications may be wide and there is a need of an adapted measurement method.

In this thesis, we propose a set of signal processing contributions in order to improve the non-intrusive estimation of transitory flow velocity through pipes, by removing the conventional measurement methods limitations. In Chapter 3 we create a signal processing framework for single-path ultrasonic active sensing, aimed to increase the flow velocity accuracy estimation in the case of misaligned transducers. We use the compressive sensing signal's reconstruction in order to improve the matched filter response which leads to a better estimation of the acoustic time of arrival, hence of the flow velocity.

In the fourth chapter, we propose a multi-path acoustic measurement method using emitted wide band signals, in order to estimate flow velocity profiles. The spatial distribution of the flow profiles is not obtained by adding ultrasonic sensor but by changing the sensing properties, in terms of relative phase delays between receiving sensors, providing also additional acoustic paths that increase the number of measured velocity points.

In the same chapter, we present a mathematical processing model for strain gauge sensors measurements, in order to detect the hydraulic turbine's operational points where the

cavitation vortex appears. We propose also a 3D representation for cavitation vortex presence visualization, based on the gyroscope rotation principle.

In order to prove the applicability of all the signal processing contributions presented in the third and the fourth chapters, we discuss their experimental tests results in the Chapter 5. We show improvements in flow velocity estimation provided by the use of signal's compressive sensing reconstruction, when the signal is perturbed by the pipe induced vibrations and by the misaligned transducers.

The efficiency of the multi-path acoustic transducer configuration for flow velocity estimation is proven with two experimental tests. The undesired presence of the "flow blow" effect is compensated with the use of multiple receivers and with beamforming processing at the reception. We also emphasize the advantage of using the adaptive beamforming principle for symmetric and asymmetric open channel flow velocity profiling, under different flowing regimes: laminar and transitory.

Hydraulic phenomena in non-stationary state

Contents

1.1	Introduction	12
1.2.1	Fluid mechanics generalities	12
1.2.2	Flow velocity profiling methods.....	13
1.2	Transient flows	13
1.2.1	Obstructed flow	14
1.3	Cavitation	15
1.4	Summary	16

Depending on the variation in time of the fluid flow parameters, the flow can be: steady or unsteady. Steady flows are constant over time and they can be achieved mainly in laboratory conditions, while unsteady flows are spread everywhere in nature and in industrial applications, due to the fluid parameters change over time.

Non-stationary flows are by definition unsteady. The fluid velocity or pressure of a non-stationary flow is time varying. Depending on the application, the flow may turn into a stabilized turbulent flow. The fast changing of flow parameter can introduce large pressure forces and rapid fluid accelerations, which are a real threat to the hydraulic system's safety.

For industrial applications it is very important to estimate the magnitude of fast varying flow parameters corresponding to a certain fluid flow application. Transient flows (and also turbulent flows) are the object of multiple studies and numerical simulations, in order to improve their prediction and to control their effects.

Today, the turbulence is an unpredictable phenomenon and a great challenge for scientists. The experimental researches and simplified numerical simulations (with respect to the real physical phenomenon) are used to study the turbulence. In this chapter, the transient flow characteristics, their causes and impact are presented, in the context of a pipeline water system.

1.1 Introduction

1.1.1 Fluid mechanics generalities

Fluid mechanics is the physics branch that studies the way that fluids flow in all their form and conditions. A fluid flow is characterized by the variation in time of its parameters: density, temperature, velocity and pressure. All these parameters are related by the generalized Navier-Stokes equation of fluid mechanics. It is considered the case of incompressible flow (the fluid density is constant over time) [Gra95 pp. 204]:

$$\frac{\partial U}{\partial t} + (U \cdot \nabla)U = g - \frac{1}{\rho} \nabla P + \nu \nabla^2 U \quad (1.1)$$

where U is the velocity vector, g is the gravity force, ρ is the fluid density, P is the fluid pressure and ν is the fluid kinematic viscosity. The term $\frac{\partial U}{\partial t}$ represents the local acceleration of the fluid particle at a fixed point in space. For steady flow, this term is zero. The term $(U \cdot \nabla)U$ is the convective term and it predicts how the flow differs from one space location to another, at the same instant of time. The terms g and $\frac{1}{\rho} \nabla p$ represent the acceleration due to gravity, respectively due to pressure gradient. The last term, $\nu \nabla^2 U$, is the viscous deceleration and it is due to the fluid's frictional resistance to objects moving through it [Gra95].

The internal flow velocity is not constant in a pipe cross-section: near pipe walls, the flow velocity is almost zero, and it increases until its maximum, in the pipe centerline. This flow velocity distribution is named **velocity profile** and it is one of the most important quantities in fluid mechanics, being a fluid flow behavior descriptor.

For the same circular pipe, the flow can have different velocity profiles, depending on the flow regime. In Figure 1.1, the flow velocity profiles are displayed, for fully developed laminar and turbulent flows. In both cases, the velocity profiles are symmetrical with respect to the central pipe axis.

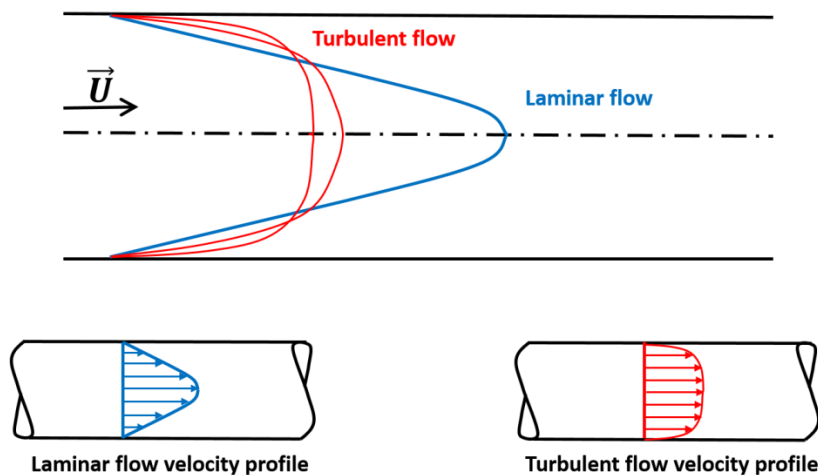


Figure 1.1 Laminar and turbulent flow velocity profiles

The laminar flow velocity profile is parabolic, with an important difference between the velocities from central pipe axis and near pipe wall. The velocities distribution in the turbulent flow is logarithmic, being much equilibrated with the velocity difference between the pipe center and its walls.

1.1.2 Flow velocity profiling methods

Velocity profiling has always been a great challenge in all applications concerning fluid flow. Starting from flow visualization techniques, with the support of numerical simulations, the velocity profiling methods have been improved. There exist measurement methods being able to detect instantly flow variations. Only non-intrusive methods will be mentioned, as they constitute the context where our works have been defined. The non-intrusive flow profiling techniques, with very good accuracy, are based on different principles: particle tracking, particle imaging velocimetry, laser Doppler anemometry and ultrasonic Doppler method.

The optical method for flow visualization, which uses the principle of particle image velocimetry (PIV) [RWW07] can be applied for wide range of flowing regimes [TMY03]. PIV technique uses small tracking particles to determine the fluid velocity field. Looking at particles displacement during a known period of time allows determining the velocity field. The drawback of this method is that it cannot be used for opaque fluids visualization. Also, in industrial applications, where pipes are also opaque (different metals or plastic based wall pipes), this method is not applicable.

The ultrasonic velocity profile (UPV) measurement method using the Doppler frequency shift principle, was proposed in order to overcome the PIV drawbacks. “The UVP method is based on pulsed ultrasound echography. An ultrasound pulse is emitted from the transducer along the measuring line, and the same transducer receives the echo reflected from the surface of micro particles suspended in the liquid” [Tak95]. This measurement method is complementary to another optical method, the Laser Doppler Anemometry (LDA) [Tro95], from the point of view of the spatial and time resolutions. UVP method has a weaker time resolution (greater than 10ms) than the LDA method, while the spatial resolution is better (less than 1mm on the beam direction), as we can find in [Tak95].

The work of this thesis focusses on the flow velocity parameter measurement in different configurations and for different flowing regimes.

1.2 Transient flows

Hydraulic transients in closed pipe flows introduce instabilities and may represent even a source of hydraulic system failure. Hence, the system monitoring is important in order to contribute to the system safety. For all hydraulic systems, different devices are conceived for safety measures, in order to ensure the system robustness to transients: bypass pumps

valve, surge tanks, control valves, air chambers [WCS03]. Despite those safety measures, transients monitoring is still vital for maintaining the safety of system exploitation.

The rapid flow parameters changing, characteristic to transient flows, in the context of a pipeline system can be generated at:

- the sudden start and stop of the hydraulic system;
- the gates and valves operation during closing and opening.

The transients pressure rapidly changing can result in excessive high pressure increasing (positive pressure) or in excessive lowering of pressure (negative pressure), with respect to the pipeline pressure ratings. According to the type of pressure variation, the impact of transients can be of different types. Further, we will discuss the different situations.

If transients caused by the rapidly and high pressure increase, pipeline system damage can occur (examples: joint rupture and leakage, elbow movement or pipe fissure).

In the case of negative pressure, there is the risk of implosion and pipe internal material damage. If the pressure drops under the water vaporization pressure, the phenomenon of cavitation appears. Air bubbles are formed and during the pressure drop, and they collapse when the pressure starts to increase. Their implosion generates high shock-wave and can damage the internal material of the hydraulic system in the area where this phenomenon takes place.

Types of transitory flows that make the object of our study, are the partially obstructed flows and the turbulent high flow rates.

1.2.1 Obstructed flow

We call obstructed flow, a sudden contraction followed by a sudden expansion of the flow domain. The flow can be partially obstructed by conception or it can become obstructed during the system exploitation, such a gate opening/closing.

In sudden contraction, the cross-sectional are of the flow domain is reduced and the fluid flow is accelerated locally (Figure 1.2). At the contraction entrance, reversed flow exist and downstream the contraction, there is a pressure drop due increased flow velocity (see Figure 1.2.a).

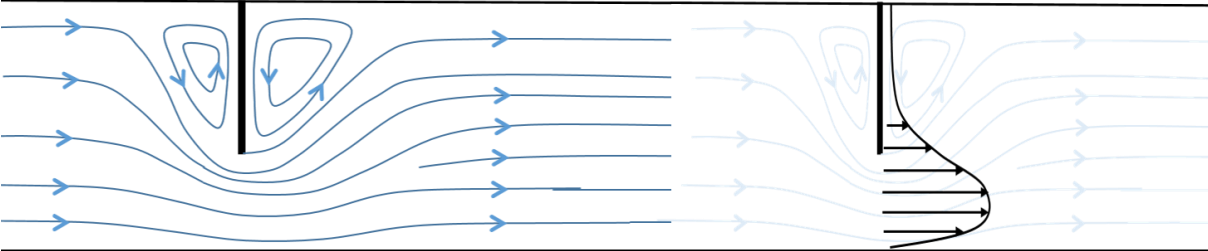


Figure 1.2. a) Contracted flow pipe streamlines and b) the corresponding velocity profile

The flow, just after the contraction, enters in a transitory region, it is unstable and its velocity profile is asymmetrical with respect to the flow direction, as we can see in Figure 1.2.b.

1.3 Cavitation

Pure and homogeneous liquids can be tensioned by pressure drop or temperature variations. When the liquid tension reaches a certain value, called critical value, cavities appear and so it becomes a diphasic system formed by liquid and vapors.

Generally, a liquid under pressure or an overheated liquid can reach a critical state. If this critical state is passed by, liquid vaporization appears under the phenomenon of cavitation, respectively boiling appears. Thus, the liquid vaporization is of two types. The first one is the well-known phenomenon of boiling: the increasing temperature creates a separation surface between the liquid and the vapors. The second type of liquid vaporization, the cavitation, takes place at constant temperature and pressure drop (Figure 1.3), when the liquid pressure is equal to the vaporization pressure (p_v).

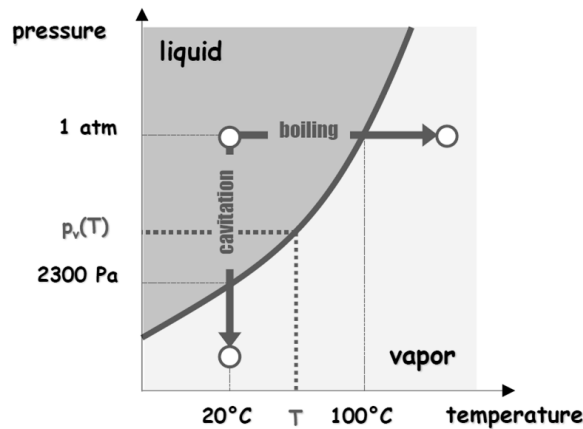


Figure 1.3. Cavitation phase diagram. Source [Fra05 pp.2]

Usually, liquids contain dissolved in gases, in small quantities. If the liquid pressure drop under a specific value, the vapor cavities appear, they are amplified as the liquid pressure continues to drop and cavities continue to be generated, creating the phenomenon of cavitation.

The cavitation has multiple forms. Transient isolated bubbles may appear in low pressure regions. They have a rapidly growth and when they will reach an area with high enough pressure, the bubbles will collapse. Another cavitation form are the attached cavities, formed on the low pressure side of the leading edge of a hydraulic system component (as the turbine/pump blades, see Figure 1.4).

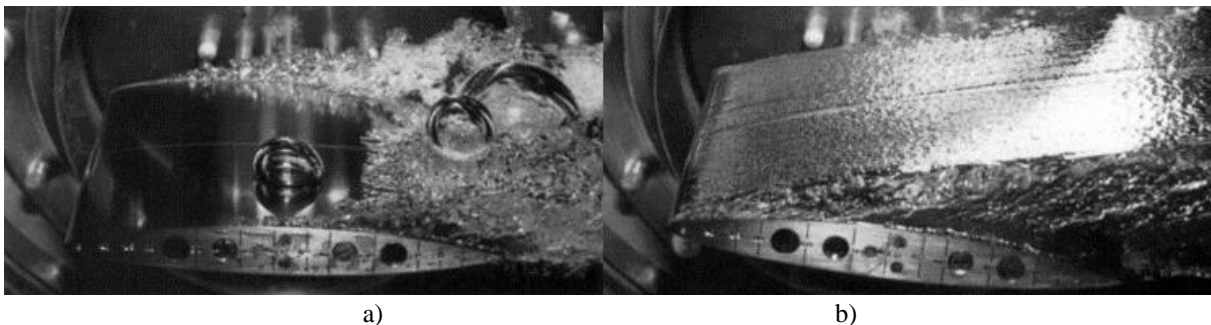


Figure 1.4. Bubbles cavitation a) and attached foil cavitation b). Source [FM85]

Also, specific to turbomachines, is the cavitation vortex. It appears in the low pressure core of a rotational flow, at the propellers outlet (Figure 1.5).



Figure 1.5. Vortex cavitation development downstream a Francis turbine. Source [ICA08]

The vapor cavities are unstable, being created by a pressure variation field. Their collapse, when they reach an increased pressure zone, is associated with mechanical shocks. The following effects are expected:

- efficiency drop, in the case of turbomachines;
- noise and vibrations;
- internal material erosion.

In industry, the cavitation phenomenon is undesirable and there where conducted multiple studies in order to have a better knowledge about its behavior and effects. Numerical simulations and experimental analysis at reduce scale for cavitation vortex characterization during turbine exploitation are suddenly encountered in the specialized literature [ICA08], [SGA06].

1.4 Summary

We have presented the hydraulic phenomena of interest in our study and a brief overview of the corresponding conventional measurement methods. Our work is focused on the improvement of the non-intrusive acoustic flow metering, for applications with transient flow, with high flow rates and cavitation. A second interest is given to the optimization of the ultrasonic flow velocity profiling, using a minimum number of ultrasound transducers. In the further chapters, the existing limitations in these area of interests are presented, along with the solutions that we propose in order to eliminate them.

Ultrasound flow monitoring

Contents

2.1	Acoustic flow monitoring principle	18
2.1.1	Passive and active acoustics	18
2.1.2	Doppler ultrasound flow monitoring	19
2.1.3	Time of flight method.....	19
2.2	Measurement issues.....	21
2.2.1	Flow domain characteristics	21
2.2.2	Fluid flow impact.....	22
2.2.3	Fluid phase state	23
2.3	Summary	23

In hydraulic systems, it is mandatory to monitor and measure the flow parameters (velocity, pressure, flow rate, phase change) of different fluids, through pipes and ducts, at every moment of time. Today, multiple methods for pipe fluid flow monitoring are available, each one being suitable for different applications. As we have already mentioned, we are interested in water pipe flow monitoring. There are some classical pipe flow meters, employed since the use of the first hydraulic systems [Mill96]:

- obstruction flow meters: venturi flow meter;
- velocity flow meters: Pitot tube;
- positive displacement meters: axial or radial turbine flow meter;
- variable area meters: rotameter.

All these instruments are more or less accurate, depending on their application, and all of them perform intrusive measurements. The classical flow meters have to be set up at the same time with the hydraulic system's installation. For later install, the system has to be stoped and new adjustment may be necessary. From practical point of view, they are inefficient.

This is why the non-intrusive techniques have been introduced. Among the class of non-intrusive measurement techniques, we mention here the Particle Image Velocimetry technique that may be used for velocity flow profiling and cavitation area for the two phase flows characterization [ICA08], [MBC17], [RWW07] and the non-intrusive acoustic techniques on which we focus further our discussion.

2.1 Acoustic flow monitoring principle

2.1.1 Passive and active acoustics

The alternative to the mechanical flowmeters are the ultrasound flowmeters. The greatest advantage is that the acoustic flowmeters are non-intrusive measurement instruments and they can be implated independently of the hydraulic system operation (Figure 2.1). Compared with other non-intrusive techniques, the acoustic measurements can be placed in many applicative contexts, for much lower costs than PIV, for instance.

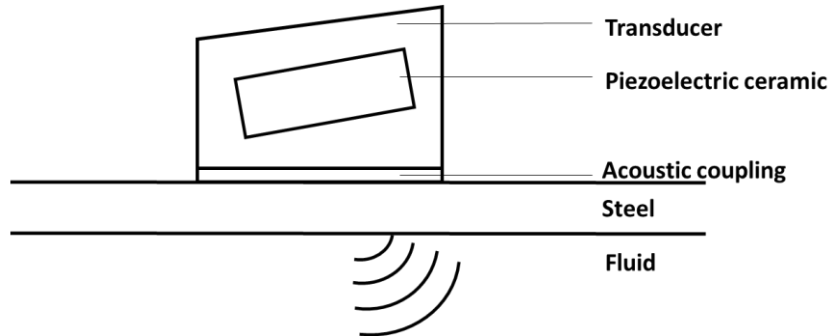


Figure 2.1. Ultrasonic transducer principle

Acoustic flowmeters can be used to monitor almost any pipe sector, being easilly to install. The acquisition of pressure field variation is realised at every instance of time, using two main approches: passive and active acoustics (Figure 2.2).

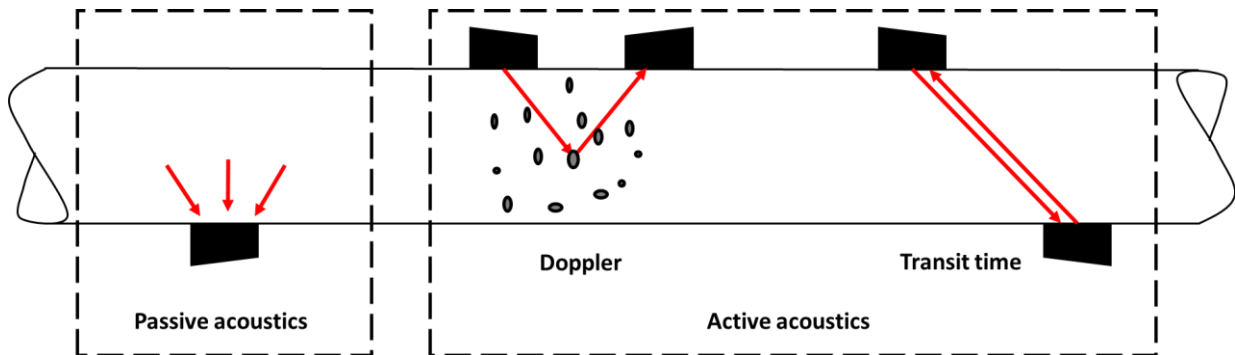


Figure 2.2. Ultrasonic flow monitoring principles

In Figure 2.3, a classical acquisition chain is presented, for passive and active ultrasonic measurements. Passive acoustics uses transducers to record the waves generated by the phenomena. Flow turbulences and vortices generate vibrations at certain frequencies and they can be found in the information carried by the recorded signal (Figure 2.3.a).

The active ultrasonic method is based on the fluid-wave interaction, transmitting an ultrasonic beam across the pipe by a transducer called emitter. The propagating beam is recorded using a second transducer called receiver (Figure 2.3.b). The beam interacts directly with the flow and so the processing of the received signal provides information about the flow parameters. The emitter and the receiver can be fixed adjacently, on the same side of the pipe (in “Z”, “V” or “W“ configuration), or on opposite sides [San02].

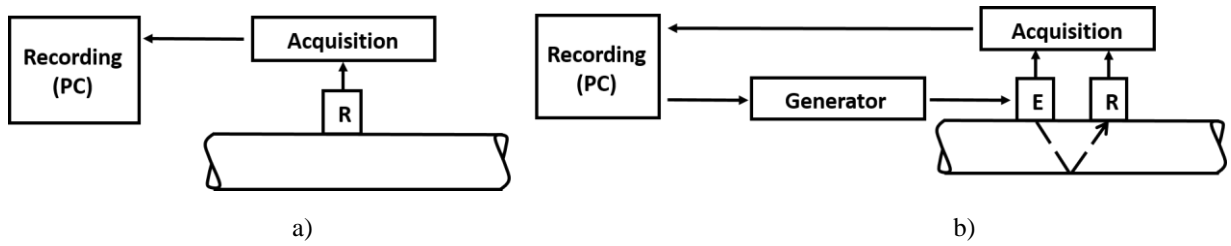


Figure 2.3. a) Passive ultrasonic method uses one or more transducers to record acoustic waves generated by the flow; b) The active ultrasonic method uses at least one emitter (E) to generate an acoustic wave to propagate through the flow, and at least one receiver (R) to record the travelling acoustic wave.

The ultrasound flow monitoring studied in our research is based on active acoustics. The transducers configuration depends on the concerned application and the choice of parameters such as the transducer numbers or the optimal distance between them, will be discussed in the following section of this chapter.

2.1.2 Doppler ultrasound flow monitoring

The oldest acoustic method for flow measurement uses the Doppler effect. An acoustic beam is emitted under a certain angle with respect to the direction of the flow. The beam is scattered by the moving particles. A frequency shift, Δf , between the emitted and the received wave is induced [SAF09]. The difference in frequency is related to the flow velocity:

$$u = \frac{c \cdot \Delta f}{2 \cdot \cos\theta \cdot f_0} \quad (2.1)$$

where f_0 is the emitted frequency and θ is the angle between the beam direction and the flow.

This method is easy to implement and is non-invasive, but it has a restrained application field due to the nature and size of the particles which varies the attenuation of the ultrasonic beam, and due to the fact that it is assumed that the particles move with the same velocity as the fluid flows [GP14 section 5.4.2.].

An accuracy improvement of this method is the use of pulsed beam in order to characterize the flow velocity in pipes profile or even to estimate the water depth in open channel flows [SAF09].

2.1.3 Time of flight method

The time of flight method (called also transit time method) is the one with the widest range of application and highest accuracy. It is successfully used for more than 30 years not just for flow rate estimations but also to provide information about the type of fluid flow inside pipes, based on fluid velocity estimation.

Now we will present the principle of the time of flight method. An acoustic wave travels through a water filled pipe, from point A towards B, in the same direction of the flow,

during time t_{AB} . Another acoustic wave, similar to the first one, travels backwards, from point B towards A, during time t_{BA} (Figure 2.4). The transducers from both points are alternatively emitters and receivers.

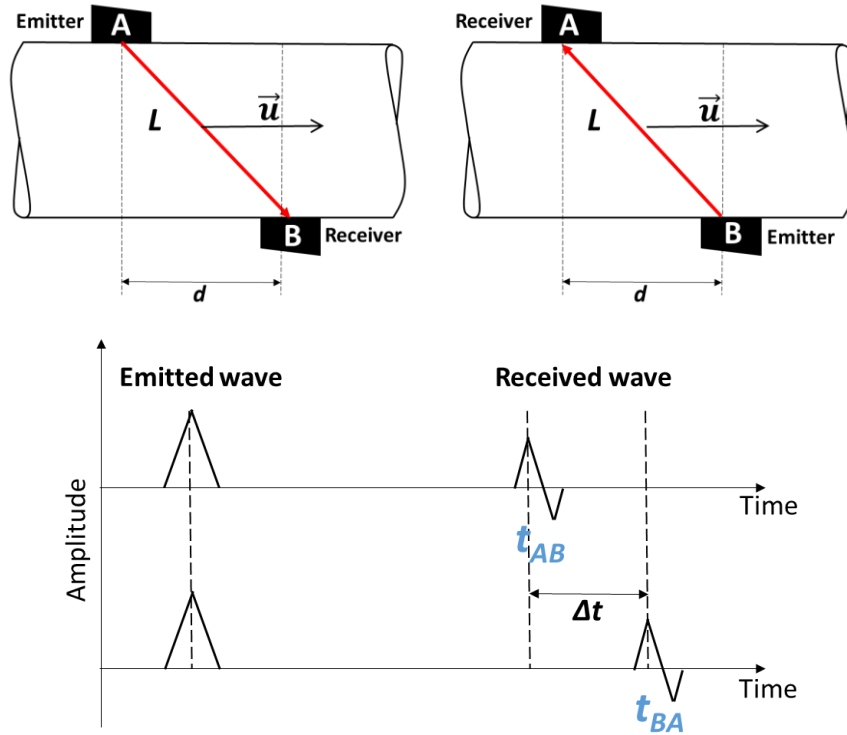


Figure 2.4. Propagation time difference estimation: $\Delta t = t_{BA} - t_{AB}$, where d is the distance between the emitter and the receiver

The times of flight of the two waves depends on the flow velocity, u , and on the traveled ultrasonic wave physical distance, L :

$$t_{AB} = \frac{L}{c + u \cdot \cos\theta} ; t_{BA} = \frac{L}{c - u \cdot \cos\theta} \quad (2.2)$$

The difference between the times is proportional with the velocity component of the flow in the direction of the wave propagation [GP14]:

$$\Delta t = \frac{2Lu}{c^2 - u^2} \quad (2.3)$$

For most fluids, $c^2 \gg u^2$, and using equation (2.1), the mean flow velocity is given by the following relationship:

$$\bar{u} = \frac{\Delta t \cdot c^2}{2 \cdot L \cdot \cos\theta} \quad (2.4)$$

where θ is the longitudinal wave's incident angle.

The flow rate can be easily estimated if we know the mean flow velocity: it is the product between the pipe cross-sectional area and the mean flow velocity.

A hydraulic correction coefficient is applied [Web99 pp. 807], that depends on the flow's Reynolds number. The estimation of the flow rate is performed using the following relation:

$$Q = k_h \cdot u \cdot \frac{\pi D^2}{4} \quad (2.5)$$

with the hydraulic coefficient, k_h , for circular pipe cross-section is given by:

$$k_h = \frac{1}{1.125 - 0.011 \cdot \log(Re)} \quad (2.6)$$

2.2 Measurement issues

Except the theoretical interaction between the fluid flow and ultrasound wave during its propagation (such as absorption and attenuation), there are some wave's parameters (frequency, phase, amplitude and deviation) that are impacted by different factors related to the flow domain and the type of fluid. The type of the fluid flow is important to be known: its density and temperature give the corresponding sound velocity and sound attenuation.

The flow velocity distribution and the fluid phase of state impact the acoustic wave propagation and the measurement method has to be adapted accordingly. The pipe size, material and thickness; the transducers configuration and the installation conditions matters also. In this section, we will discuss the influence of this factors in the case of water pipe flow since these factors impacts the shape of received signals.

2.2.1 Flow domain characteristics

The transducers installation has to take into account characteristics of the flow domain. The transducers installation where hydraulic transients occur will increase the measurement errors, the acoustic wave being widened and strongly attenuated by the non-uniform pressure field (Figure 2.5).

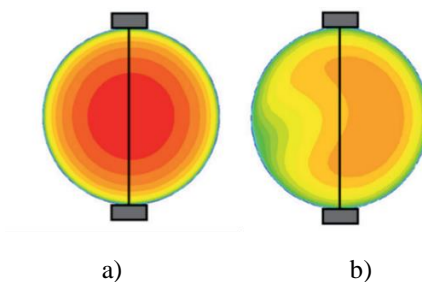


Figure 2.5. Circular pipe cross section: a) Fully developed velocity flow profile; b) Disturbed velocity flow profile. Source: [Tuv16]

If the hydraulic system integrates particular hydraulic components that are disturbing sources, such as flow contractions/expansions, bends or gates, the transducers placement has to take into account their presence.

2.2.2 Fluid flow impact

Laminar flow conditions are never encountered in real life applications and they represent an idealized measurement conditions. In such conditions, the fluid mean velocity is constant in time and the velocity profile in the axial direction of a cross-section of a pipe is symmetric (Figure 2.5.a) with respect of the flow direction. All the other types of flow represent scenarios where the current measurement techniques are used, but not always efficiently, due to hydraulic transients. When hydraulic transients appear, the velocity profile becomes asymmetric, and there are important pressure variations in a pipe cross-section. This is specific to transient or turbulent flow, which are characterized by a Reynolds number over 4000, meaning that the flow velocity increases or the flow domain geometry is variable.

Further, we will discuss the ultrasonic wave propagation in both situations, from transmitter-receiver propagation path perspective. Firstly, suppose that we are in the case of flow velocity increasing and constant flow domain geometry. The excessive flow rate leads to a phenomenon called the “flow blow” effect (Figure 2.6). The energy of the received signal is weakened due to the high flow velocity and the acoustic beam is shifted in space and widened. In the same time, too low flow rate can generate measurement errors. Low flow rate will generate low propagation time differences and inaccurate flow rate estimations.

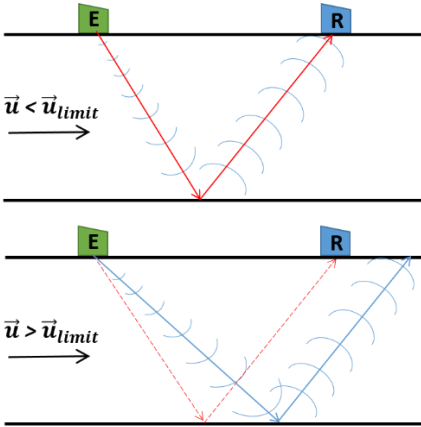


Figure 2.6. The “flow blow” effect

Secondly, if the flow rate is constant and the flow domain geometry varies, the flow velocity will increase locally, and turbulences are likely to appear. In this case, in order to ensure a satisfying measurement accuracy, the classical transducer configuration (Figure 2.4) has to be adapted to this type of flow monitoring. The contributions that will be presented in the next chapters, for these issues compensation, consists in the use of a multiple emitter – multiple receivers configuration (for one path) in order to compensate the emitted acoustic beam shift, compensate the time of flight estimation errors and thus increase the flow meter’s robustness in case of the “flow blow” effect and transient/rapid flow rate/velocity changes.

2.2.3 Fluid phase state

The fluid flow can be single phase or multiphase flow, if at least two fluid phases are present: solid, liquid or gaseous. In most applications, initially, the fluid flow is a single phase flow, and during exploitation two-phase flow may appear. The phase change, from liquid to gas and/or from gas to liquid is conditioned by the fluid pressure or fluid temperature variation. In industry, there are multiple applications when the pressure field of the working fluid is variable, [Ant84 pp. 94] for example, in the case of hydraulic machines: turbines, pumps, water cooling systems, chemical and oil industry.

In our research we are interested on high pressure variations. There are types of fluid flow with great interest for industrial applications, when the fluid pressure decreases dramatically and it becomes lower than a reference value, called the vaporization pressure (the value of the liquid vaporization pressure at atmospheric temperature). Vapor cavities and air bubbles can appear and because of rapid pressure field variation, the pressure increases again and bubbles collapse generating shock waves.

When the emitted acoustic beam interfere with the vapor cavities, it is scattered and attenuated. The degree of attenuation and scattering depends on the size and distribution of the air bubbles.

2.3 Summary

In further chapters, we focus on ultrasound signal processing measurement methods that we propose in order to overcome the limitations discussed in this chapter. We propose to use single acoustic path measurement technique in order to achieve an improvement of the ultrasound flow metering precision, along with a compressive sensing based matched filtering framework for the signal processing part. For the flow velocity profiling we propose a multiple acoustic paths technique, with a beamforming processing of these multiple paths.

Single path ultrasound processing

Contents

3.1	Wide band signals.....	26
3.2	Matched filtering for TOA estimation.....	27
3.3	Compressive sensing based signal reconstruction.....	28
3.3.1	Introduction	28
3.3.2	LFM representation in the warped domain.....	29
3.3.3	L-statistics and discrete time-frequency analysis	31
3.3.4	Compressive sensing reconstruction	32
3.4	Numerical example.....	33
3.5	Summary	39

As we presented in the previous chapter, the flow velocity variation out of a (limited) performing range produces the acoustic beam deviation and/or multi-path propagation, affecting the received signal shape. Other cases, such as the mechanical misalignment of the sensors due to the uncontrolled vibrations, can produce undesired effects on the received signal.

This chapter presents the improvement we propose from a single sensor's perspective. Two main contributions are proposed. First, we show how the matched filter concept can improve the velocity accuracy estimation and robustness. Second, we propose to use the compressive sensing reconstruction of the received signal, in the warped domain, in order to overcome the effect of the misaligned transducers.

The received signal reconstruction will allow the compensation of *TOA* estimation errors and thus will contribute to increase the flow meter's robustness in case of such undesired effects. Using the new signal processing algorithm based on compressive sensing that take advantage of the signal reconstruction, the new flowmeters can achieve a higher accuracy in terms of *TOA* estimation. The time of arrival estimation for acoustics signals can also be performed using another methods such as: thresholding, curve fitting or sliding-window.

These target methods are simpler but suboptimal compared to the detection method described in this section, based on matched filtering [BA98]. They provide a good compromise between accuracy and system complexity.

3.1 Wide band signals

In order to increase measurement performances, the studies that we perform are focused on the use of wide band signals, analyzed using matched filtering. At the basis of this signal processing methodology we find the wide band signals (linear modulations, cubic, logarithmic chirps or discrete frequency modulations, discrete phase, etc.) that have been primarily studied in the radar field, due to their excellent resolution and noise robustness properties. These properties are possible due to the instantaneous signal frequency variation, which provides a wide band duration product being operated by the principle of matched filtering [CBD14], [DPC14].

There are two main reasons why we have chosen to use the wide band emitted signals. The first one is related to the time resolution improvement. Wide band signals allow a precise estimation of wave transit time, implicitly a precise estimation of the flow velocity, and also robust propagation compared to pulse signals.

The second reason of using wide band signals, is motivated by the interest of simultaneous signal emission in the direction of the flow and in the opposite one. This type of emission gives the possibility to work with very short repetition periods, and also to carry out measurement with a very high rate.

In the same time, the electronic system gets simplified because we don't have to switch between emission/reception level, in order to perform measurement in the same direction with the flow and in the opposite direction. The use of LFM waves with different rate, ensure the "orthogonality" in the time-frequency domain, avoiding in this way the interferences between the emitted waves in the same time.

The simultaneous emission principle consist in emitting LFM signals, with positive rate, respectively, negative rate, defined by:

$$e_1(t) = A_1 \exp[j2\pi(f_0 + kt^2)], \quad t \in [kT_r, kT_r + D]$$

$$e_2(t) = A_2 \exp[j2\pi(f_0 - kt^2)], \quad t \in [kT_r, kT_r + D] \quad (3.1)$$

where f_0 is the transducer's central frequency, k is the linear modulation rate that allows frequency sweeping around f_0 , in the desired frequency band, T_r is the repetition period of emission and D is the signal duration. Figure 3.1 shows spectrograms examples of emitted signals used in our studies, which correspond to the simultaneous emissions with positive and negative slopes.

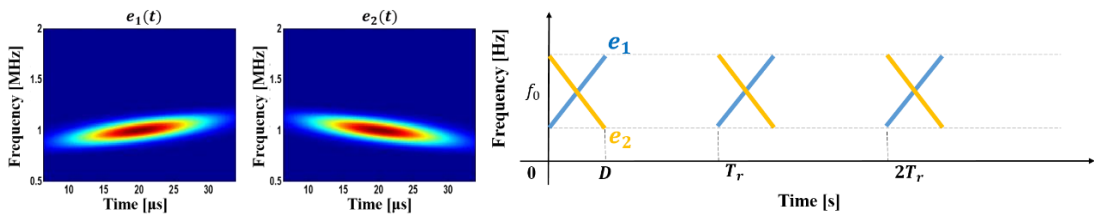


Figure 3.1. LFM signals with different chirp rates, used for simultaneous emission in the direction of the flow and in the opposite direction.

3.2 Matched filtering for *TOA* estimation

As we have seen in the first chapter, the *TOA* estimation impacts strongly the flow measurement accuracy. We estimate the acoustic *TOA* of a single-path configuration, using matched filtering.

The matched filtering is a signal processing method widely used in digital communications, radar or sonar applications. The interest is to detect the presence of the desired signal by using set of data from an another related signal [MIK05]. The matched filter can be succesfully applied if there is a significant corelation or statistical dependence between the two signals involved.

The definition of the matched filtering with the emitted signal $s(t)$ and applied to the received one $x(t)$, is given by the correlation between these two signals. Thus, given a wide band signal, the impulse response of matched filtering of this signal (i.e. relative to shifted versions of the signal) is constructed with the following expression (the assumption of a stationary configuration is made):

$$h(t) = a * s(t_0 - t) \quad (3.2)$$

where a is a normalization factor, t_0 represents a time reference and the operator “*” is the Hermitian operator. As this expression indicates, the filter impulse response, $h(t)$, is obtained by time reversal of the original signal.

Let’s consider the simplest model for the received signal through the measuring system:

$$x(t) = A \cdot s(t - TOA) + \varepsilon(t) \quad (3.3)$$

where A and TOA represents, the attenuation, respectively the time of arrival of the emitted signal and $\varepsilon(t)$ represents the additive Gaussian signal noise. The application of the matched filter on the signal $x(t)$, expressed as a convolution between x and h , leads to:

$$y(t) = \int_{-\infty}^{\infty} x(\tau) \cdot h(t - \tau) d\tau \quad (3.4)$$

The estimation of the *TOA* is now reduced at the instant of time computation for which the matched filter response is maximal:

$$TOA = \arg \max[y(t)] - t_0 \quad (3.5)$$

The diagram of this approach is displayed in Figure 3.2, from which results the formula for the time of arrival of the matched filter.

In acoustic monitoring, wave’s propagation and reception are conditioned by factors related to: wave’s propagation physics (such as attenuation, absorption, scattering, geometrical spreading or propagation losses) and to geometrical set-up of the acoustic system.

In this second category, the acoustic transducers inappropriate alignment is one of the frequently encountered situation.

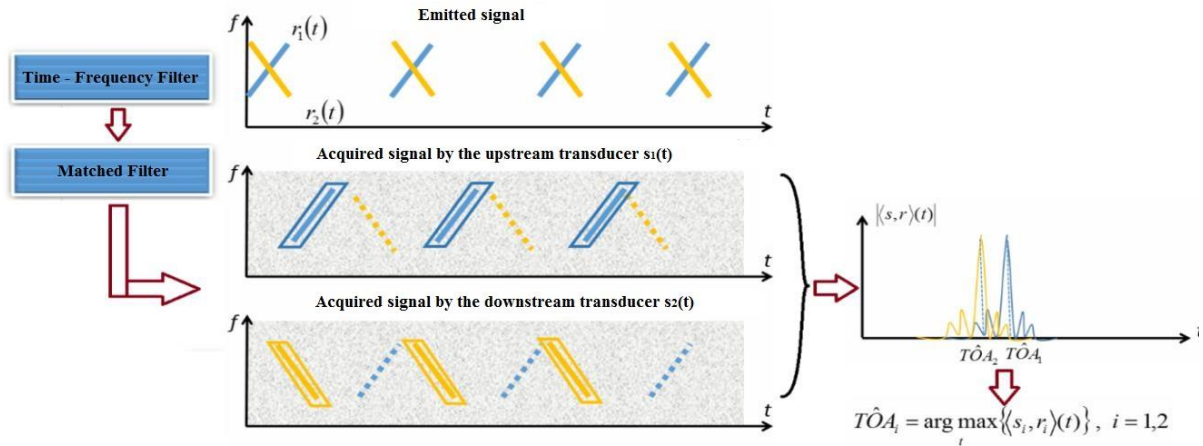


Figure 3.2. The diagram of the received signal processing using matched filtering technique

In most of acoustic applications, due to underwater unsteady conditions, vibrations, or geometrical misalignments, a position offset of the acoustic transducers appears. In terms of received signals, the misalignments between sensors conduct to the loss of the signal's energy and informational content, fact that can affect the processing at the receiver level. The transducers relative position is important for applications involving direction of arrival estimation, localization or source detection. When the transmitter-receiver transducers configuration is inappropriate, the received signal's informational content is not the same as the one of the emitted signal. As we will present later, in our context, the misalignment of the transmitting/receiving sensors will conduct to the generation of two propagation paths. The received signal will be then composed by two close arrival, characterized by destructive interferences, affecting the accuracy of TOA estimation.

Consequently, it is important to maintain the signal's informational content between emission and reception, in order to preserve an optimal signal processing performing. Hence, the effects of transducers position offset need to be compensated to avoid dramatically errors of the data processing results. For some simple applications, with fixed experimental configurations, the position offset can be geometrically quantified and its compensation is trivial. In most cases, where the geometric quantification is not possible, its compensation demands more complex methods, one of possible solution being presented in next session, based on the compressive sensing concept.

3.3 Compressive sensing based signal reconstruction

3.3.1 Introduction

This section presents a method that contributes at performances improvement of a sensing array by recovering the incomplete information, in the case of misaligned transducers.

In previous studies, the compressive sensing concept has been successfully used for separation of linear and non-linear frequency modulation signals [OSS14], [SOS13], in applications of radar, sonar, Doppler effect or underwater mammal vocalization [BIO15]. Multiple signal's overlapping components may exist in the time-frequency domain. That's why the conventional windowing or filtering operations [LSB11], [JW92] are not useful for signals separation.

A consequence of this compressive sensing based separation method is that there are missing samples or observations, corresponding to the frequency values where the multiple signals components are overlapped. In [BIO15] the separation of an underwater mammal vocalization numerical model, composed by two non-linear frequency modulated signals superposed in the time-frequency domain has been proposed. The compressive sensing concept allows the missing samples recovery [Bra07], if the signal is expressed into another analysis basis.

In our work, we take advantage from the signal recovery capability of the compressive sensing concept. The difference is that in our applications, we are not interested in signal's components separation, but just in their recovery, in order to ensure the accuracy of TOA estimation. Here, the compressive sensing concept aiming is to reconstruct signals that are recorded with informational loss, thus, they already have a sparse basis representation in the frequency domain [Bra07], [PB10], [SOS12].

In a standard formulation of the compressive sensing concept, the observations are made in the time domain [JAS13]. In our work, we deal with non-stationary signals that may be sparse in the time-frequency domain and we apply the compressive sensing algorithm in a warped domain, in order to stationarize them and to perform their reconstruction [SOS13].

We consider that the emitted signals are linear frequency modulations. Their Instantaneous Frequency Law (IFL) coordinates will be used to estimate the warping transform function (or time axis transform). The warping transform is used to stationarize the received LFM signal, hence, to turn it into a stationary sparse sinusoid in the warped domain. In our work, the aim of the compressive sensing concept is to reconstruct the stationarized sinusoid with missing sample. Then, an unwarping transform will turn the reconstructed sinusoid into the signal's original basis.

3.3.2 LFM representation in the warped domain

Consider a LFM emitted signal defined by:

$$s(t) = Ae^{j(2\pi f_0 t + c_r t^2)} \quad (3.6)$$

where f_0 is the central frequency and c_r is the chirp rate. The acoustic wave propagation environment is a source of noise, while the measurement configuration misalignments will impede a complete signal reception. Consider then the following received signal model:

$$x(t) = s'(t) + \varepsilon(t) \quad (3.7)$$

where $s'(t)$ is the received fraction of $s(t)$ and it represents an incomplete spectral information, while $\varepsilon(t)$ is the additive noise.

As the emitted signal is known, the first step is to use the available information, the signal's IFL, to construct the warping law attempting to stationnarize the signal's time-frequency content. In a general case, we consider an arbitrary IFL, $\varphi(t)$, and a finite set of coordinates $\{\varphi(t_k)\}_{k=\overline{1,L}}$, with L divided segments of the signal $s(t)$. We consider a bijective function $w(t)$, called **warping function**, defined by the following equations system:

$$\begin{cases} \varphi(w(t_k)) = w(\varphi(t_k)) = t_k, k = \overline{1,L} \\ w_k^{(0)} = \frac{1}{2}(I_k + I_{k+1}) \end{cases} \quad (3.8)$$

where $w_k \stackrel{\text{def}}{=} w(t_k)$ and $[I_k, I_{k+1}]$ is centered around t_k . Warping function bijectivity will allow the signal unwarping into its original basis.

IFL has to be monotone on each of L intervals. This fact will ensure the existence of the inverse warping function. Thus, the local solution of this equation system, for a point p is given by:

$$w_k^{(p)} = w_k^{(p-1)} - \text{sgn}(\varphi(w_k^{(p-1)}) - t_k) \frac{I_k - I_{k-1}}{2^{p+1}} \quad (3.9)$$

with the solution convergence condition:

$$\left| w_k^{(p+1)} - w_k^{(p)} \right| < \varepsilon \quad (3.10)$$

We define a warping operator, W , as:

$$\{W, \quad w(t) \in C^1, \quad w'(t) > 0: \quad s(t) \rightarrow W(s(t))\} \quad (3.11)$$

where C^1 is the class of differentiable functions and $s(t) \in \mathcal{L}(\mathbb{R})$.

The signal time axis transformation introduced by the warping operator is defined by:

$$W(x(t)) = \left| \frac{dw(t)}{dt} \right|^{\frac{1}{2}} x(w(t)) \quad (3.12)$$

The envelope of the warped signal is represented by the term $\left| \frac{dw(t)}{dt} \right|^{\frac{1}{2}}$. As we are not interested in signal energy conservation, but in modulations recovery, this term can be neglected. Hence, we can define the warping operator as [BIO15]:

$$W(x(t)) = x(w(t)) \quad (3.13)$$

For non-stationary signals encountered in real life applications, the time-frequency content is not possible to be expressed analytically. Using the time axis transformation, [JIQ06] proves that any kind of signal can be expressed by non-disturbed sinusoids, pure sinusoids.

Consider $x[n] \in \mathbb{R}, n = 1, \dots, N$, being the sequence obtained by uniform sampling of the continuous signal $s(t)$, defined by:

$$x[n] = \int x(t) \delta(t - nT) dt = s'[n] + \varepsilon[n] \quad (3.14)$$

with T the sampling rate and δ the Dirac function.

The associated warped discrete sequence is given by $x_w[m] \in \mathbb{R}, m = 1, \dots, N_{warping}$. As it is necessary to estimate new values, the warped discrete sequence need to be more important in terms of number of samples, thus we usually choose $M = 3N$. Then, the sampled non-unitary discrete time warping operator is defined as:

$$W(x[n]) = x_w[m] = x \left(w_d \left(\frac{m}{N_{warping} - 1} \right) (N - 1)T \right) \quad (3.15)$$

where w_d is the normalized function of $w(t)$. Then, using the linearity property of the warping transform, we have:

$$W(x[n]) = W(s'[n]) + W(\varepsilon[n]) \quad (3.16)$$

3.3.3 L-statistics and discrete time-frequency analysis

$W(s'[n])$ represents the warping transform of the signal fraction to be reconstructed and due to this transform, it is turned into a sinusoid that is supposed to be sparse in the frequency domain:

$$W(s'[n]) = \alpha e^{jf_w n} \quad (3.17)$$

with α the amplitude of the sinusoid of frequency f_w . Once the warped signal is available, its discrete *STFT* is computed:

$$STFT[n, k] = \sum_{p=0}^{M-1} W(x[n + p]) e^{-j2\pi kp/M} \quad (3.18)$$

where M is the length of the Hamming window used to compute the *STFT*.

The $W(x[n])$ analysis in the time-frequency domain is performed in order to separate the desired part of the signal from perturbations (see Figure 3.3). When the desired signal part and the disturbances generate the same frequency components, they will generate high frequency amplitudes. When they are opposite in phase, low frequency amplitudes will be generated. The disturbing components can be then partially or completely removed if the strongest and the weakest values of $STFT[n, k]$ are eliminated [OSS14]. This technique is named L-statistics and it is successfully used in the case of highly noised signals [SDT13], [SOS13].

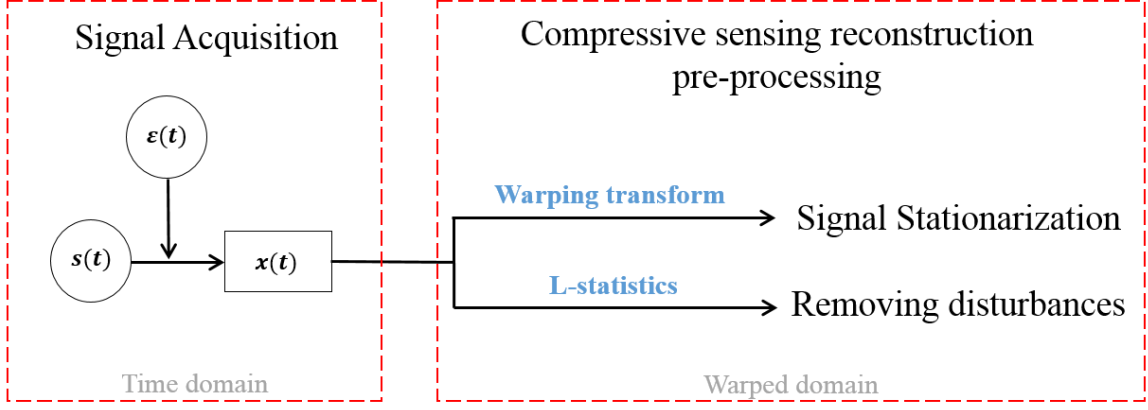


Figure 3.3. Warping transform and L-statistics purpose in signal pre-processing before the compressive sensing reconstruction

In order to remove the strongest and the weakest values of $STFT[n, k]$, we sort its values for each frequency k , along the time axis n :

$$S_k(m) = \text{sort}\{STFT[n, k], n = 1, \dots, N\} \quad (3.19)$$

Consider N_H the number of highest values of S_k and N_S the number of the smallest ones. In this case, when we apply the L-statistics to equation (3.18), we get:

$$STFT_{CS} = \sum_{m=N_S}^{N-N_H} S_k(m) \quad (3.20)$$

Equation (3.19) expresses that for each frequency k , instead of N samples, a certain number of samples is left and it will be used in further calculations [SOS13]. The L-statistics selected values contain the stationary sparse part of the signal, to be reconstructed using the compressive sensing concept.

3.3.4 Compressive sensing reconstruction

If we define a $M \times M$ matrix, as the coefficients matrix of the $STFT$, then we can rewrite the equation (3.18) as follows:

$$STFT_M[n] = C_M \cdot W(x[n]) \quad (3.21)$$

where $STFT_M[n]$ and $W(x[n])$ are vectors of the form:

$$STFT_M[n] = [STFT[n, 0], \dots, STFT[n, M - 1]]^T \quad (3.22)$$

$$W(x[n]) = [W(x[n]), W(x[n + 1]), \dots, W(x[n + M])]^T$$

Considering non-overlapping windows, the vectors from (3.21) can be expressed in one equation:

$$STFT = C_M \cdot W[n] \quad (3.23)$$

Let's consider W_{DFT} , the discrete Fourier transform of W , with C_{DFT} the corresponding DFT matrix. Then, the discrete warped signal can be expressed in the Fourier domain by:

$$W = C_{DFT}^{-1} \cdot W_{DFT} \quad (3.24)$$

Relation (3.23) can be rewritten as:

$$STFT = C_M \cdot C_{DFT}^{-1} \cdot W_{DFT} = C_{FULL} \cdot W_{DFT} \quad (3.25)$$

where the matrix $C_{FULL} = C_M \cdot C_{DFT}^{-1}$ maps the global frequency information from W_{DFT} into local information in $STFT$ [SOS13]. Now, we will use the L-statistics discussed in the previous sub-section. Hence, the sorted values of $STFT$ that are expressed by the relation (3.21), are related to the sparse DFT vector of W , by the matrix C_{CS} , named the compressive sensing mask. We can proceed now to the signal samples reconstruction, based on the following minimization problem:

$$\min \|W_{DFT}\|_1 = \min \sum_{k=0}^{N-1} |W_{DFT}(k)| \quad \text{subject to} \quad (3.26)$$

$$STFT_{CS} = C_{CS} \cdot W_{DFT}$$

This reconstruction technique has firstly been introduced in [SOS13]. It states that the missing values of $STFT_{CS}$ can be recovered such as to provide a minimum l_1 -norm of the warped signal DFT. The reconstruction performance is not affected by the L-statistics removed samples, if the corrupted samples are discarded and there are enough information left about the desired signal.

After completing the compressive sensing reconstruction in the time-frequency domain, of the warped signal, its representation in the original basis is achieved through the unwarping function: the inverse function of $w(t)$.

3.4 Numerical example

In this section, we present a numerical example that illustrates the steps of the algorithm presented in the section 3.3. The scenario is described as follows. The acoustic propagation environment is a filled water steel pipe. In the case of optimally aligned transducers, as it is shown in Figure 3.4.a), the emitted acoustic wave, $s(t)$, travels into the water, between the two transducers. At the reception the wave is attenuated and noised.

The emitter and the receiver transducers can be misaligned, hence the initial receiver position from Figure 3.4.a), that is displayed in grey in Figure 3.4.b), is changed due to the ultrasonic wave deviation during its propagation through the water and the steel pipe walls. In this case, at the reception, the wave propagating in the water is additionally delayed in time

and superposed on the wave propagating through to the main propagation direction of the transmitting transducers and then, in the steel.

The wave propagation through the environment of interest and through the pipe, for this type of application, is modeled using band-pass filters. The wave's propagation through steel, water and also during the transducer emission, alter the wave's spectral content by frequency filtering and attenuation. Hence, in accordance with our experimental tests on misaligned transducers, we chose to use a band-pass filter in order to numerically describe a simplified phenomenon's case of study.

Let consider an emitted LFM signal, defined by (3.6), with a frequency variation between 98 and 138 Hz for a sampling frequency of 1024 Hz. The chirp bandwidth was chosen in order to ensure a proper frequency resolution during the CS reconstruction algorithm and also to avoid a high computational cost.

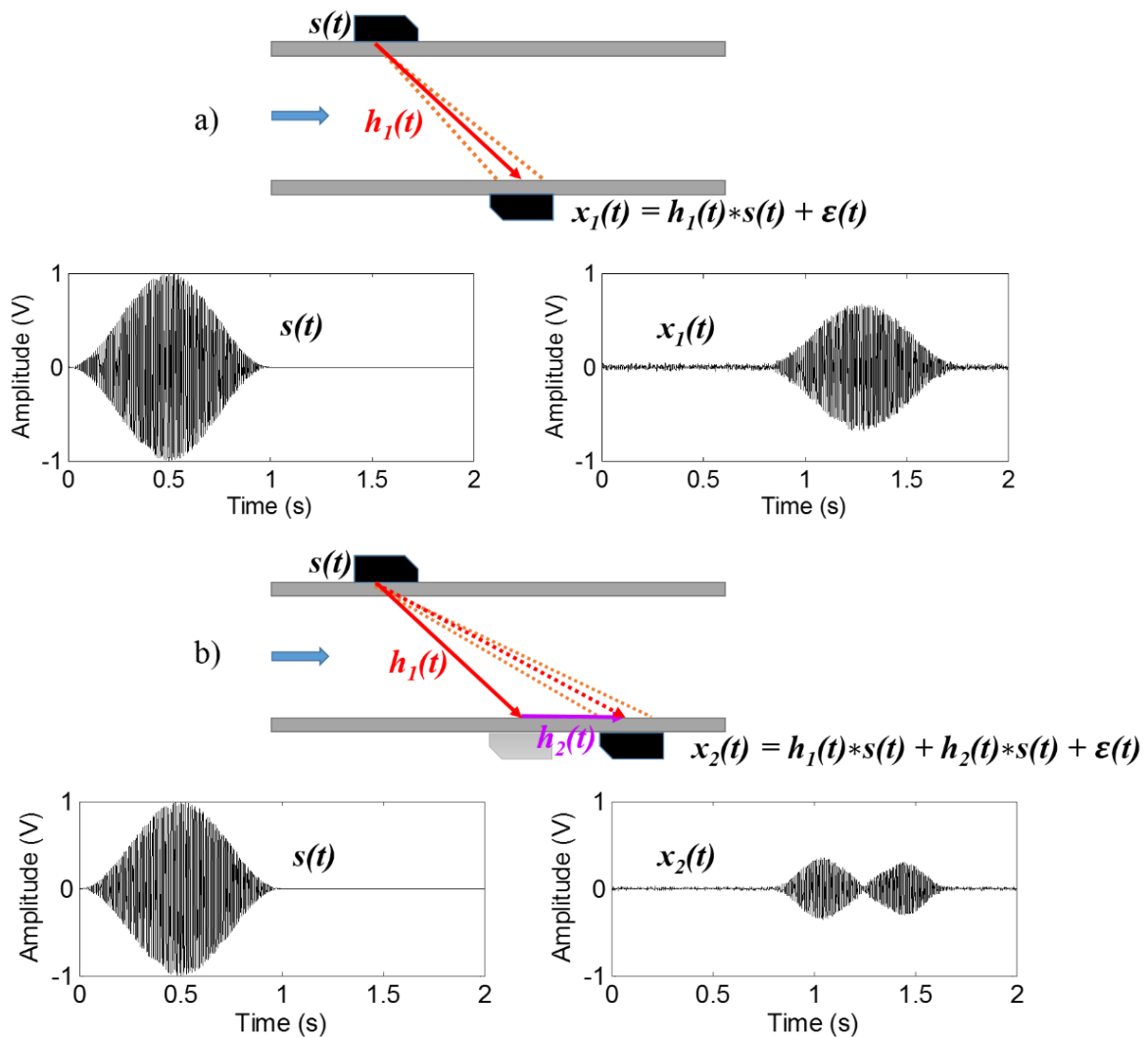


Figure 3.4. a) Emitted and received signals in the case of perfectly aligned transducers and b) misaligned transducers.

The received signal from the configuration described in the Figure 3.4.b) can be modeled as:

$$x_2(t) = s(t) * h_1(t) + s(t) * h_2(t) + \varepsilon(t) \quad (3.27)$$

where “*” is the convolution operator, h_1 is the impulse response of the filter modeling the propagation in the water, h_2 is the impulse response of the filter modeling the propagation through water and steel, before arriving to the receiving transducer and ε is the additive Gaussian noise.

In this way, we obtained a modeled received signal $x_2(t)$ that is attenuated, band-pass filtered and shifted version of the emitted signal $s(t)$. Due to the interferences, some samples may be missing with respect of the emitted signal $x_2(t)$ due to the destructive interference. Consequently, the attenuated and time shifted wave has a deformed spectral information (Figure 3.5).

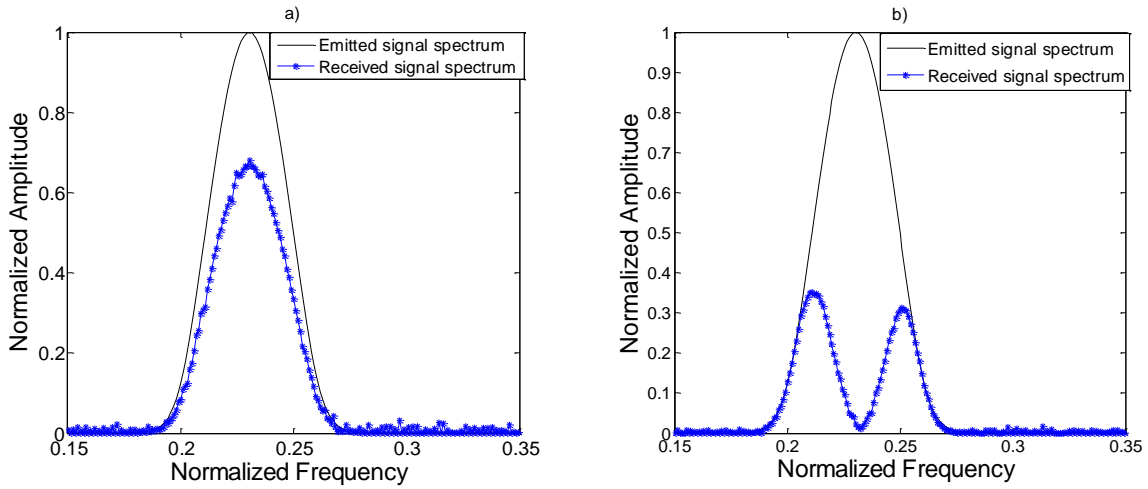


Figure 3.5. a) Emitted/received spectrums in the case of perfectly aligned transducers and b) emitted/received spectrums, in the case of misaligned transducers.

In this context, the aim is to reconstruct the missing samples from $x_2(t)$ in order to perform an accurate TOA estimation of $x_2(t)$ between the two transducers: the emitter and the receiver. The proposed solution for the missing signal samples recovery is the warping based compressive sensing reconstruction.

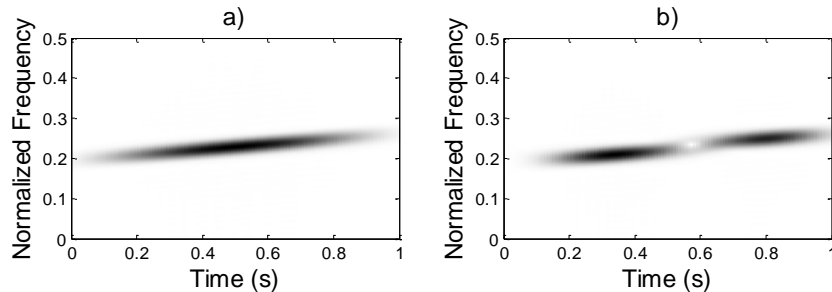


Figure 3.6. a) Spectral content of the emitted signal and b) of the received one. The received signal spectral information are sparse compared to the one of the emitted signal

In order to estimate the warping function, first, the corresponding signal’s IFL is used to design the associated warping function [IQS06]. The signal reconstruction pre-processing

is completed with the signal time-frequency stationarization in the warped domain, which is performed using the estimated warping function (Figure 3.7).

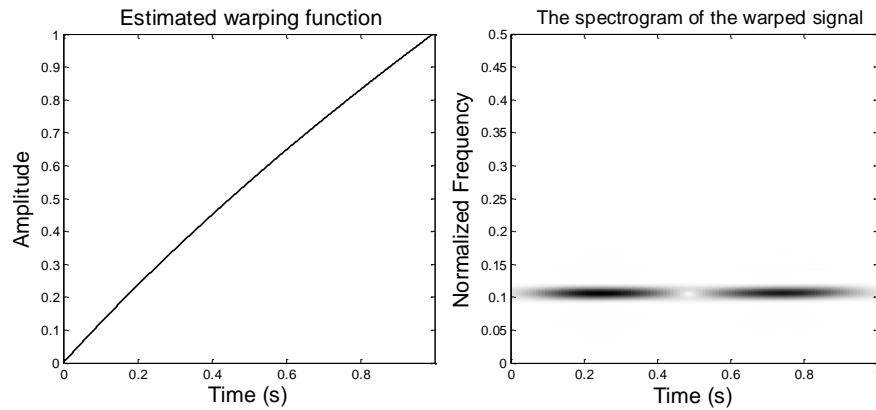


Figure 3.7. Estimated warping function that stationarizes the signal’s time-frequency content and the warped signal spectrogram.

The next step is to perform the recovery of the warped signal missing components. The CS reconstruction algorithm is now applied. The following figure shows the reconstructed signal’s spectrogram in the warped domain.

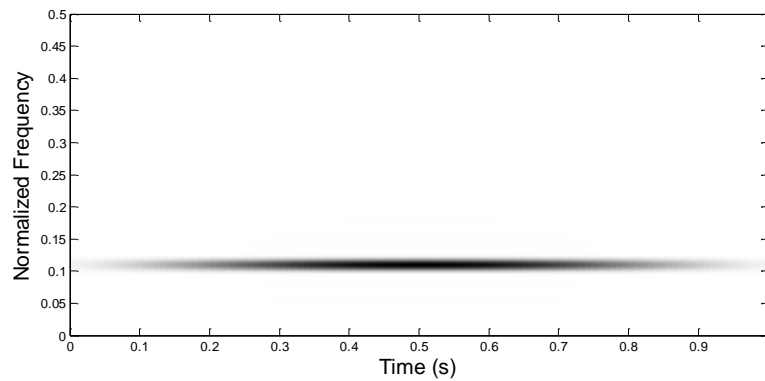


Figure 3.8. The spectrogram of the recovered signal in the warped domain

In order to return in the original time domain, an inverse warping transform is used. We obtain the reconstructed signal, $x_2'(t)$. As indicated in Figure 3.9, after the compressive sensing samples recovery, the time-frequency support of the received signal $x_2(t)$ is almost completely reconstructed.

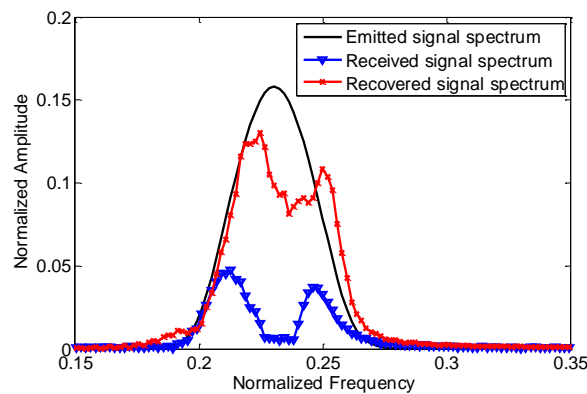


Figure 3.9. The spectrum of the emitted signal $s(t)$, of the received signal $x_2(t)$ and of the CS-based recovered one $x_2'(t)$.

The spectrogram of the recovered signal is no more sparse (Figure 3.10) due to the compressive sensing reconstruction, which indicates also the signals missing information recovery.

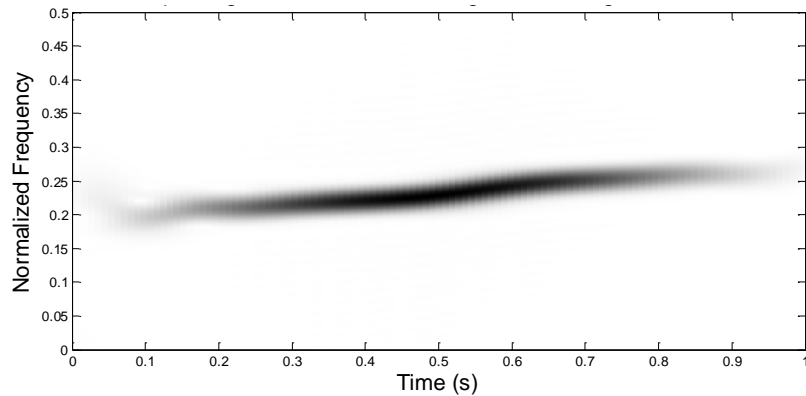


Figure 3.10. The recovered signal's spectrogram in the original time axis domain

Further, the wave's time of flight can be estimated by matched filtering of the reconstructed signal with the emitted LFM.

The steps procedure of the TOA estimation are summarized in the following figure, for both cases: when using the signal processing based only on the matched filtering and when the processing is done on the reconstructed one.

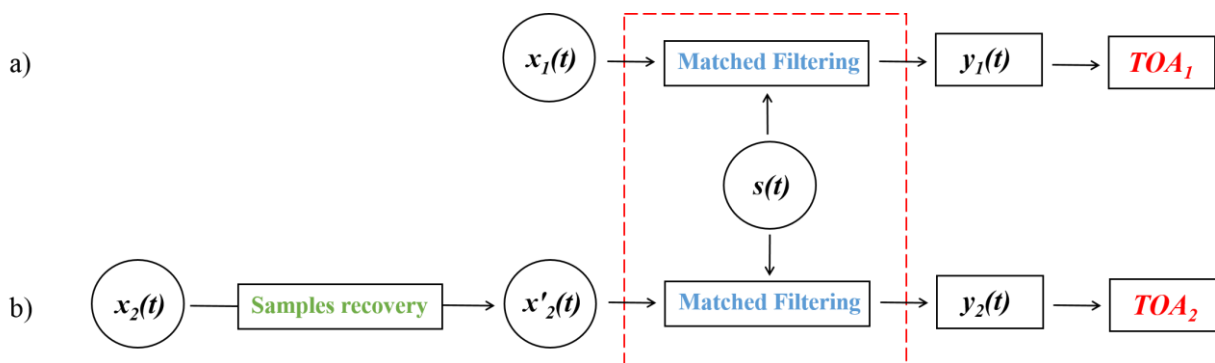


Figure 3.11. a) Classical TOA procedure estimation and b) TOA estimation based on compressive sensing reconstruction before matched filtering.

The matched filter responses, $y_1(t)$ and $y_2(t)$ are definitely different. If the signal's samples are not recovered, the matched filter response is not accurate. In our example, $y_1(t)$ has two local maxima, (marked with red dots in Figure 3.12.a), none of them being the precise one. The real TOA is estimated using the matched filter response from Figure 3.12.b).

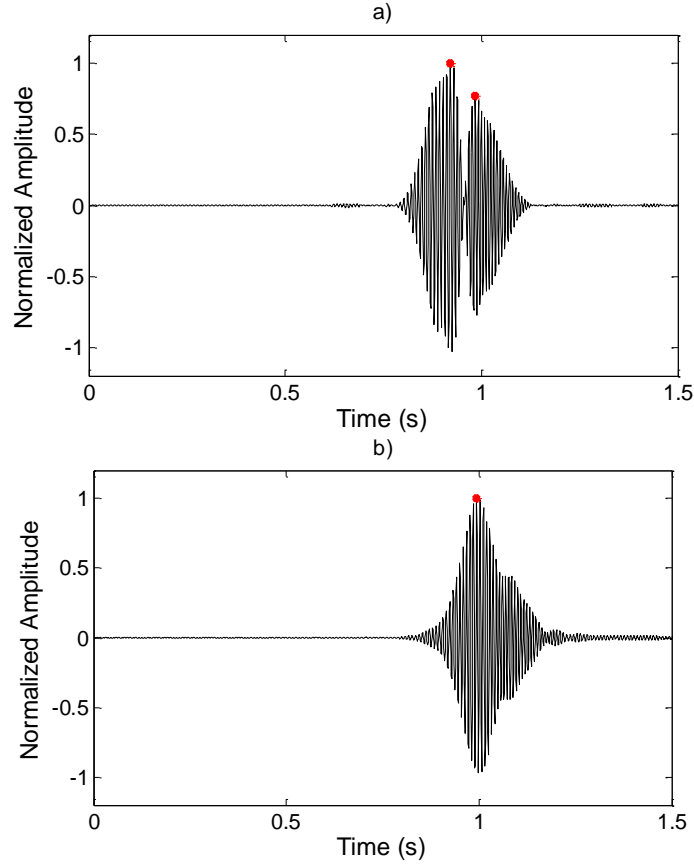


Figure 3.12. Matched filter responses for TOA estimation using a) the corrupted signal and b) the reconstructed signal.

A statistical analysis is performed, aiming to compare the improvement of the compressive sensing reconstruction in the warped domain, with respect to the matched filtering using the original received signals. As comparison criterion, we use the TOA relative estimation error, given by:

$$Error = \frac{|TOA_{estimated} - TOA_{theoretical}|}{TOA_{theoretical}} \cdot 100 \quad (3.28)$$

In order to test the compressive sensing reconstruction method robustness, in the case of our numerical example, the SNR of the received signal varies between -15 and 25 dB. For each SNR, a set of 100 noise samples is generated and each one is added to the signal. For each of these trials, the TOA estimation error is calculated.

The average of these TOA estimation errors, for both original signal and compressive sensing reconstructed signal, is computed for 8 different SNR values (Figure 3.13). As shown in Figure 3.13, the TOA estimation is improved when the signal is reconstructed, showing lower relative estimation error, even at low SNR.

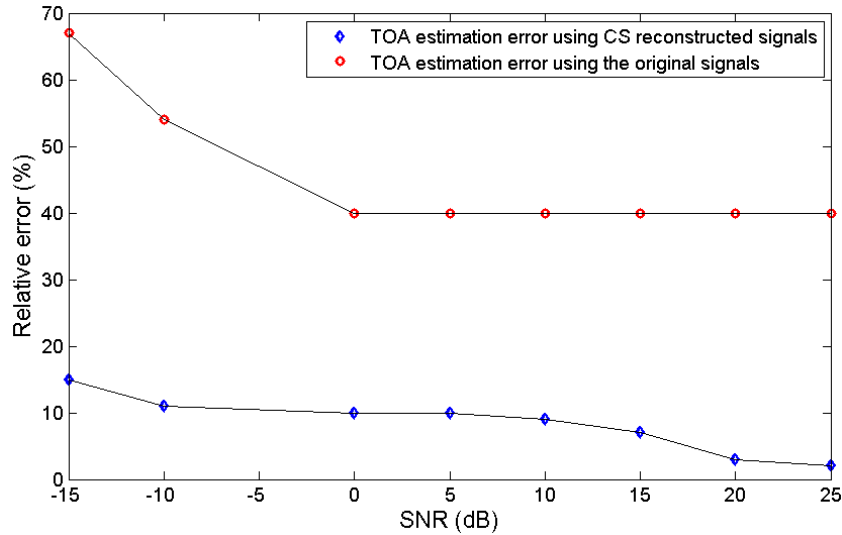


Figure 3.13. Variation of the TOA error estimation with the SNR of the received signal.

3.5 Summary

A warping based compressive sensing reconstruction method for wide band signals is presented. The general applicative context of this work is related to the cases where the waves propagating in dispersive environments are subject of interferences that produce the loss of some samples of the signals. A method to recover these samples is proposed in this chapter, based on the use of compressive sensing reconstruction applied in the warped domain. Signal's recovery lead to better results in terms of matched filtering. In this case, the estimation error is considerably reduced, as it has been proven by the presented numerical example and simulations.

Tests were also conducted in a reduced scale experimental facility, in order to prove the interest of using the signal compressive sensing recovery for the signal's time of arrival estimation and to quantify the improvement introduced by this signal processing method. The applications and the results that will be presented in Chapter 5 of the manuscript, show that the time of arrival estimation can be considerably improved after the received signal's samples recovery, with the matched filter response improvement.

Active and passive multi-sensor sensing

Contents

4.1 Active multi-sensor sensing	42
4.1.1 Introduction	42
4.1.2 Classical adaptive beamforming principle	43
4.1.3 Adaptive beamforming for flow velocity profiling	48
4.2 Passive multi-sensor sensing.....	50
4.2.1 Mathematical model	50
4.2.2 Gaussian noise input.....	52
4.2.3 Sinusoidal with additive noise input.....	53

Current ultrasonic flow meters are based on direct time of arrival estimation by matched filtering of the received and emitted signals. Narrow band signals are used, as well as a single emitter/receptor transducer configuration. Although simple, this configuration presents a series of limitations such as energy losses due to pipe wall/water interface, pressure/flow transients, sensitivity to induced vibrations and embedded turbulence. The errors associated with these limitations reduce the overall robustness of existing flow meters, as well as the measured flow rate range and lower accuracy. In order to overcome these limitations, two major innovations implemented for active sensing, at the signal processing level. The first one concerns the use of wide band signals and it has been already introduced in Chapter 3. The second innovation consists in the use of a multiple emitter – multiple receivers configuration (for one path) in order to compensate the emitted acoustic beam shift, compensate the time of flight estimation errors and thus increase the fluid flow estimation's robustness in case of undesired effects such as the “flow blow” and transient/rapid flow rate/velocity changes.

In the first part of this chapter, we will present the signal processing algorithm that take advantage of the controlled wide band content coming from multiple receivers, and that allows to achieve a higher accuracy in terms of flow velocity over a wider velocity range than the existing systems. In the second part, we propose a mathematical model for passive sensing processing, in order to perform vortex detection and 3D vortex presence visualization. Its visualization is constructed on the gyroscope principle, translating the strain gauge vertical elongations into a nutation movement.

4.1 Active multi-sensor sensing

4.1.1 Introduction

Multi-sensor sensing deals with analysis and processing of signals recorded from multiple sensors. It is widely used for detection in sonar and radar applications, and the processing methods are adapted for each particular case. In our research we take advantage of the adaptive directivity diagram of multi-sensor sensing in order to overcome the undesired effects that may appear during water pipes flow.

Generally, a sensing array is formed by a 2D transducers grid as it is displayed in Figure 4.1. The grid is composed by M transducers along the x -axis and N transducers along the y -axis. This sensing array can be seen as a linear series of M arrays with N elements each.

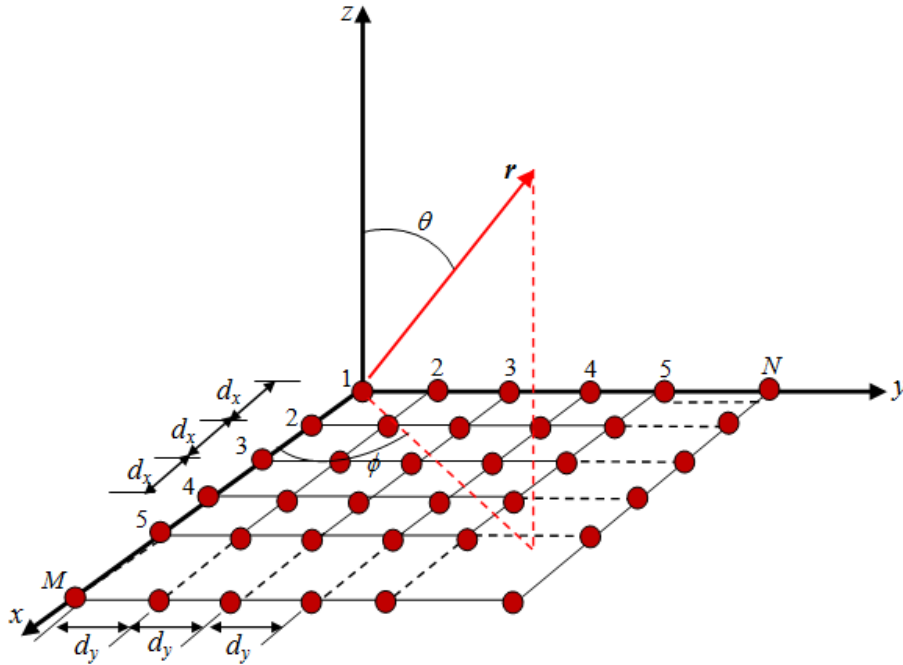


Figure 4.1. Diagram of 2D sensing array with $M \times N$ transducers. d_x and d_y are the distances between elements along x -axis, respectively along y -axis. θ is the angle of observation normal to the array and ϕ is the angle with the x -axis.

The expression of the directivity diagram is [Mai03 section 2.2.2]:

$$G(\theta, \phi) = \left[\frac{1}{M} \frac{\sin\left(M \frac{\psi_x}{2}\right)}{\sin\left(\frac{\psi_x}{2}\right)} \right] \cdot \left[\frac{1}{N} \frac{\sin\left(N \frac{\psi_y}{2}\right)}{\sin\left(\frac{\psi_y}{2}\right)} \right] \quad (4.1)$$

where

$$\begin{aligned} \psi_x &= kd_x \sin\theta \cos\phi + \beta_x \\ \psi_y &= kd_y \sin\theta \sin\phi + \beta_y \end{aligned} \quad (4.2)$$

and (β_x, β_y) are the phase shift for two successive elements of the array, in the x -direction, respectively in the y -direction. In (4.2), a coefficient named propagation constant is applied: $k = 2\pi/\lambda$, with λ the wave length. The principal and the secondary lobes of G are localized by:

$$\begin{aligned} kd_x \sin \theta_m \cos \phi_m + \beta_x &= \pm 2m\pi, m = 0,1,\dots \\ kd_y \sin \theta_n \sin \phi_n + \beta_y &= \pm 2n\pi, n = 0,1,\dots \end{aligned} \quad (4.3)$$

If we want to redirect the principal lobe towards a certain point (θ_0, ϕ_0) , the phase shifts are:

$$\begin{aligned} \beta_x &= -kd_x \sin \theta_0 \cos \phi_0 \\ \beta_y &= -kd_y \sin \theta_0 \sin \phi_0 \end{aligned} \quad (4.4)$$

For given (β_x, β_y) , the direction angles of maximum radiation are defined by:

$$\begin{aligned} \tan \phi_0 &= \frac{\beta_y d_x}{\beta_x d_y} \\ \sin \theta_0 &= \pm \sqrt{\left(\frac{\beta_x}{kd_x}\right)^2 + \left(\frac{\beta_y}{kd_y}\right)^2} \end{aligned} \quad (4.5)$$

These equations prove the interest of using multi-path sensing. Due to (β_x, β_y) phase shift adapting, it is possible to redirect the acoustic beam in order to obtain an maximum level of energy for the reception diagram, for any spatial fluctuation that may appear.

In the context of our research, the possibility to redirect the acoustic beam is presented as an adaptive solution in order to overcome the fluid flow dynamics and to improve the flow velocity profiling. Further, we will present the signal processing techniques for this multi-sensor sensing.

4.1.2 Classical adaptive beamforming principle

Before applying the adaptive beamforming principle in our context, there are two constraints that must be taken into consideration: the distance between transducers and emitted wave's characteristics.

Distance between transducers

Consider a 2×2 sensing array defined as presented in Figure 4.2, the main parameters are: the distance between the emission and the sensing array, L , the distance between two transducers, d , the radius of the emitted beam angle, R , and the acoustic beam wide angle, α .

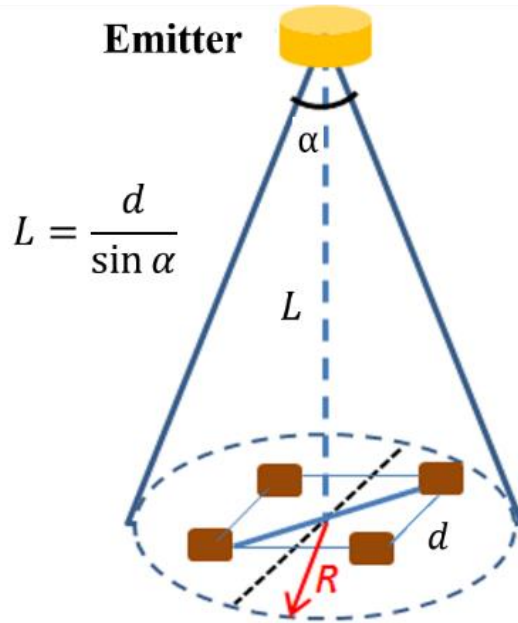


Figure 4.2. Parameters definition for a sensing array of 2×2 transducers.

Hence, there is a constraint to be imposed in order to ensure that all the receivers will “see” the emitted waveform, which is fundamental for adaptive beamforming principle: the diagonal distance between two transducers has to be equal to $d\sqrt{2}$, which means less than the emitted beam diameter, $2R$:

$$\begin{aligned}
 d\sqrt{2} < 2R &\Leftrightarrow d\sqrt{2} < 2 \cdot L \cdot \tan\left(\frac{\alpha}{2}\right) \Rightarrow \\
 \Rightarrow d < \sqrt{2} \cdot \frac{d}{\sin \alpha} \cdot \tan\left(\frac{\alpha}{2}\right) & \quad (4.6)
 \end{aligned}$$

This equation gives, in general case, the upper limit of the distance between two transducers, for which the beamforming algorithm can be applied.

Spatial sampling theorem constraint

An important result in the array sensing theory is the spatial sampling theorem which impose that the distance between transducers, d , has to be inferior to the wave length, λ . For example, in the case of a frequency $f_0 = 1$ MHz and a sound velocity in water of 1480 m/s, the wave length is 1.48 mm. If this condition is not respected, side lobes may appear and it will be impossible to estimate the angles of arrival.

For the considered 2×2 sensing array defined earlier, if the transducers are placed in direct contact with the water and without respecting this rule, we obtain the directivity diagram shown in Figure 4.3.

For a non-intrusive measurement, the directivity computation has to take into account the wave propagation in the steel-water-steel environment. The emitted acoustic wave excites first the metallic pipe’s walls and then the receiver.

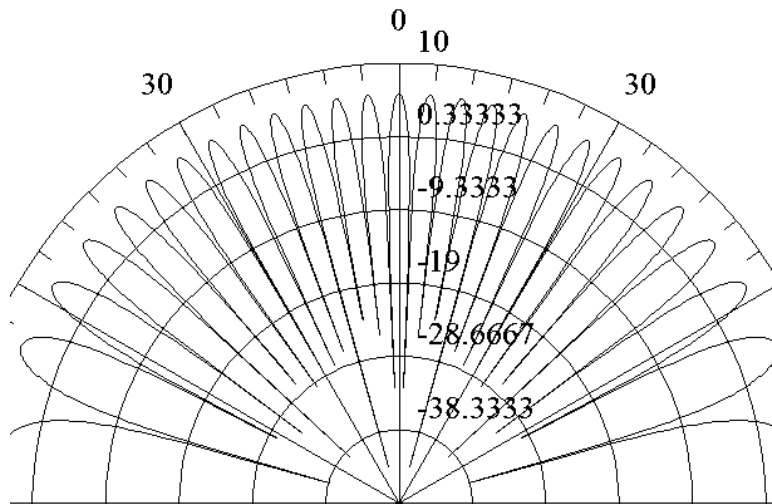


Figure 4.3. Directivity diagram for a 2×2 sensing array that doesn't satisfy the spatial sampling theorem.

We can imagine that the four transducers array is a grid composed by a four sub-arrays, each of them being defined by the pipe wall in front of which they are placed. In this situation, the main lobe has a much better angular resolution (see Figure 4.4), which justifies the use of the beamforming algorithm, presented in the next sub-section.

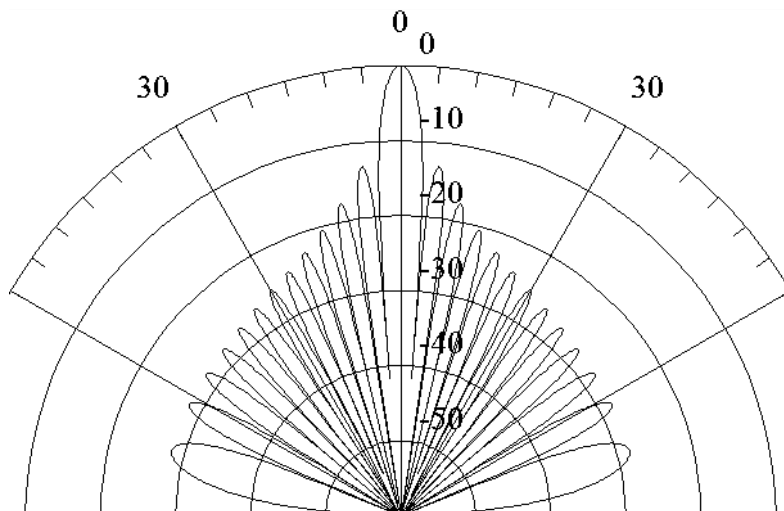


Figure 4.4. Directivity diagram for a non-intrusive 2×2 sensing array that follows the rule imposed by the spatial sampling theorem, considering the propagation first in the steel.

The adaptive beamforming technique consists in shifting the received signals of each series, and selecting the optimum set of phase shift that will maximize the power after the four signals summation. The Figure 4.5 describes the beamforming algorithm diagram in the case of multiple receiving sensors network.

Each reception is shifted with its corresponding delay, ϕ , computed with matched filtering method. The global TOA that will give the average flow velocity is obtained by matched filtering the shifted receptions sum with the emitted signal.

We can see that this method offers two possible TOAs computing. The first one is to estimate TOAs for the optimal set of phase shifts and to transmit them to the processing center. The second one is to provide a global TOA, after adaptive beamforming optimization.

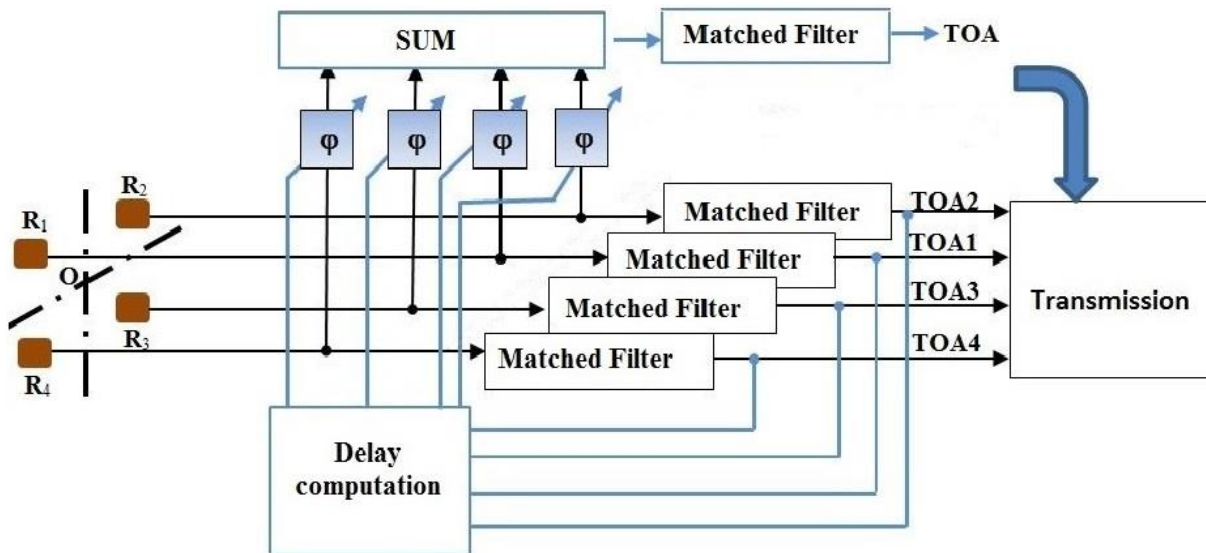


Figure 4.5. The beamforming algorithm diagram.

The flexibility offered by the adapted beamforming algorithm gives greater robustness and accuracy in hydraulic parameters estimation such as flow rate, respectively the acoustical time of flight.

We will explain in detail this process, by taking an example with intuitively illustrated signals, in Figure 4.6.

Let's consider the emitted and the received signals, for two consecutive periods of time. We show in the same time the signals in the stationary case, i.e. without flow (during period n , in red dashed line).

Given an appropriate transducers alignment at the reception level, the received signals by transducers R_1 and R_2 , respectively, R_3 and R_4 , arrive at the same instance of time. This time of arrival is estimated using the matched filter. The estimated TOAs are used for signals phase shift from period $n+1$, such as all four receptions are in phase. The individual TOAs estimated during the period $n+1$ will be used for phase control during period $n+2$, and so on.

The phase shift is established having as reference the first arrived signal from all four received ones. Here, we assume that the TOAs don't have an important variation, from one period of time to another.

The shifted signals summation will allow to have a high power signal and achieve two objectives of beamforming algorithm: ensure a correct signal level (avoid signal loss due to the dynamic nature of the environment) and precisely measure the global TOA/Doppler effect for a precise flow rate estimation.

A priori, in this case, it is assumed that the TOAs are quasi-constants from one emission to the next one: during the repetition periods of order of micro-seconds, the hydraulic parameters do not vary so to impact the wave's propagation time and shape.

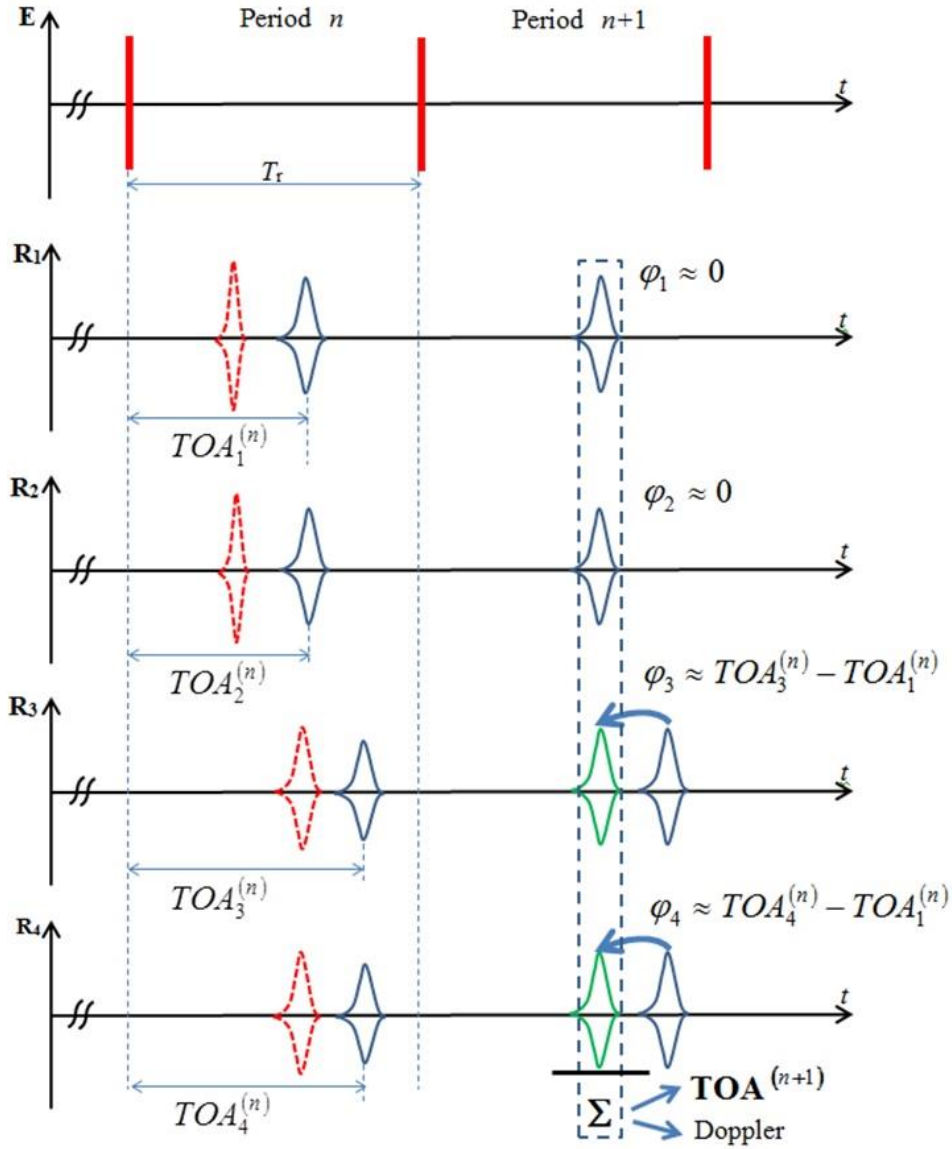


Figure 4.6. The beamforming algorithm principle.

To ensure maximum algorithm accuracy, a local optimization method is used: suppose that $x_i^{(n)}(t), i = 1, \dots, 4$ are the received signals, during the period n and Δ is the shift operator, then:

$$\Delta\{x_i^{(n)}(t)|\varphi_i^{(n)}\} = x_i^{(n)}(t - \varphi_i^{(n)}) \quad (4.7)$$

The shift operator, Δ , in the simplest case, is identified with a translation operation, for shift values named $\varphi_i^{(n)}$ (corresponding to signal i and period n). In this context, the power of coherent signal summation, for the period n , is defined by the following expression:

$$P^{(n)}(\varphi_i^{(n)}) = \left| \sum_{i=1}^4 \Delta\{x_i^{(n)}(t)|\varphi_i^{(n)}\} \right|^2 \quad (4.8)$$

which is a function of $\varphi_i^{(n)}$. The optimal time shifts set, $\{\hat{\varphi}_i^{(n)}\}$, that maximizes the relation (4.8) is defined by the following expression:

$$\hat{\varphi}_i^{(n)} = \arg \max_{\varphi_i^{(n)}} P^{(n)}(\varphi_i^{(n)}) \quad (4.9)$$

with an interval of search of phase differences defined as the neighborhood of the optimum phase shifts obtained during the period n-1:

$$\hat{\varphi}_i^{(n)} \in [\hat{\varphi}_i^{(n-1)} - \varepsilon_i, \hat{\varphi}_i^{(n-1)} + \varepsilon_i] \quad i = 1, \dots, 4 \quad (4.10)$$

where $\hat{\varphi}_i^{(n-1)}$ represents the optimal shift for the transducer i and ε_i is the interval width.

This adaptive beamforming technique is illustrated in the next chapter in the case of flow velocity profiling.

4.1.3 Adaptive beamforming for flow velocity profiling

The flow velocities encountered in most hydraulic applications may have high variations. Thus, the method presented previously solves this drawback with the use of the emitted wide band signals. In addition, the spatial distribution of the flow profiles is not obtained by adding more ultrasonic sensors but by changing the sensing properties, in terms of relative phase delays between receiving sensors, providing also *additional virtual acoustic paths* that increase the number of velocity points.

In the previous chapter, the use of wide band signals and the associated matched filtering is defined as a way to accurately estimate the TOA along one acoustic propagation path.

Measuring the velocities in multiple points requires classically the definition of the corresponding additional paths by many pairs of transmitter/receiver sensors. As alternative, we propose the use of adaptive beamforming technique presented earlier, and based on the coherent multi-transducer reception measurement principle [BBL07].

According to this principle, the use of multi-element transmitting and/or receiving elements allows to change the directions of wave propagation by modifying the phase delays between the signals transmitted/received by the elements of the sensing array.

In order to illustrate the use of this principle in our case, let us consider one acoustic path defined by one emitting element and two receivers – Figure 4.7 (this is actually the configuration that was used in our experimental setup and which will be presented in the following chapter).

The first case (Figure 4.7.a) concerns the symmetric propagation paths where the emitter transducer is located at the same ranges with respect of the receiving transducers. If the transmitted signal is $s(t)$, then the received signal corresponding to the array composed by the two receiving sensors (R1 et R2) is (ignoring the amplitude attenuations):

$$x(t) = s\left(t - \frac{D_1}{c + v_1 \cos \alpha_1}\right) \quad (4.11)$$

where α_1 is the angle between the axis D_1 and the flow direction.

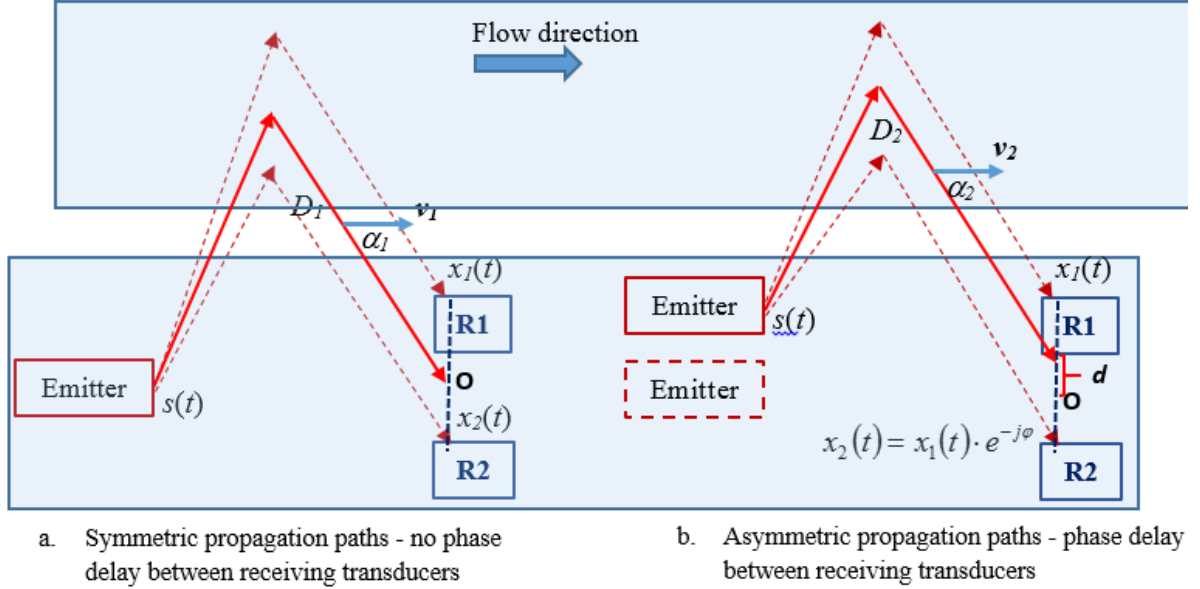


Figure 4.7. Principle of adaptive beam-forming in the case of two element receiver.

The signal $x(t)$ is obtained by combining the signals received by the both receiving sensors. If these signals are in phase, their combination corresponds to the acoustic path. This acoustic path is defined by the emitting sensor-bouncing on the opposite wall of the channel and the point \mathbf{O} that is placed at the half distance between the both sensors. Using the phase summation of the both received signals we obtain the signal x and, by matched filtering processing and considering the same diagram but in the opposite sense of the flow, we obtain the flow velocity along this acoustic path.

In the case of asymmetric propagation paths, if the received signals are delayed in phase with a controlled value, ϕ , this is equivalent to consider that the emitter has another position (Figure 4.7.b) and that the propagation paths don't have the same range. These new propagation paths are created by electronically modifying the line of sight of the both transducers by a controlled delay, which allow estimating the velocity in these new axes. This is done by processing the signals defined as:

$$x(t) = s\left(t - \frac{D_2}{c + v_2 \cos \alpha_2}\right) \quad (4.12)$$

by considering also the signals received when the transmission is in opposite sense of the flow.

This signal corresponds to an acoustic path defined by a virtual position of the emitter that corresponds to a receiving point located at a range d with respect of point \mathbf{O} .

By setting the phase delays from 0 to +/- maximum admissible value it is possible to define many propagation paths, for each one a flow velocity being estimated. The admissible value is defined as the maximum phase delay for which the two receiving transducers remain in the radiating zone of the emitter.

More accuracy may be achieved by using many elements at the emission and/or receiver. This technique is very interesting to measure the velocity profile since it does not require to physically define the acoustic paths.

4.2 Passive multi-sensor sensing

Nowadays, for hydraulic system monitoring, intrusive pressure sensors can be used in order to detect pressure fluctuations. Mathematical simulations and reduce scale test are also performed for flow prediction. Due to instabilities and turbulences, these methods cannot be generalized, despite that they may provide satisfying results [Ili07], [KT97], [HLNZ08].

Multiple sensors of different types are used in order to perform constant hydropower plant monitoring, especially in the case of the rotational components. In particular, the time evolution of the axial efforts is measured using extensometers. Having the extensometer elongations measurements at the bearing unit level, we propose a novel processing method, in order to visualize the turbine off-design behavior in terms of the generated axial efforts.

Our study is based on a mathematical model, presented in the following section. The model is applied to a real calibration dataset, for different turbine's operating conditions.

4.2.1 Mathematical model

In order to characterize the vortex cavitation presence, we perform a mathematical and statistical interpretation of passive measurements, for instance, the axial efforts. The proposed method performs a conversion of the measured elongations in a way that the axial efforts can be directly interpreted with the nutation movement [But06] of a gyroscope (see Figure 4.8). This axial effort's measurement is crucial in quantifying the instabilities levels at the current operational point of the turbine. The analogy between the extensometer measurements and the nutation movement provides a new virtual monitoring instrument of the machine instabilities. In the proposed framework we expect to obtain a minimum level of instabilities for the best efficiency point, and larger one for lower efficiency operating points.

Let consider a circle, C , in a spherical coordinates system (r, φ, θ) , to which we apply a set of three rotation matrices, R_x , R_y and R_z , for each of the three directions x, y respectively z. The rotated circle, C_r , is given by the following system of equations:

$$C_r = R_z \times R_x \times R_y \times C, \quad (4.11)$$

Here, $t \in [0, T]$, with T being the duration of one full rotation of a disk around the Oz axis and $\varphi, \theta \in [0, 2\pi]$. We define the rotation angle φ as a function of the extensometer elongations measurements, $S_{in}(t)$:

$$\varphi(t) = \text{arctg}\left(\frac{S_{in}(t)}{r}\right) \quad (4.12)$$

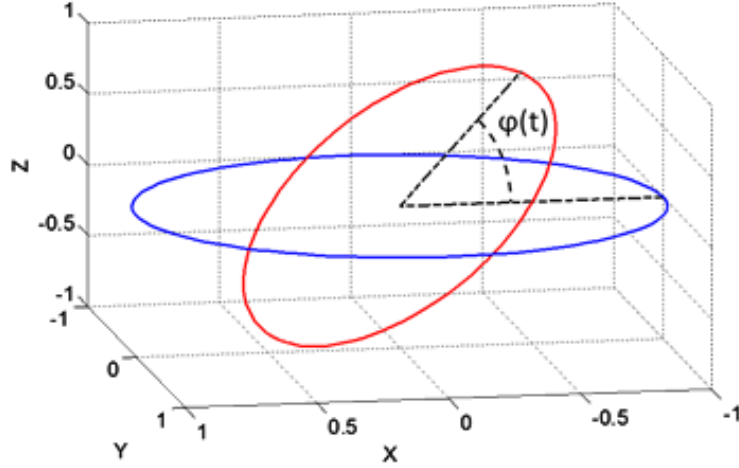


Figure 4.8. 3D rotation of a circle with angle φ , around the y -direction.

Let us consider a nonlinear operator: X . If the X operator is applied to our signal $S_{in}(t)$, the response is given by:

$$X\{S_{in}(t)\} = \frac{1}{1 + S_{in}^2(t)} \quad (4.13)$$

We rewrite the equations system (4.11) as follows:

$$\begin{aligned} C_r &= r \cdot \begin{pmatrix} \sin[\theta(t)] & \cos[\theta(t)] & -\sin[\theta(t)] \\ \cos[\theta(t)] & \sin[\theta(t)] & \cos[\theta(t)] \\ 0 & -\sin[2\varphi(t)] & \sin[\varphi(t)] \end{pmatrix} \cdot \\ &\cdot \begin{pmatrix} \cos[\alpha(t)] & 0 & -\cos[\alpha(t)] \\ 0 & \cos[\alpha(t)] & 0 \\ 0 & \sin[\alpha(t)] & 0 \end{pmatrix} \cdot \begin{pmatrix} \cos^2[\varphi(t)] \\ \cos[\varphi(t)] \\ 1 \end{pmatrix} = \\ &= r \cdot M(t) \cdot \begin{pmatrix} \cos^2[\varphi(t)] \\ \cos[\varphi(t)] \\ 1 \end{pmatrix} \stackrel{r=1}{\Leftrightarrow} M(t) \cdot \begin{pmatrix} X\{S_{in}(t)\} \\ (X\{S_{in}(t)\})^{\frac{1}{2}} \\ 1 \end{pmatrix} \end{aligned} \quad (4.14)$$

In (4.14), the unity circle is considered. Further, we study the response of different input signals, when we will apply the proposed operator X . The general input signal pattern is: a steady state component, $s(t)$ (which corresponds to a deterministic process, in this case the turbine rotation frequency) and additive noise:

$$S_{in}(t) = s(t) + \varepsilon(t)$$

Generally, the probability density function for an experimental data can be predicted, if it has a Gaussian or sinusoidal shape [Che87]. Deterministic signals have periodic amplitudes that allow harmonic decomposition related to sin waves, thus $s(t)$ will be the sine wave corresponding to the turbine rotation. The additive noise, $\varepsilon(t)$, present in the frequency bandwidth which corresponds to the cavitation vortex, is assumed to be Gaussian.

In the following sections we will analytically estimate the response of each component, sinusoid and noise, to the X operator.

4.2.2 Gaussian noise input

Let us consider the case of independent and identically distributed Gaussian noise input, $\varepsilon(t)$. The corresponding probability density function, pdf, is given by the following relation:

$$p_n(x) = \frac{1}{\sigma\sqrt{2\pi}} e^{-\frac{(x-\mu)^2}{2\sigma^2}}, \quad -\infty < x < \infty \quad (4.17)$$

We want to see how $p_n(x)$ is changed if we apply the X operator. We will perform a pdf variable change [Ven73]. Let us consider a random and continuous variable x , normally distributed, with the pdf given by (4.17). The variable change that we propose is:

$$x \rightarrow \frac{1}{1+x^2} \quad (4.18)$$

Hence, consider the function $X_n(x) = \frac{1}{1+x^2}$, which is strictly increasing on the interval $(-\infty, 0]$ and strictly decreasing on the interval $[0, \infty)$. On both intervals, X_n is continuous and differentiable. The equation $X_n(x) = y$ has the following two solutions:

$$x_1 = \sqrt{\frac{1-y}{y}} \quad \text{and} \quad x_2 = -\sqrt{\frac{1-y}{y}}.$$

Thus, we have:

$$\begin{aligned} p_n(y) &= \frac{p_n(x_1)}{|X'_n(x_1)|} + \frac{p_n(x_2)}{|X'_n(x_2)|} = \\ &= \frac{1}{\sigma y \sqrt{2\pi y(1-y)}} \cdot \left[e^{-\frac{(\sqrt{\frac{1-y}{y}}-\mu)^2}{2\sigma^2}} + e^{-\frac{(-\sqrt{\frac{1-y}{y}}-\mu)^2}{2\sigma^2}} \right] \quad (4.19) \end{aligned}$$

for $y \in (0,1)$. An example of the estimated and calculated X transform of a Gaussian noise pdf is displayed in Figure 4.9.

According to (4.19), the pdf domain of definition is restrained to the interval $(0, 1)$.

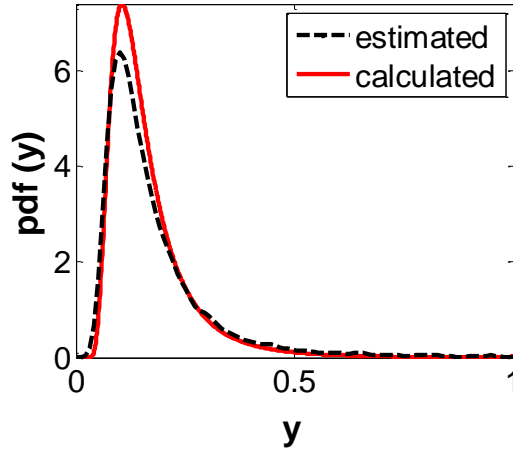


Figure 4.9. Probability density function of the X transform of a Gaussian noise $\sim N(2.5, 0.5)$ has the mean=0.15 and the variance=0.01 if it is computed using (7), and it has the mean=0.17 and the variance=0.3 if it is numerical estimated.

4.2.3 Sinusoidal with additive noise input

In this section, we will perform the pdf analysis of the X transform of a sinusoidal wave with Gaussian noise. Consider a sinusoidal wave of the form: $s(t) = A \cdot \sin(2\pi ft + \theta)$. Firstly, we compute the joint pdf of one sinusoid and an additive noise, supposed to be Gaussian noise. It is given by the convolution of their corresponding pdfs [Che87]:

$$\begin{aligned}
 p_{S_{in}}(x) &= \int_{-\infty}^{\infty} p_s(x - \tau) * p_n(\tau) d\tau \\
 &= \frac{1}{\sigma\pi\sqrt{2\pi}} \int_0^{\pi} e^{-\left(\frac{x - A\cos(\theta)}{4\sigma}\right)^2} d\theta
 \end{aligned} \tag{4.20}$$

where σ is the noise's standard deviation. A and θ are the sinusoidal wave's amplitude and phase.

If we develop, in Taylor- MacLaurin series, the exponential term from (4.20), then $p_{S_{in}}(x)$ can be rewritten as follows [Appendix A]:

$$p_{S_{in}}(x) = \frac{\alpha}{\sigma\sqrt{2\pi}} e^{-\left(\frac{x}{4\sigma}\right)^2} \tag{4.21}$$

where $\alpha = \alpha(A, \sigma, N)$ is a constant depending on the sinusoid amplitude, noise standard deviation and the number of series terms, N . For calculus simplicity, we suppose N is an odd number.

Secondly, we perform for $p_{S_{in}}(x)$ the same variable change as in the previous section, and we will get the pdf of $X(S_{in})$:

$$p_{X(S_{in})}(y) = \frac{\alpha}{\sigma\sqrt{2\pi y^3(1-y)}} \cdot e^{\frac{y-1}{(4\sigma)^2 y}} \quad (4.22)$$

The k-th order moments of $p_{X(S_{in})}(y)$, $n \geq 1$, are given by the following relation [Ven73]:

$$m_k = \int_{-\infty}^{\infty} y^k \cdot p_{X(S_{in})}(y) \quad (4.23)$$

As mentioned in previously, $y \in (0,1)$. We perform the variable change $\frac{1-y}{y} = t$ and we obtain:

$$m_k = \frac{\alpha}{\sigma\sqrt{2\pi}} \int_0^{\infty} \frac{1}{\sqrt{t}} \cdot \frac{1}{(1+t)^k} \cdot e^{-at} dt \quad (4.23)$$

with $a = \frac{1}{(4\sigma)^2}$. If we compute the integral from (4.23), for the first moment [Abr64], we get:

$$m_1 = \pi \cdot \frac{\alpha}{\sigma\sqrt{2\pi}} \cdot e^a \cdot \operatorname{erfc}(\sqrt{a}) \quad (4.24)$$

As (4.24) proves, the pdf's moments are functions of sinusoid amplitude and noise standard deviation. The sinusoid describes a deterministic process, hence A is known, and σ can be estimated.

In order to test the robustness of our proposed transform, we perform an SNR level test. The moments of first and second order are calculated for a SNR range between -30 and 10 dB. Their variation is displayed in Figure 4.10.

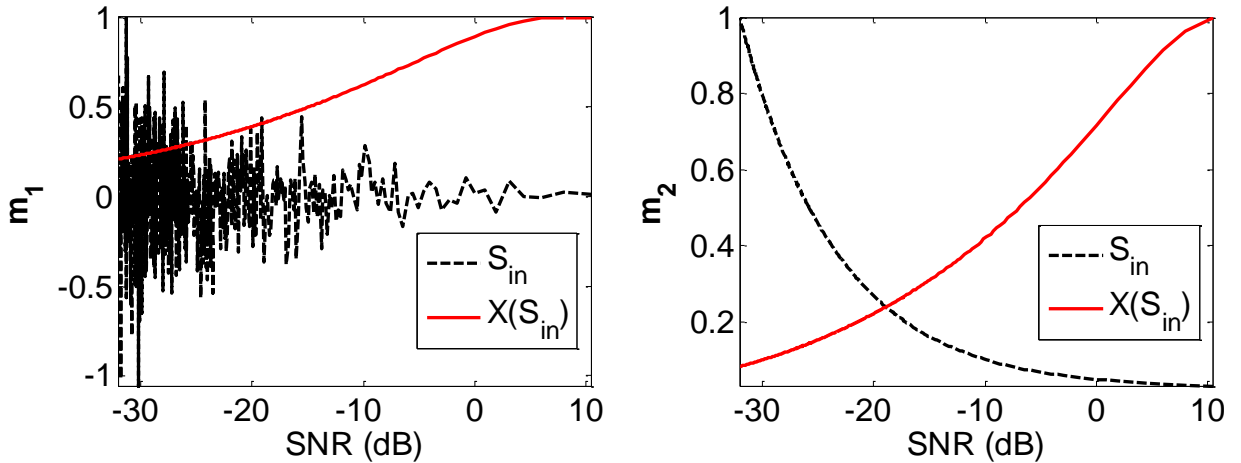


Figure 4.10. SNR level test.

4.3 Summary

The multi-sensor sensing is an innovative technique that can be used for rapid transient flow monitoring. This contribution is based on a theoretical signal processing principle named adaptive beamforming, in the context of non-intrusive multi-sensors sensing of the flow velocity.

The adaptive beamforming brings spatial resolution improvement and it allows the use of a finite number of sensors with different sensing directions, in order to achieve better performances in both dynamic(transient) flow sensing and velocity profile estimation.

Results in applicative contexts

Contents

5.1	Transducers position offset compensation	58
5.1.1	Experimental set-up	59
5.1.2	Results	60
5.1.3	Conclusion	61
5.2	Asymmetric velocity profile construction	61
5.2.1	Experimental set-up	61
5.2.2	Results	64
5.2.3	Conclusion	65
5.3	Acoustic flow metering.....	65
5.3.1	Experimental set-up	65
5.3.2	Results	66
5.4	Cavitation vortex detection	70
5.4.1	Experimental set-up	70
5.4.2	Results	71
5.4.3	Conclusion	74

In this chapter we present four applications in order to prove the interest of the proposed theoretical approaches described in previous chapters. The first application concerns the use of the compressive sensing reconstruction algorithm for transducers position offset compensation. In the second application we show how the adaptive beamforming technique can be used to estimate the asymmetric velocity profile of an open channel-flow with the use of a minimal number of transducers (much fewer than the velocity profile points). The third application presented in this chapter shows the acoustic flowmeter's improvements that we propose, for water pipes with excessively high flow rates. The last application uses a new method for vortex rope detection in the case of hydraulic turbines.

5.1 Transducers position offset compensation

As we have discussed in the second chapter, the acoustic transducers position offset impacts the propagation quality between the emitter and the receiver: the wave's shape and frequency content can be corrupted in the case of misaligned sensors. In this section we consider the practical case of a transmitter (E) and receiver (R1) configuration presented in Figure 5.1.

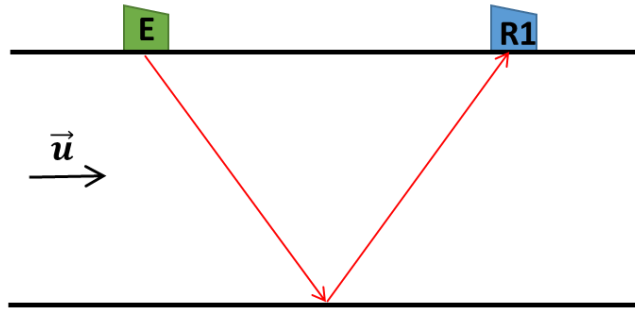


Figure 6.1. Example of an acoustic emitter-receiver configuration.

When the pipe flow induces vibrations and if the sensors are not perfectly fixed, the transducers may be misaligned. In this case, the acoustic reflected wave may be deformed at the receiver R1 position. We say that the receiver R1 is misaligned with respect to the reflected wave's path (see Figure 5.2).

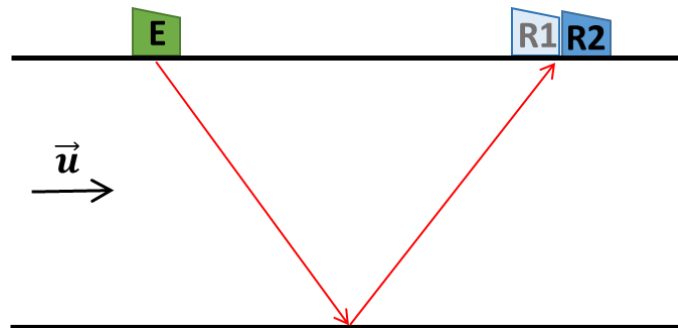


Figure 6.2. Misaligned transducers. R1 is the misaligned receiver that is supposed to record the reflected acoustic wave, while the receiver R2 is positioned where the acoustic wave is actually reflected.

The transducers misalignment conducts to the attenuation and deviation of the received signal affecting the final application results. Consequently, it is important to maintain the signal's informational content between emission and reception, in order to preserve an optimal signal processing performing. Hence, the effects of transducers position offset need to be compensated to avoid dramatically errors of the data processing results. We propose to performe a information recovery of the received signal using the compressive sensing reconstruction.

5.1.1 Experimental set-up

In order to demonstrate the results of the warped CS-based reconstruction algorithm, we have performed an experimental test in which we reproduce, at reduce scale, the phenomenon previously described. A chirp with a frequency variation between 0.5 MHz and 1.1 MHz is emitted and the reflected signal is recorded by the receivers R1 and R2, with a sampling frequency of 50 MHz.

Figure 5.3 illustrates the emitted signal in this contex. In the ideal case when the emitting and the receiving sensors are perfectly aligned, the received signal is just delayed and attenuated. Where the alignment is not well done, the received signal has informational missing content.

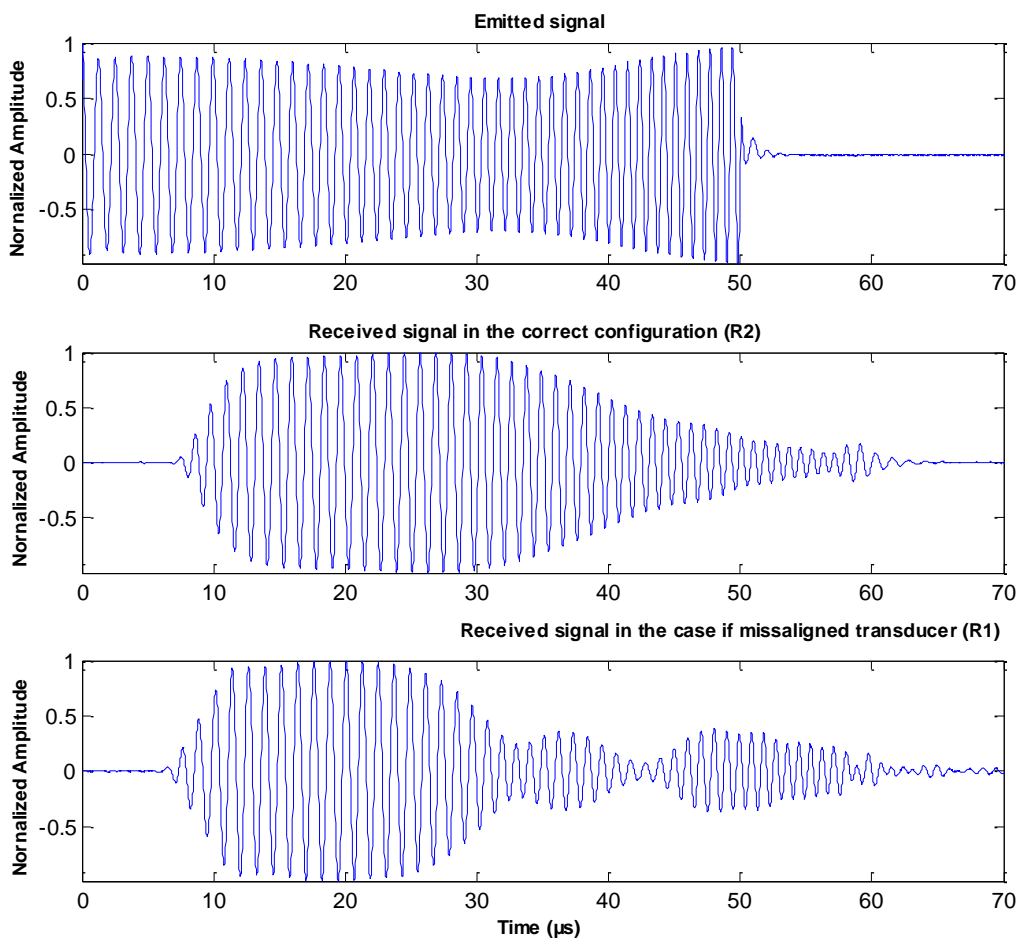


Figure 6.3. Emitted and received waveforms for the optimal alignment and misaligned case, respectively.

The need to reconstruct the received signal is given by the fact that the TOA estimation is considerably affected by the transmitted information between the emission and reception. The TOA estimation is generally performed using matched filtering. The strong deformation of the reflected signal (as is the presented case in Figure 5.4) will conduct to an innacurate TOA estimation.

The matched filter response provides two points of local maximum, none of them being the one which will provide the signal TOA.

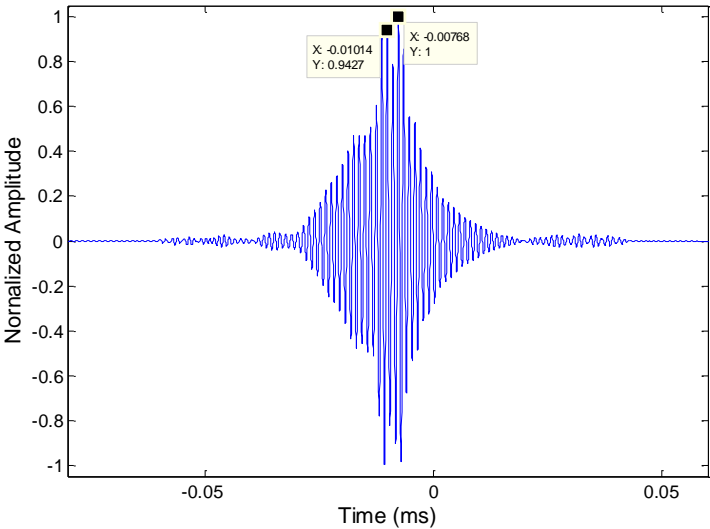


Figure 6.4. The result of the matched filter applied in the case of misaligned transducers.

5.1.2 Results

The purpose of the signal reconstruction was to recover the informational content. Now, if we compare the spectral content on the initial received signal with the recovered one, we can see an important spectra reconstruction (Figure 5.5).

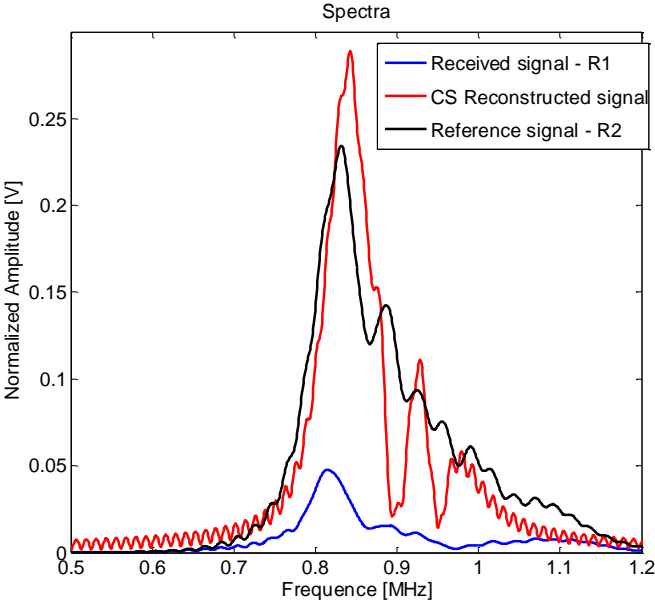


Figure 6.5. The spectrums of the: reference received signal in the proper configuration, E-R2, (in black line); received signal in the case of misaligned transducers, E-R1 (in blue line); the recovered signal (in red line).

This spectral recovery, achieved by the warping based CS reconstruction algorithm, improves considerably the TOA based matched filter estimation since only one local maximum point is detected, at the right position (Figure 5.6).

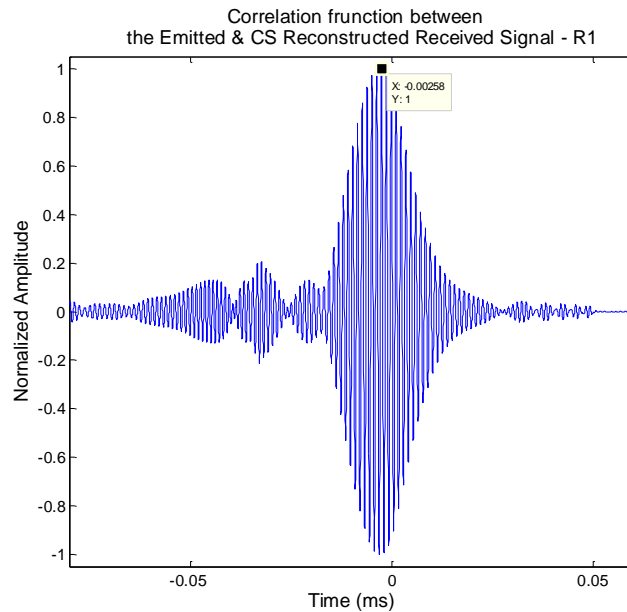


Figure 6.6. The matched filter response for the recovered signal.

5.1.3 Conclusion

The general applicative context of this application is related to the cases where the waves propagating in dispersive environments are subject of interferences that produce the loss of some samples of the signals. The proposed method for samples recovery was tested in this section, based on the use of compressive sensing reconstruction applied in the warped domain. Signal's recovery lead to better results in terms of matched filtering [MDCI16].

The perspectives are to extend the present work to different emitted frequency modulation waveforms. We look also to apply this study in the case of multi-transducer configurations in order to allow their application in other fields of research.

5.2 Asymmetric velocity profile construction

5.2.1 Experimental set-up

The aim of this application is to estimate an open-channel flow velocity profile, using acoustic time of flight flow metering based on matched filtering and adaptive beamforming.

The facility test, located at the National R&D Institute in Electrical Engineering from Bucharest - Romania, is a closed loop where the water is circulated through a rectangular

plexiglas channel (see Figure 5.7). We estimate different velocity profiles: symmetric and asymmetric profiles, for multiple flow mean velocities values which do not exceed 1.1 m/s. The obtained results are validated by velocity measurements using a Pitot tube installed downstream the acoustic system.

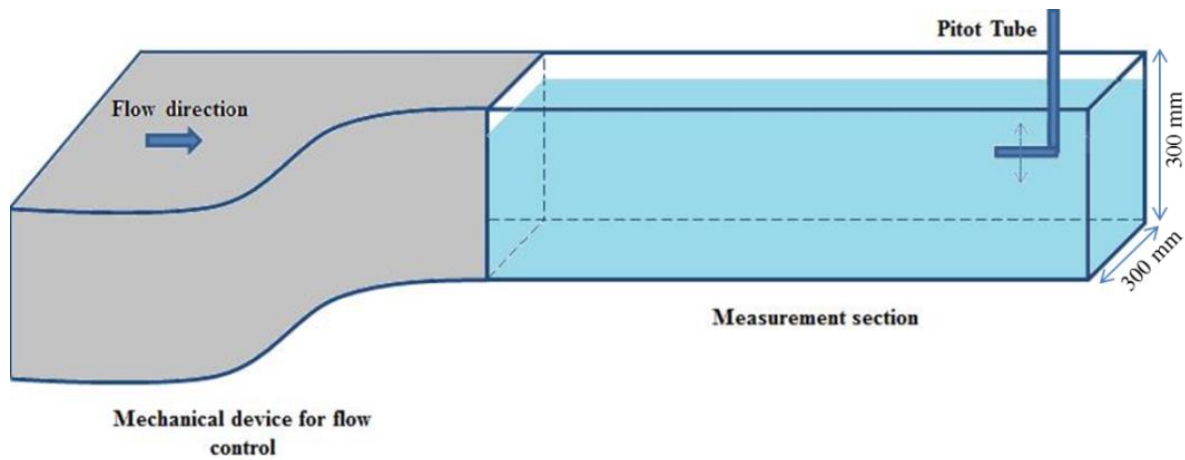


Figure 6.7. Experimental facility used for velocity profile estimation.

For all acoustical measurements, 45 degrees acryl wedge transducers of 1 MHz frequency band have been used. The generated waveforms are 800 - 1200 kHz linear frequency modulations and they are recorded with a sampling frequency of 200 MHz. Thus, the temporal resolution of 5 ns ensures the estimation of flow velocities down to 0.2 m/s.

Each pair emitter-receiver is placed in “V” configuration which means that both the emitter and the receiver are clamped-on the same channel side. For simplicity, the acoustic measuring system is adapted to each velocity profile.

In the case of a fully developed flow with a velocity range between 0.2 and 1.1 m/s and symmetric velocity profile, an acoustic flow metering configuration composed by two emitters and two receivers is proposed. Accordingly, two “V” paths are used for the symmetric velocity profile estimation (see figure 5.8), which means that there are two flow velocity values available. More values, required to complete the flow velocity profile, will be obtained by phase shifting these two received signals.

In order to create a flow with an asymmetric velocity profile, the open-channel inlet was restrained with about 60% from its complete opening. In these conditions, the flow velocity is increased at the channel bottom and the difference in flow velocity between all the flow layers demand a new acoustic flow metering configuration. The new configuration allows an accurate estimation of the velocity variation in the flow domain section of interest. Two “V” paths (see Figure 5.9) between one emitter and two receivers are created. The third one is established between the two emissions: because the waves in the flow direction and in the opposite direction are generated alternatively, the non-active emitter can record also the wave emitted by the active one. Thus, these transducers configuration allows the flow velocity measurement in three points of the flow domain transversal section. Using the same principle as for the symmetric velocity profile estimation, also in this case, the complete velocity profile can be constructed without changing the transducers position.

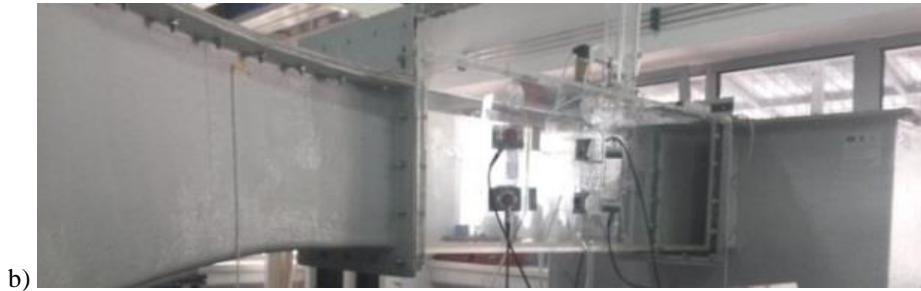
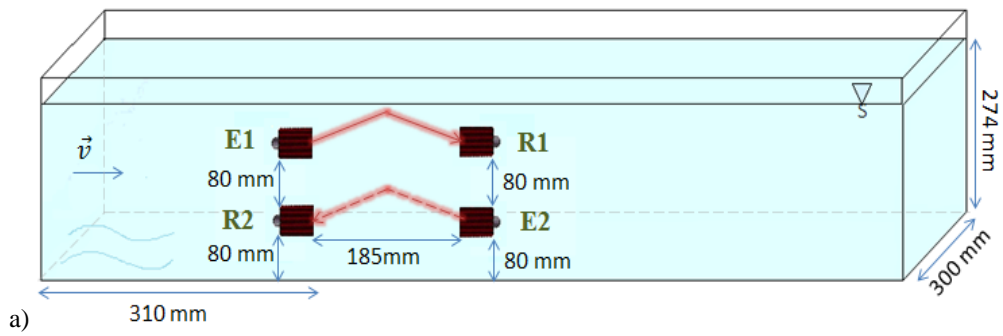


Figure 6.8. Experimental configuration for the symmetric velocity profile estimation: a) the two “V” paths [E1-R1] and [E2-R2] correspond to emitted signal in the flow direction (the red continuous line), respectively in the opposite direction (the red dotted line); b) The transducers clamp-on open-channel side.

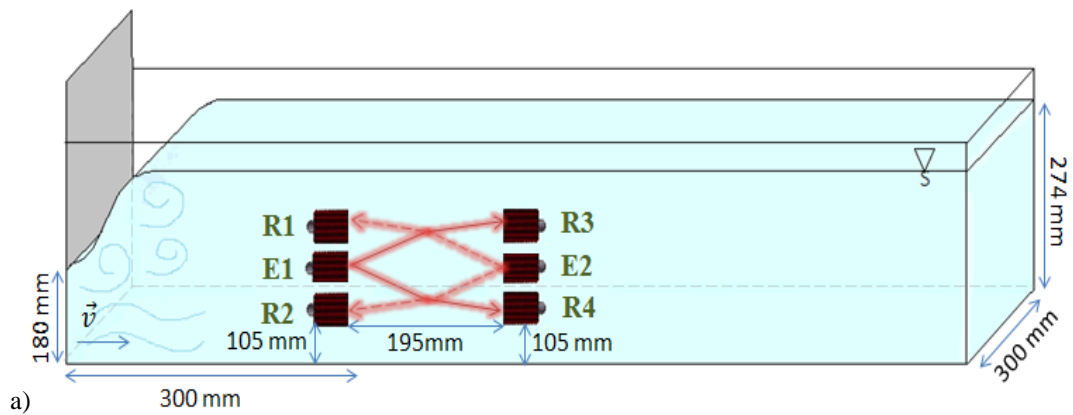


Figure 6.9. Experimental configuration for the asymmetric velocity profile estimation: a) each three sets of “V” paths [E1-R3, E1-E2, E1-R4] and [E2-R1, E2-E1, E2-R2] correspond to emitted signal in the flow direction (the red continuous line), respectively in the opposite direction (the red dotted line); b) The transducers clamp-on open-channel side.

5.2.2 Results

One example of results is presented the two following figures, for the flow velocity profile estimation when the flow rate is equal to $0.0276 \text{ m}^3/\text{s}$, i.e. the instantaneous flow velocity in the case of the symmetric velocity profile estimation lies between 0.29 m/s and 0.30 m/s (see Figure 5.10) and in the case of the asymmetric velocity profile between 0.16 m/s and 0.68 m/s (see Figure 5.11). Table 1 contains the measured flow velocities using the Pitot tube installed on the experimental facility and the estimated flow velocities using the acoustic method developed in section 4.1.2.

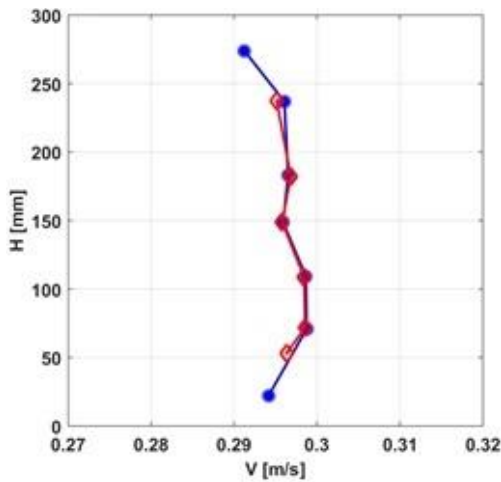


Figure 6.10. Symmetric flow velocity profile measured with Pitot tube (the blue curve) and estimated with acoustic time of flight meter (the red curve)

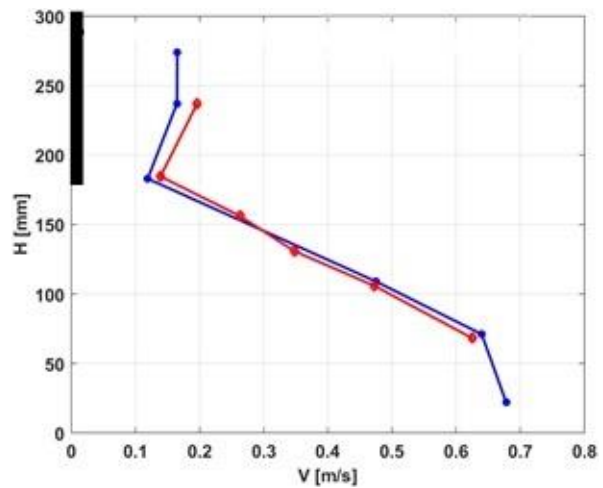


Figure 6.11 Asymmetric flow velocity profile measured with Pitot tube (the blue curve) and estimated with acoustic time of flight meter (the red curve)

The number of points used to construct the velocity profile is chosen by the user taking into account the measurement purpose and conditions.

Table 1. Flow velocity values measured with the Pitot tube and estimated with the acoustic time of flight flow meter for the symmetric and asymmetric flow profiling

H (mm)	Symmetric velocity profile		Asymmetric velocity profile	
	V _{measured} (m/s)	V _{estimated} (m/s)	V _{measured} (m/s)	V _{estimated} (m/s)
22	0.2941	-	0.6779	-
52	-	0.2964	-	-
71	0.2987	0.2986	0.6398	0.625
109	0.2986	0.2984	0.4746	0.4723
128	-	-	-	0.3482
149	0.2959	0.2958	-	0.2631
183	0.2965	0.2968	0.2190	0.1389
237	0.2960	0.2952	0.1646	0.1959
277	0.2912	-	0.1650	-

5.2.3 Conclusion

The adaptive beamforming technic implementation allows to define arbitrary direction of emission/reception. The main difficulties are related to the geometric constraints for the multi-transducers configuration installation. We have shown that the adaptive beamforming algorithm applied to wide band signals provides a robust estimation of flow velocity despite different flow regimes and transducers mechanical misalignments [MCBD16].

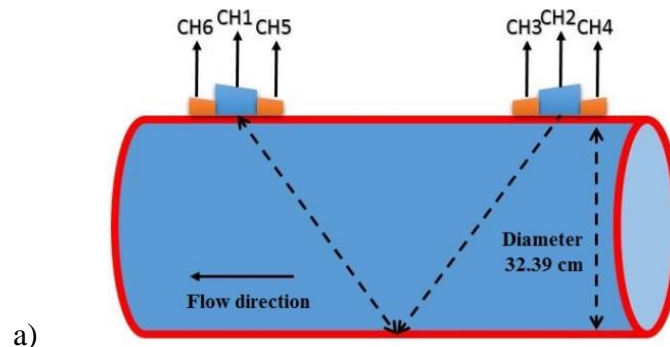
In the further works, we will closely investigate the propagation effects between the sensors and the inside parts of the pipe. Namely, it is obvious that the propagation in the solid part of the pipes deforms the transmitting signals but estimating carefully this deformation could be useful to improve the both matched filtering and adaptive beam-forming performances. Also, it will help us defining the ultrasonic wide-band phase interferometry that will lead to the design of agile and high resolution ultrasonic sensing systems.

5.3 Acoustic flow metering

5.3.1 Experimental set-up

The results presented in this section concern the flow velocity measurement through an experimental facility of Centre d'Etudes et de Recherche de Grenoble (see Figure 5.12), which is able to reproduce ultrasonic flowmeter tests on low diameter pipe with large variation of flow rates (between 0 and 11.5 m/s). The experimental test were conducted by the Direction Technique Générale. The objectives of these tests are: the flow blow effect study under high flow velocity conditions and matched filtering and adaptive beamforming technics performance estimation in the case of wide flow velocity range.

The measurement configuration implementation is composed by two emitter transducers and two receiver transducers, all of them are 1MHz transducers with an emission angle of 45°. The 'V' transducers displacement is illustrated in Figure 5.12.a. The signals were transmitted to transducers by a dual channel generator and acquired with three oscilloscopes (see Figure 5.12.b). The received signals are amplified with a variable gain preamplifier between 12dB and 24dB.





b)

Figure 6.12. a) The transducers displacement in ‘V’ configuration and b) the equipment used for the experimental tests.

For this experimental configuration, the emitted signals parameters are: linear frequency modulation in opposite directions (see Figure 5.13), frequency modulation period of $40\mu\text{s}$, signal period repetition of 2ms , frequency band between $800\text{kHz} - 1200\text{kHz}$, 5V signal amplitude and the sampling frequency of 100MHz .

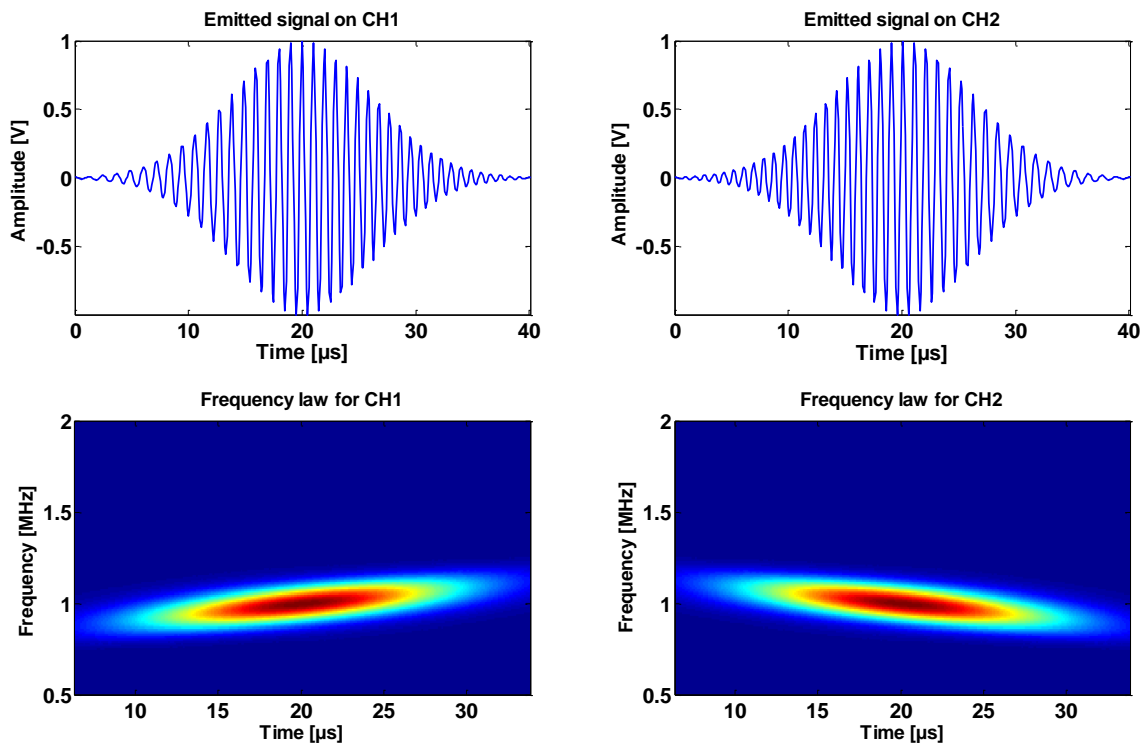


Figure 6.13. The emitted signals on CH1 and CH2 with their corresponding time-frequency contents.

5.3.2 Results

In order to illustrate the important contribution of the adapted beamforming algorithm, in Figure 5.14, the signal processing results for two different flow velocities are presented: 5 and 10 m/s . One can see that the matched filters results have different amplitudes, as well as the physical pulses without interest for the present study, but with great chances to skew the time of flight calculations.

With the help of the adaptive beamforming algorithm, higher amplitude of the processing system responses is observed, while the artifact pulses are considerably reduced.

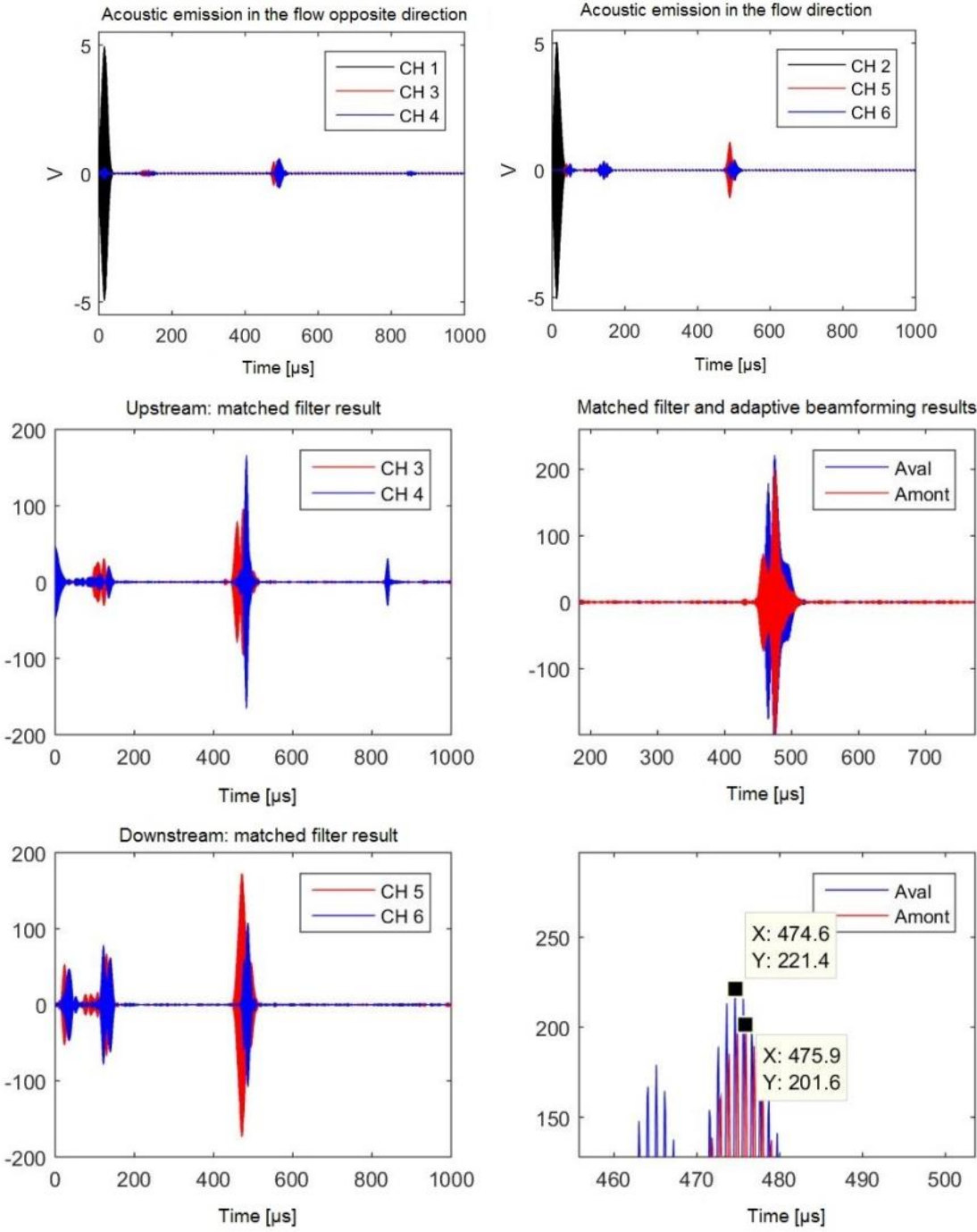
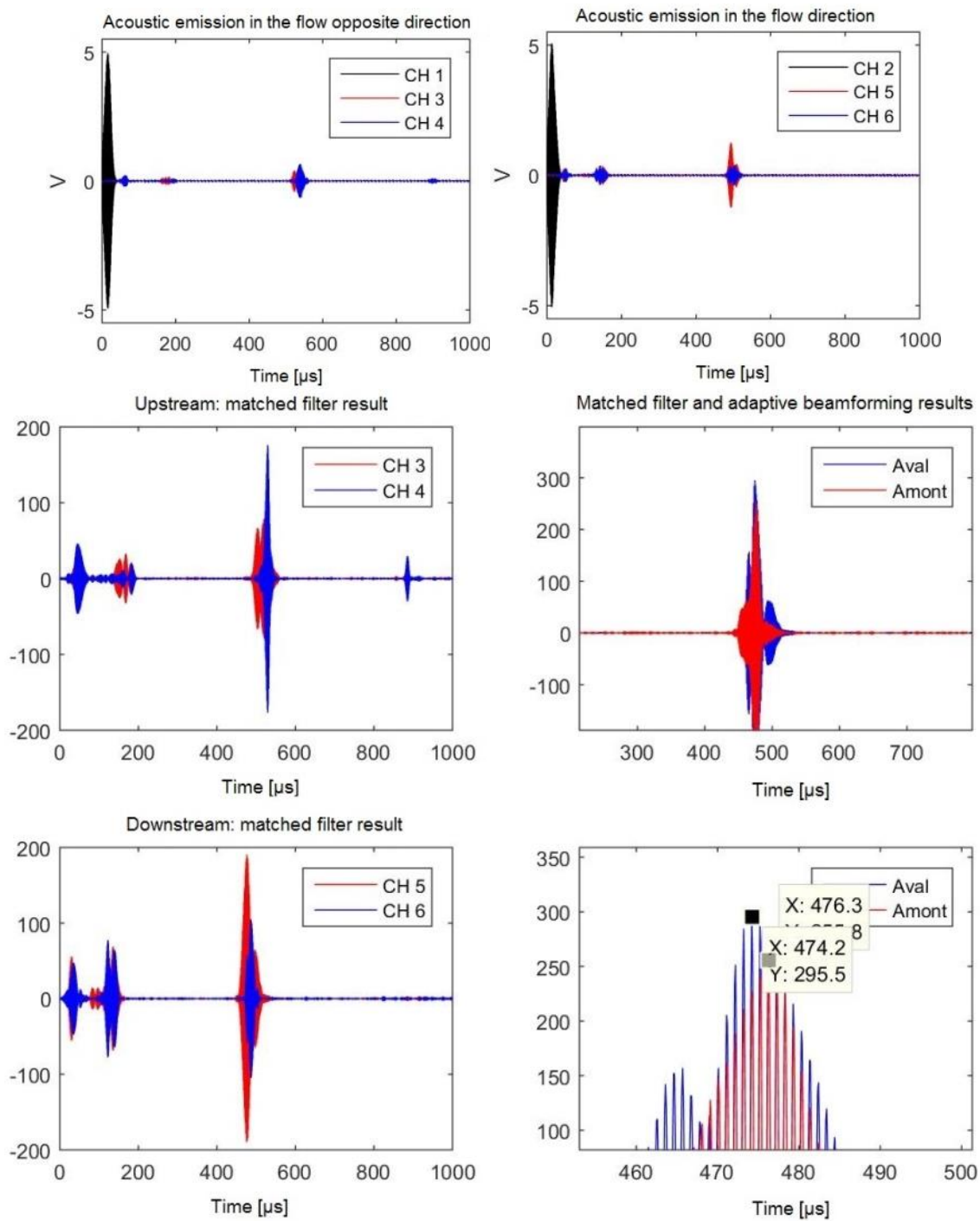


Figure 6.14.a. Signal processing results, for one emission period, at 5 m/s.



b. Signal processing results, for one emission period, at 10 m/s

Figure 5.14. Illustration of results for one emission/reception period and two different velocities

These clear advantages result in better flow rate performance estimation, shown in Figure 5.15, for the entire flow velocity range: from 1 m/s to 12 m/s.

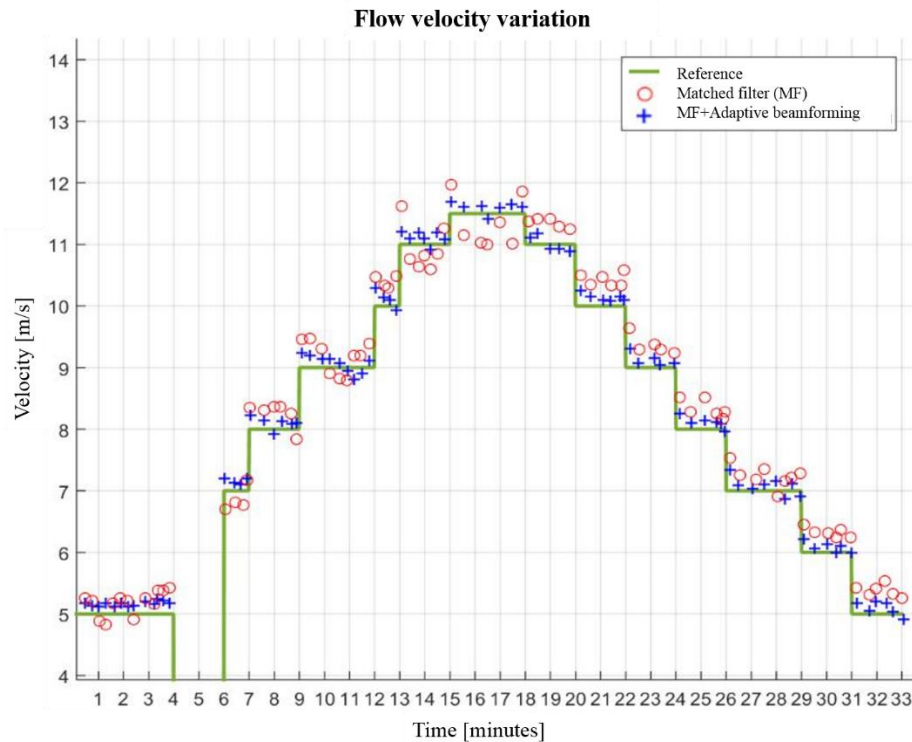


Figure 6.15. The estimation of flow velocity average using matched filtering and matched filter with adapted beamforming techniques

Another way to visualize these results is to look at the global errors (see Figure 5.16) for each flow velocity value and each algorithmic configuration: matched filter (MF) and matched filter with adaptive beamforming, and for the original recorded signals during few minutes (i.e. approximately 200 000 signals).

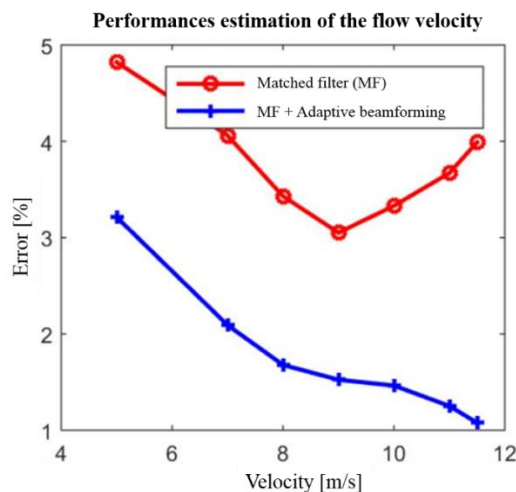


Figure 6.16. The error variation for flow velocity estimation using the matched filter and the matched filter with adaptive beamforming

Concerning the results obtained with the matched filter, one can see that the flow velocity error estimation diminishes for low values, between 3 and 9 m/s. This observation is also true for the matched filter with adaptive beamforming results, and this can be explained

by the better estimation of the time of flight difference for higher flow velocities values rather than for the small ones.

When the flow velocity is over 9 m/s, the results obtained with matched filtering have higher errors. Contrary, in the case of the matched filter with adaptive beamforming, the errors are even lower, meaning that the flow velocity is more precisely estimated. This result shows the motivation for the matched filter with adaptive beamforming method use in order to eliminate the flow blow phenomenon's effects.

5.4 Cavitation vortex detection

Hydraulic machinery monitoring using non-intrusive sensors is today's trend in the hydroelectric power industry. The phenomena of cavitation vortex occurs mostly at off-design regimes, which reduces the turbine's efficiency. In this section we propose a mathematical model for vortex detection and a 3D vortex presence visualization. Its visualization is constructed on the gyroscope principle, translating the strain gauge vertical elongations into a nutation movement. The mathematical model for vortex detection computes the data statistical moments. The model is tested on experimental data recorded using an extensometer. In this section, we will show how this mathematical model is applied on experimental data.

5.4.1 Experimental set-up

Data acquisition and the experimental setup were performed by "Électricité de France" (EDF). For the experiment, SCAIME Epsimetal extensometer sensors with a resolution better than $1\mu\text{m/m}$ is used [RVL15] are placed on the alternator bearing conical support at 150mm distance from its outer edge and at 300mm distance from the alternator bearing of a Francis turbine (see Figure 5.17).

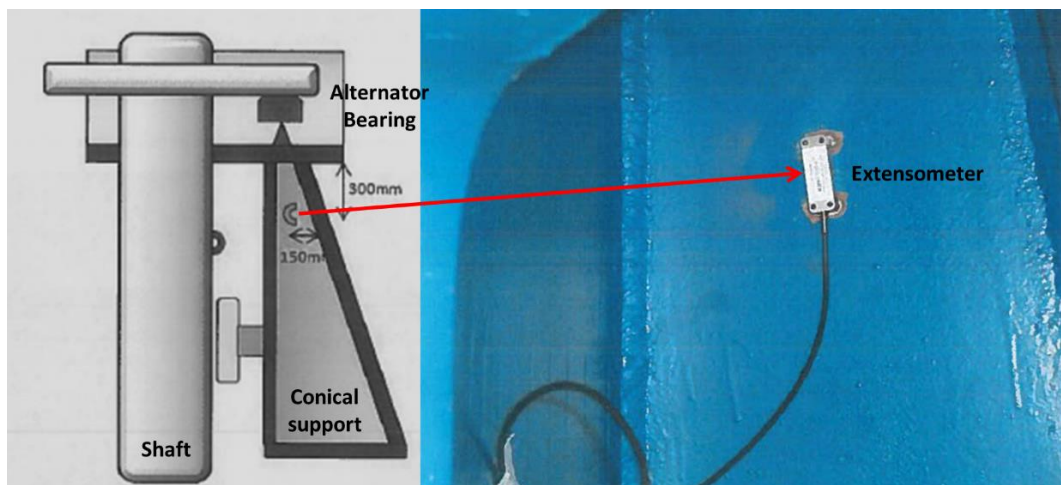


Figure 6.17. The extensometer placement on the alternator bearing.

Using 18 different operating conditions (different water flow rates, between 80 and 350 l/s), elongations variations were recorded with a sampling rate of 5120 Hz. The extensometer measurements are related to the turbine mechanical behavior. The link with the hydraulic phenomenon is made by the presence of low frequencies, under 1Hz, in the spectral analysis of the recorded data.

5.4.2 Results

The theoretical framework presented in section 4.2, will be used now to detect and visualize the cavitation vortex presence (Figure 5.18). The input signal, $S_{in}(t)$, is composed by the sum of one sinusoids, corresponding to the turbine rotation frequency and the noise in the corresponding vortex frequency bandwidth: between 0.5 and 1 Hz.

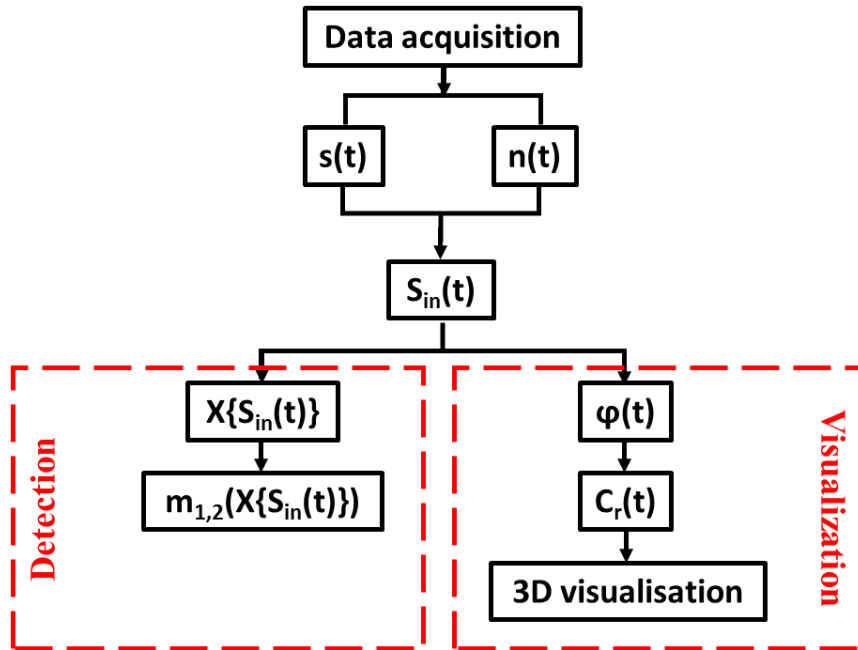


Figure 6.18. Measured data processing method.

The vortex detection is performed by computing the first and second order statistical moments of S_{in} and $X\{S_{in}\}$, for several working regimes. In order to apply (4.24), the sinusoid parameters are constants, no matter the turbine's working regime, and σ is the reference noise standard deviation (the σ of recorded noise for the optimal working conditions of the turbine).

Figure 5.19 shows moments variation of S_{in} and $X\{S_{in}\}$, for all flow rates. The effect of using the proposed transform X , defined by (4.13), is that the statistical moments m_1 and m_2 of $X\{S_{in}\}$ are correlated and they vary according to the cavitation vortex appearance.

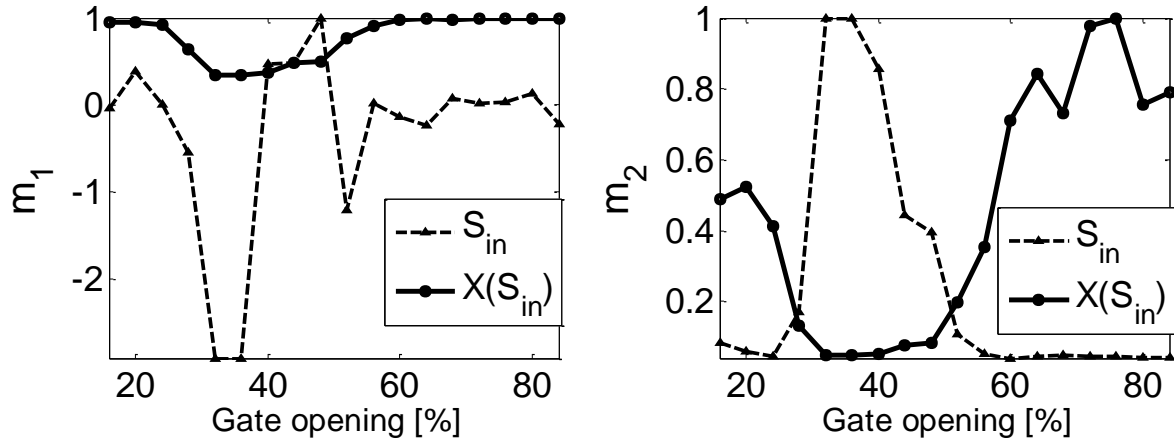


Figure 6.19 Statistical moments variation as a function of the gate opening.

One can notice a vortex detection event by the drop of the second order moment, m_2 , for a gate opening between 25-50%. The vortex presence, hence appearance of its corresponding frequency, is marked by a lower data's variance. The first order moment do not provide enough information, especially that of S_{in} .

Using (4.13), the recorded vertical elongations during turbine exploitation, are transposed to angular rotation of a circle with 3 degree of freedom: rotation around x , y and z directions. In order to obtain a 3D rotation of the circle, at every instance of time, a product of the three rotation matrices following (4.11) and (4.12), for each direction, is applied to an unitary circle in initial position: $r = 1$ and $t \in [0, 2\pi]$. The rotation period is equal to the vortex rotation period. Eq. (4.14) gives the spherical coordinates of the rotated circle, at each time instant t .

The presence of the cavitation vortex is represented in Figure 5.20, for all the operational points available. Any variation from the circle position of reference in 3D coordinates, indicated the presence of this undesired phenomenon. To better understand the correlation with each turbine's operational point, we have represented also the turbine's hill chart.

In Figure 5.21 we can visualize the presence of the cavitation vortex correlated with each operational point. Three main operating points are considered: part load (PL), the best efficiency point (BEP) and high load (HL). For PL, more than for HL, the vortex appearance is marked by the presence of low frequencies on signal's spectrum, and by the deviation from the 3D circle reference position given by the BEP.

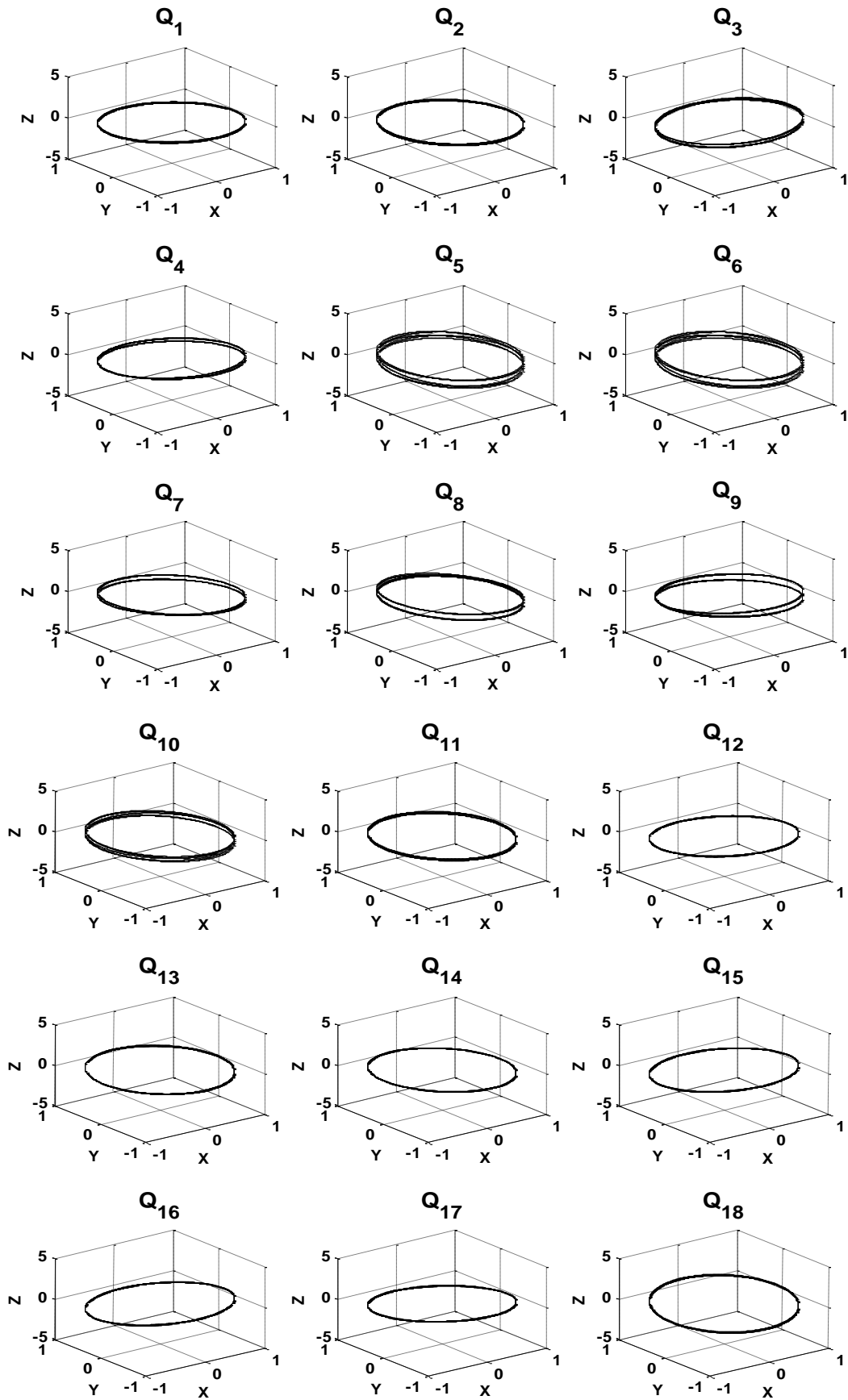


Figure 6.20. 3D interpretation of the vortex cavitation appearance during a Francis turbine operation. Q_i , with $i = \overline{1,18}$ denotes the flow rate.

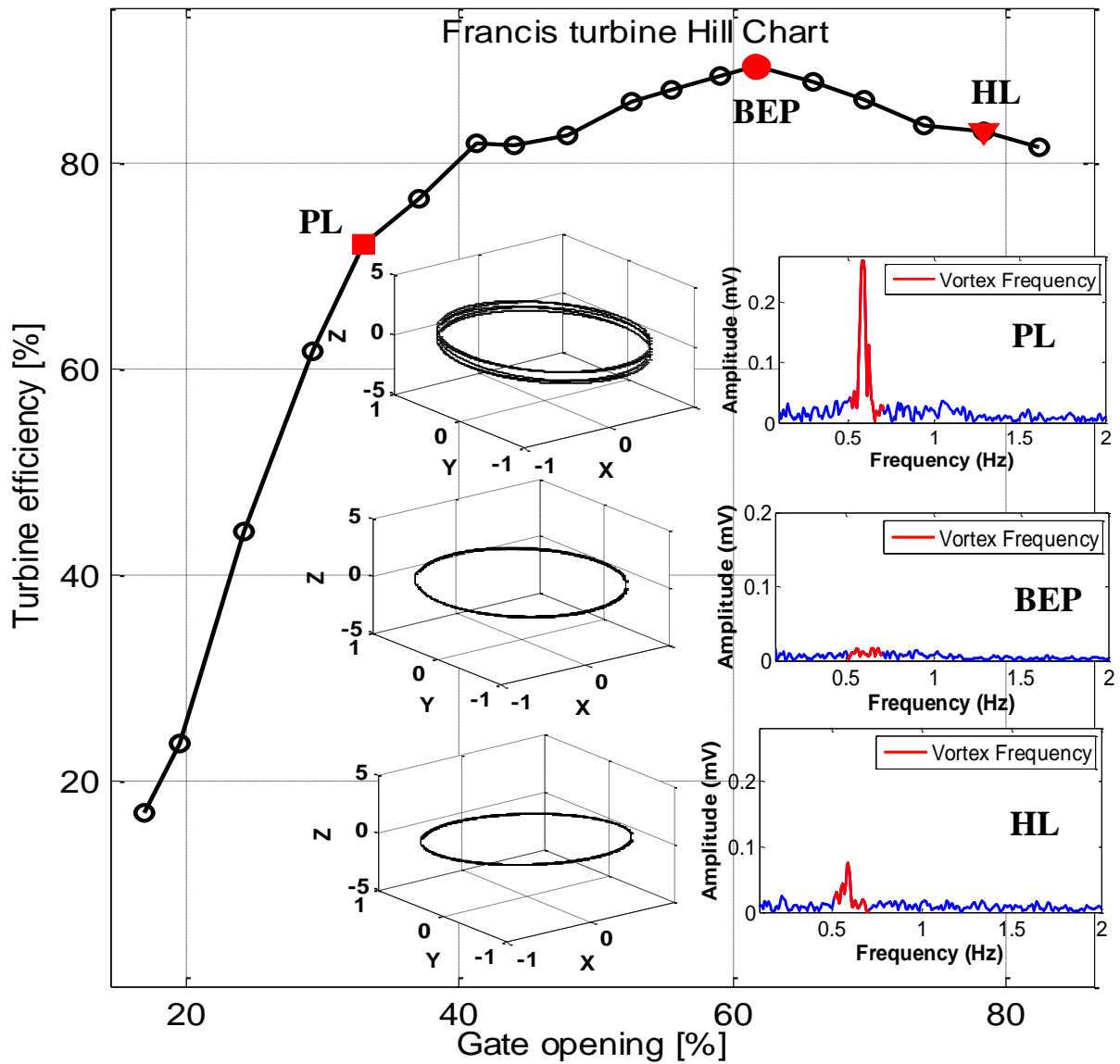


Figure 6.21. 3D interpretation of the vortex cavitation appearance.

In the case of cavitation vortex appearance, the statistical moments of the corresponding signal are close to those of a Gaussian pdf. This fact is in agreement with our initial assumption, that the additive noise present in the cavitation vortex frequency bandwidth is considered to be Gaussian.

5.4.3 Conclusion

Cavitation vortex and all flow instabilities have a major impact on hydraulic machinery efficiency. The ability to detect instantly the flow parameters changes, improves the machines monitoring and thus, low efficiency exploitation can be avoided. In this paper we have presented a new application for extensometer measurements, which provide real time information about the cavitation vortex appearance, using a mathematical model for data processing. Perspectives of study concern the adaptive estimation for the reference noise standard deviation.

Conclusion & Perspectives

This thesis brings a set of ultrasound signal processing contributions for instantaneous transitory flow measurements, with application in industrial pipes monitoring. The aim of this contributions was to compensate the measurement errors (which are quite conceivable) in order to provide an acceptable accuracy for the flow's parameters estimation, under almost measurement conditions.

Our research was focused on a specific type of ultrasound flow meters issues and limitations, presented in the second chapter of the manuscript: sensor misalignment, excessive flow velocity which leads to the “flow blow” effect, two-phase flow and/or the presence of the Doppler effect. These limitations led us to consider, within the framework of this thesis, research axes whose common objective is to provide the signal processing tools capable of lifting the operational locks.

Consequently, we have considered a set of signal processing principles in order to meet our objectives: the principle of wide-band signals which allowed a finer resolution and better robustness to disturbances of the signal processing system; the concept of compressing sensing in order to reconstruct the missing samples due to interference at the reception point; the principle of beamforming and the principle of multi-sensor sensing which made it possible to evaluate the velocity profile in a pipe section. All of these research axes have been organized in two chapters, depending on the transducers configuration: the single-sensor configuration and the multi-sensor configuration.

The framework presented in Chapter 3 contributes to the improvement of the matched filter's-based time of arrival estimation, by performing a signal pre-processing defined by the compressive sensing signal reconstruction. This method was applied in the single-path acoustic configuration, and the result was an increase in accuracy for the time of arrival estimation in the case of misaligned transducers.

Chapter 4 was focused on multi-sensor configurations, with active and passive sensing. For the active sensing, we took advantage of the adaptive directivity diagram of the emitted signals, in order to overcome the undesired effects during acoustic propagation through water pipes. This principle was applied for flow velocity profiling, reducing the requirement of high number of transducers [MCBD16].

Also, in the multi-sensor configuration section, we have presented a processing method for passive sensing, method based on a mathematical model developed in order to emphasize the presence of the cavitation vortex during a hydraulic turbine operation. In this way, we could clearly distinguish between different operational points of the turbine, having as data input only the signal's amplitude and a Gaussian noise reference [MVI17].

The methodology presented in this manuscript was implemented in the case of three real-life context applications, which are exposed in Chapter 5. The first one was performed at CERG, “Centre d’Etudes et de Recherche de Grenoble”, on a test facility which allowed non-intrusive acoustic measurements on a metallic pipe. The effect of “flow blow” was created and the results of the framework based on the signal’s compressive sensing reconstruction before matched filtering was emphasized.

Two more experimental tests were performed at the National Research Institute in Electrical Engineering from Bucharest (ICPE), aiming to create non-intrusive flow profiling. The beamforming principle was validated during this two experimental tests for two different flows, using acoustic wide band signals.

The different achievements of this work allow me to imagine different further works directions, falling in both theoretical and application fields.

The main theoretical research axis concern the generalization of the adaptive beamforming techniques by taking into consideration the propagation in the solid environments placed before the ultrasonic sensor array. In this thesis, we have shown that the presence of the solid environment before the ultrasonic sensors brings possible the adaptive beamforming principle. To go further, we will work on the modelization of the propagation in the solid environment and to take advantage of the physical modifications of the signals due to the propagation in this type of environment. We consider that the modeling of this physical deformation (generally, the dispersivity of the environment) will constitute a natural modulation that will contribute to the enhance the matched filtering and, in multi-sensor configuration, the adaptive beamforming performances.

In the applicative plan, the further research will attempt to extend the areas of applications developed in this thesis to other hydraulic contexts. Namely, one research will be to extend the approach developed in the passive context to other types de sensors, attempting to monitor other parameters of the hydraulic machine such as the efficiency, cavitating phenomena, structural behaviour, etc.

The same types of applicative contexts will be considered in the angle of active investigation techniques by using the approaches developed in the multi-sensor context.

Statistical moments of a joint pdf function

The joint pdf of one sinusoid and an additive noise, supposed to be Gaussian noise, is given by the convolution of their corresponding pdfs [Che87]:

$$p_{S_{in}}(x) = \int_{-\infty}^{\infty} p_s(x - \tau) * p_n(\tau) d\tau = \frac{1}{\sigma\pi\sqrt{2\pi}} \int_0^{\pi} e^{-\left(\frac{x - A\cos(\theta)}{4\sigma}\right)^2} d\theta \quad (\text{A.1})$$

We are interested compute the statistical moments of this pdf, so we try analytically calculate the expression of $p_{S_{in}}(x)$. Hence, we will discuss the integral from (A.1), that we name it I :

$$I = \int_0^{\pi} e^{-\left(\frac{x - A\cos(\theta)}{4\sigma}\right)^2} d\theta = \int_0^{\pi} e^{-\left(\frac{x}{4\sigma}\right)^2} e^{\frac{2xA}{(4\sigma)^2} \cdot \cos\theta} e^{-\left(\frac{A}{4\sigma}\right)^2 \cdot \cos^2\theta} d\theta \quad (\text{A.2})$$

Let us define the following coefficients:

$$f_1 = f_1(x) = -\left(\frac{x}{4\sigma}\right)^2 ; f_2 = f_2(x) = \frac{2xA}{(4\sigma)^2} ; f_3 = -\left(\frac{A}{4\sigma}\right)^2 , \forall x \in \mathbb{R} \quad (\text{A.3})$$

in order to easier express the equation (A.2):

$$I = \int_0^{\pi} e^{f_1} e^{f_2 \cdot \cos\theta} e^{f_3 \cdot \cos^2\theta} d\theta = e^{f_1} \int_0^{\pi} e^{f_2 \cdot \cos\theta} e^{f_3 \cdot \cos^2\theta} d\theta \quad (\text{A.4})$$

Both exponential functions depending on θ , will be now approximated with a Taylor-MacLaurin series:

$$I = e^{f_1} \int_0^{\pi} \left[1 + \sum_{n=1}^{\infty} \frac{f_2^n \cos^n\theta}{n!} \right] \cdot \left[1 + \sum_{n=1}^{\infty} \frac{f_3^n \cos^{2n}\theta}{n!} \right] d\theta \quad (\text{A.5})$$

where n is the number of Taylor-MacLaurin series. For calculus simplicity, we suppose that n is an odd number.

In this way, $\int_0^\pi \cos^n \theta d\theta = 0$ and $\int_0^\pi \cos^{2n} \theta d\theta = \pi \cdot \frac{(2n)!}{2^{2n} \cdot (n!)^2}$, for each $n \geq 1$.

Hence, the integral I reduces at the following expression:

$$\begin{aligned}
 I &= e^{f_1} \int_0^\pi 1 + f_3^n \sum_{n=1}^{\infty} \frac{\cos^{2n} \theta}{n!} d\theta = e^{f_1} \left[\pi + f_3^n \int_0^\pi \sum_{n=1}^{\infty} \frac{\cos^{2n} \theta}{n!} d\theta \right] = \\
 &= \pi \cdot e^{f_1} \left[1 + f_3^n \sum_{n=1}^{\infty} \frac{(2n)!}{2^{2n} \cdot (n!)^3} \right]
 \end{aligned} \tag{A.7}$$

Now, we go back to equation (A.1) to replace the integral I with this new form, and we obtain the following expression for the joint pdf of a sinusoid with additive Gaussian noise:

$$\begin{aligned}
 p_{S_{in}}(x) &= \frac{1}{\sigma\sqrt{2\pi}} \cdot e^{f_1} \left[1 + f_3^n \sum_{n=1}^{\infty} \frac{(2n)!}{2^{2n} \cdot (n!)^3} \right] d\theta = \\
 &= \frac{\alpha}{\sigma\sqrt{2\pi}} \cdot e^{f_1} = \frac{\alpha}{\sigma\sqrt{2\pi}} \cdot e^{-\left(\frac{x}{4\sigma}\right)^2}
 \end{aligned} \tag{A.8}$$

Résumé étendu

Contributions au traitement des signaux ultrasonores pour des mesures instantanées en écoulements transitoires

L'objectif de cette thèse est proposer des méthodes de traitement des signaux ultrasonores pour améliorer le calcul des vitesses d'écoulements transitoires à l'intérieur des conduites en mode non intrusive et en conditions complexes de mesure. Par conditions complexes nous entendons des fortes et, respectivement, des basses vitesses d'écoulement ainsi que des mesures en contexte d'un écoulement transitoire ou turbulent.

Classiquement, la vitesse de l'écoulement d'un fluide peut être estimée, de manière non intrusive, avec des ultrasons par le biais des débitmètres à temps de transit. Les débitmètres à temps de transit conventionnels sont basés sur l'émission alternée des pulses acoustiques mono-fréquentielles (donc, à bande étroite) et le calcul de la différence absolue entre les temps de vol dans le sens de l'écoulement (direct) et le sens opposé (inverse). La vitesse du fluide (et le débit), ou plutôt la précision de ces grandeurs, reposent principalement sur l'estimation de cette différence. Pour les débitmètres actuels, l'estimation des temps d'arrivée en mode direct et inverse a été résolue principalement par la synchronisation de l'émission (le front montant du signal/pulse émis) avec le signal reçu détecté suite à un seuillage.

La partie sensible de cette technique est le choix du seuil (en admettant que le signal reçu n'est pas affecté par d'autres phénomènes comme des échos parasites, atténuation excessive ou des effets Doppler) déterminé principalement de façon empirique : au-dessus de 50% ou 80% de la valeur maximale attendue du signal. Des techniques pour automatiser et réduire l'erreur de mesure sont tout à fait envisageables et qui assurent une précision acceptable dans des conditions de mesure presque idéales. Néanmoins, hormis les cas des figures ayant des conditions de mesure idéalisées (écoulement laminaire, une distance adéquate par rapport aux coudes, une bonne propagation du signal acoustique, etc.), il existe plusieurs scénarii où les techniques actuelles sont déficitaires :

- le désalignement des capteurs qui peut se produire soit par la mise en place initiale de l'expérimentation soit par les vibrations générées pendant le fonctionnement. L'effet produit par le désalignement des capteurs est une propagation des ondes à travers différents trajets acoustiques qui fait apparaître des interférences au niveau du capteur de réception. À cause de la propagation multivoie et des interférences, à la réception, on retrouve un signal qui porte une information souvent incomplète par rapport à la modulation émise ;

- une vitesse d'écoulement trop forte qui conduit à l'effet « flow blow » : l'énergie du signal reçu est affaiblie en raison de la fuite des particules portant la propagation de l'onde du diagramme d'émission-réception, et, ceci en raison de la vitesse d'écoulement. A l'opposé, une vitesse d'écoulement trop faible aura pour conséquence des différences de temps de propagation trop faibles, ce qui nécessite une augmentation de la fréquence d'échantillonnage;

- les écoulements bi-phasiques et/ou la présence de l'effet Doppler.

Ces constats, présentés dans le deuxième chapitre du manuscrit, nous ont conduit à envisager, dans le cadre de cette thèse, des axes de recherche qui ont pour objectif commun de fournir les outils de traitement du signal capables de lever les verrous opérationnels présentés ci-dessus. Ainsi, les principes de traitement du signal envisagés pour répondre à cet objectif sont :

- le principe des signaux à large bande qui confère au système de traitement du signal une résolution plus fine et une meilleure robustesse aux perturbations. A travers l'utilisation de ce principe, il s'agit de proposer un traitement innovant au niveau d'un élément ultrasonique du système de mesure afin d'accroître sa robustesse et précision de mesure;

- le concept de compressive sensing afin de reconstruire les échantillons perdus suite aux interférences au point de réception. La méthode proposée consiste premièrement à représenter le contenu temps-fréquence du signal reçu dans une forme stationnaire et qui permet, par la suite, la récupération de l'information manquante via la reconstruction dans le domaine spectral;

- le principe de formation de voie: les différentes conditions de mesure (une plage importante de la vitesse d'écoulement, un profil de vitesse asymétrique, des vibrations des capteurs, ...) peuvent conduire à des modifications continue du diagramme d'émission et de réception, provoquant ainsi des fluctuations du niveau du signal reçu et une perte des performances de mesure. La solution consiste à mettre en place des capteurs à plusieurs éléments dont les phases d'émission/réception seront contrôlées automatiquement de façon à pouvoir changer les diagrammes d'émission/réception et garantir toujours un niveau de signal globale optimal.

- le principe des multi-cordes qui permet d'évaluer le profil de vitesse dans une section de la conduite. Il s'agit ici de définir un ensemble de plusieurs cordes acoustiques qui, chacune, estime une vitesse moyenne dans l'axe qui relie l'émetteur et le récepteur.

L'ensemble de ces axes de recherche a été classé selon la configuration des capteurs utilisée (Figure B.1): la configuration mono-capteur (mono-élément) et la configuration multi-capteur (multi-élément). La méthodologie de traitement du signal en configuration mono-capteur est décrite dans le troisième chapitre.

La première opération nécessaire pour la mesure des paramètres hydrauliques est l'émission des ondes ultrasonore. L'émission des formes d'onde à large bande présente un double intérêt. Le premier est celui de la bonne résolution en termes d'estimation de temps d'arrivées des ondes, ce qui amène à une estimation précise des différences de temps de transit et, implicitement, à une bonne précision de mesure des vitesses d'écoulement. Par ailleurs, une bande large garantit une meilleure robustesse aux effets de propagation que les signaux impulsionnels. Le deuxième intérêt est l'émission simultanée dans le sens et le

contre-sens de l'écoulement, par la possibilité de travailler avec des périodes de répétition bien plus faibles, ayant ainsi la possibilité de réaliser des mesures avec une très forte cadence, ce qui est essentiel pour la mesure des phénomènes transitoires hydrauliques.

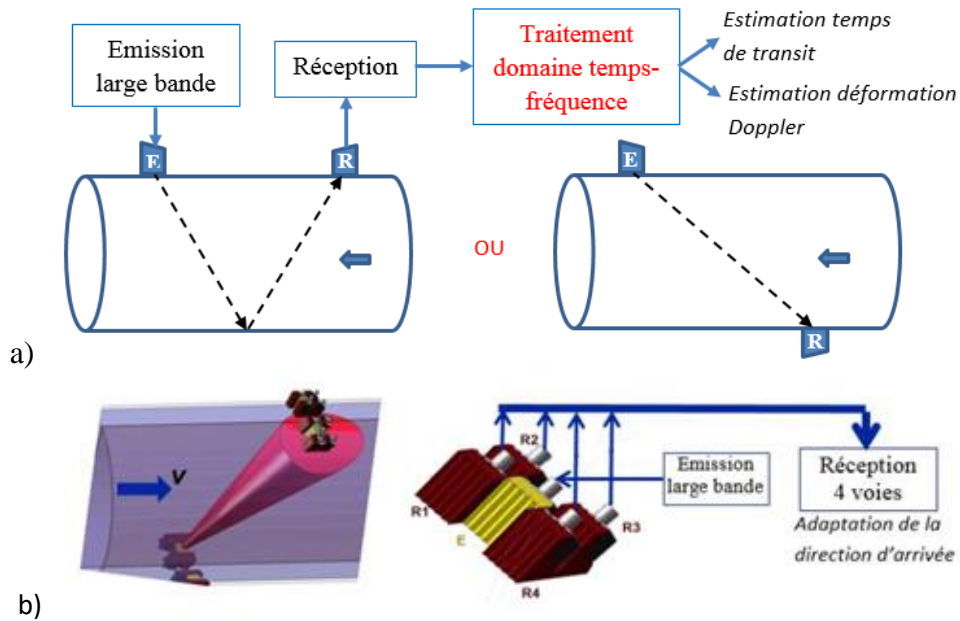


Figure B.1. Organisation globale des axes de recherche: a) la configuration mono-capteur et b) la configuration multi-capteurs.

Le principe de cette émission simultanée consiste à émettre des modulations linéaires de fréquence (MLFs) avec des pentes positives et, respectivement, négatives, définies par:

$$e_1(t) = A_1 \exp[j2\pi(f_0 + kt^2)], \quad t \in [kT_r, kT_r + D]$$

$$e_2(t) = A_2 \exp[j2\pi(f_0 - kt^2)], \quad t \in [kT_r, kT_r + D]$$

où f_0 est la fréquence centrale du capteur, k le taux de modulation linéaire qui permet le balayage de la fréquence autour de f_0 dans la bande souhaitée, T_r est la période de répétition des émissions et D est la durée des signaux. La Figure B.2 montre un exemple des spectrogrammes des signaux émis dans les expérimentations que nous avons réalisées dans le cadre de nos études.

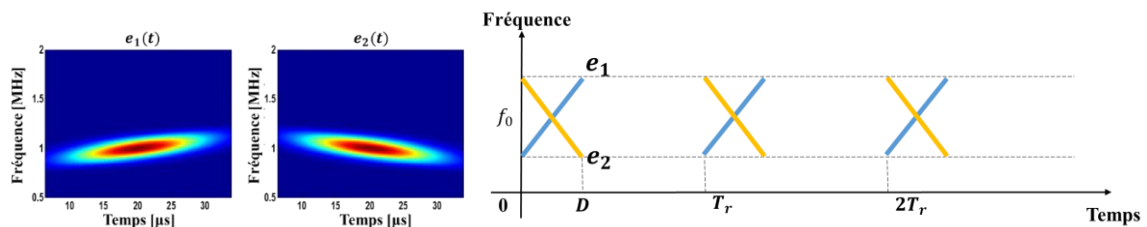


Figure B.2. Les signaux de type MLFs de pentes différentes utilisés pour l'émission simultanée dans le sens et en contre sens de l'écoulement.

L'utilisation des formes d'onde de type modulations linéaire de pentes différentes assure la quasi « orthogonalité » dans le plan temps-fréquence, évitant ainsi le risque d'interférences entre les ondes émises au même temps.

Un retard de propagation correspond à un changement de distance, donc si nous mesurons le retard et que nous connaissons la vitesse du son, nous pouvons évaluer de combien la particule s'est déplacée et comme nous connaissons le délai entre des impulsions, nous pouvons calculer la vitesse de la particule. Ce principe classique de mesure de la vitesse moyenne d'un écoulement (qui, conjointement avec la physique de la configuration, permet d'accéder au débit moyen) est illustré sur la figure suivante où nous présentons la signification de la différence de temps de propagation.

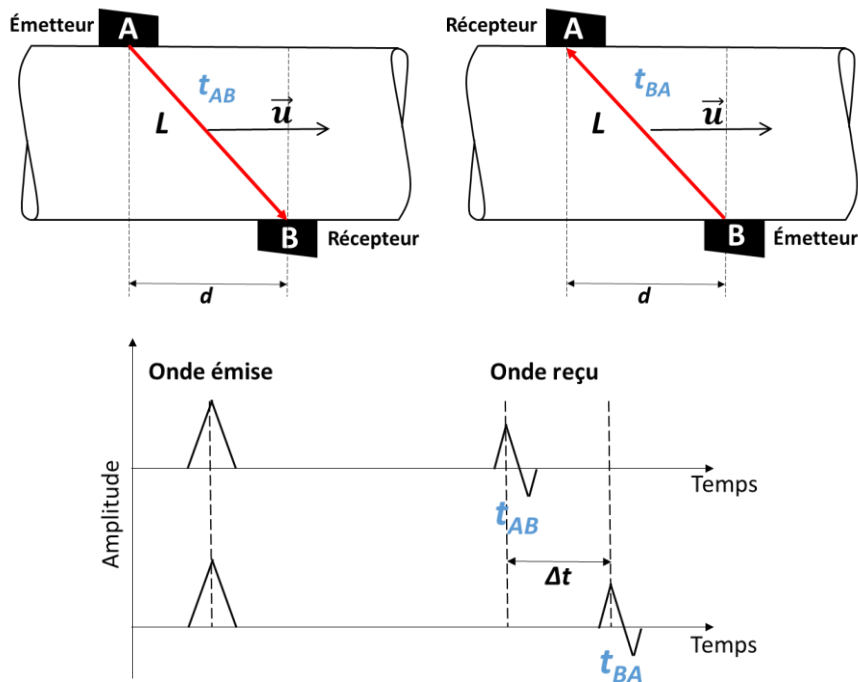


Figure B.3. Illustration du principe de mesure de vitesse d'écoulement par différence de temps de transit.

Comme nous le constatons, la précision d'estimation des temps de propagation est déterminante pour la précision de mesure de la vitesse de l'écoulement. Si les signaux reçus sont incomplets, cela pourrait influencer considérablement l'estimation du temps de propagation de l'onde.

Idéalement, pour un alignement optimal des capteurs (voir la Figure B.4.a), l'onde acoustique émise, $e(t)$, se propage dans l'eau, entre l'émission et la réception. L'émetteur et le récepteur peuvent être désalignés (voir la Figure B.4.b), la position du récepteur étant différente de celle idéale (représentée en gris dans la Figure B.4.b). Dans ce cas, à la réception, l'onde acoustique qui se propage dans l'eau a un retard plus important et elle sera donc superposée à l'onde qui se propage à travers le sens de propagation principal des capteurs d'émission-réception puis, dans l'acier (voir la Figure B.4.b).

Afin d'accroître les performances de mesure de temps de propagation, dans le contexte des capteurs désalignés et un signal incomplet à la réception, le positionnement de nos études est constitué par l'utilisation du filtrage adapté et le concept du compressive sensing. La propagation à travers ces deux trajets de propagation de la Figure B.4.b, se traduit par des interférences destructives qui conduisent à l'atténuation voir la perte de certains échantillons du signal émis. L'information manquante du signal reçu, $r_2(t)$, doit être récupérée afin d

estimer précisément le temps de propagation. La méthode proposée consiste premièrement à représenter le contenu temps-fréquence du signal reçu dans une forme stationnaire et qui permet, par la suite, l'application des algorithmes de compressive sensing afin de reconstruire les échantillons perdus suite aux interférences au point de réception.

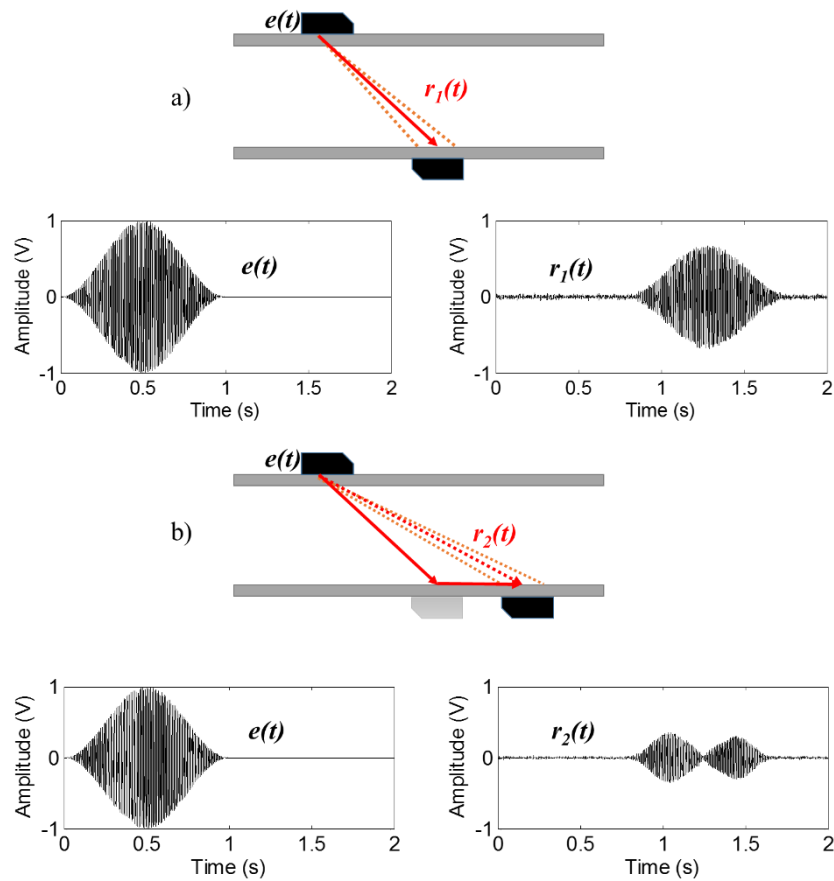


Figure B.4. Les ondes émises et reçues a) dans le cas des capteurs parfaitement alignés et b) dans le cas des capteurs désalignés.

Le fonctionnement d'un système de débitmétrie par temps de transit est souvent affecté par les paramètres physiques comme la gamme de variation de la vitesse d'écoulement ainsi que la précision de positionnement des capteurs qui, en présence des vibrations, peuvent se décaler par rapport à la position idéale. Ces deux types de perturbations, malgré leur origine différente, provoquent le même effet – la variation aléatoire du diagramme d'émission/réception et, par la suite, des fluctuations quant à l'amplitude et la forme des signaux reçus. Ces fluctuations provoquent une diminution des performances du filtre adapté et, donc, une perte de précision de mesure de vitesse d'écoulement.

Plus précisément, dans le cas d'une vitesse d'écoulement très élevée les particules portant l'onde sortent, en grande partie, du diagramme d'émission/réception, en raison de leur grande vitesse (l'effet que on l'appelle « flow blow »). Cet effet conduit à une atténuation voir une perte complète du signal en réception, ce qui implique une diminution des performances d'estimation des vitesses d'écoulement.

A partir de ces constats, nous proposons dans le quatrième chapitre, une technique de mesure à plusieurs éléments qui, par le principe de formation de voie, auront la possibilité d'adapter leur caractéristique de directivité en fonction du contexte opérationnel. Dans des conditions de débit variable (la vitesse d'écoulement varie d'une mesure à l'autre) ou de profil des vitesses asymétrique, le diagramme de directivité d'émission/réception se modifie. Cette modification est perçue par les capteurs de réception comme une distribution non uniforme de l'énergie acoustique reçue. Ainsi, en conditions de vitesse zéro, l'angle de la voie acoustique avec la direction d'écoulement a une valeur fixe, connue. En conditions de vitesse, cet angle change de valeur (Figure B.5).

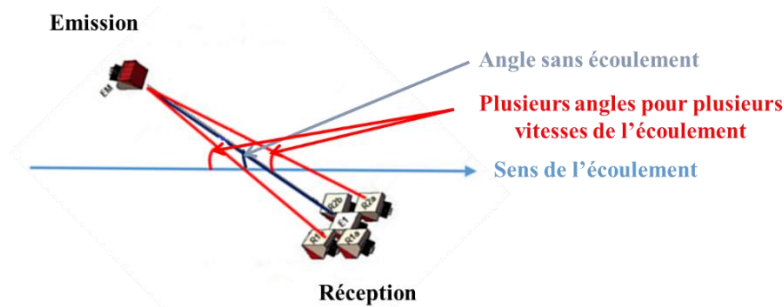


Figure B.5. Le déplacement du diagramme de directivité vue à la réception.

La différence d'angle est une source potentielle d'erreurs car la valeur d'angle est un paramètre important dans la formule du calcul du débit. Le déplacement du diagramme de directivité du capteur est donc une source d'erreurs de la mesure. Pour ce raison, la configuration multi-capteurs en réception est utilisée. Le but est de suivre les modifications de l'angle de la voie acoustique avec la direction d'écoulement et de les corriger, afin d'avoir la même précision de mesure que dans le cas optimal.

Les résultats expérimentaux des méthodes proposés dans le cadre de cette thèse, sont présentés dans le **chapitre 5**, en comparaison avec les méthodes classiques. Nous présentons les améliorations apportées dans l'estimation du TOA dans le cas des capteurs désalignés. Dans la mesure où la réponse du filtre adapté est perturbée par une réception incomplète, l'estimation du TOA n'est plus précise car la sortie du filtre adapté présente plusieurs maximales locales (Figure B.6).

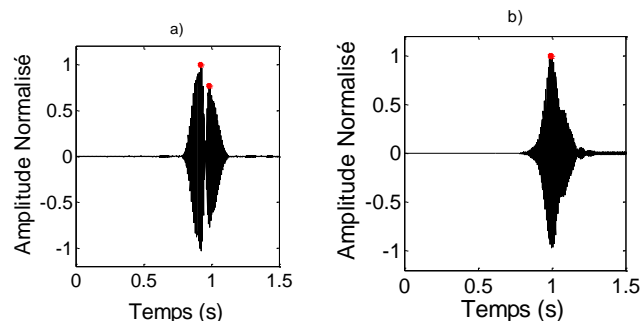


Figure B.6. Le résultat du filtrage adapté pour le signal reçu dans a) la configuration des capteurs désalignés et b) pour le signal reconstruit par le compressive sensing.

La contribution consiste alors à réaliser, avant le filtrage adapté, un prétraitement qui vise la reconstruction du signal reçu et qui contribue à améliorer la réponse du filtre adapté.

La récupération d'échantillons à l'aide du compressive sensing, de l'information manquante du signal reçu, dans les conditions des capteurs désalignés améliore considérablement l'estimation du temps de propagation de l'onde acoustique. Ceci peut être observé dans la visualisation de la sortie du filtre adapté à la réception dans le cas du signal reçu avec les échantillons manquants et, respectivement, avec les échantillons récupérés (Figure B.7). L'information spectrale du signal reconstruit avec le compressive sensing dispose d'une information spectrale plus riche que celle du signal reçu initial.

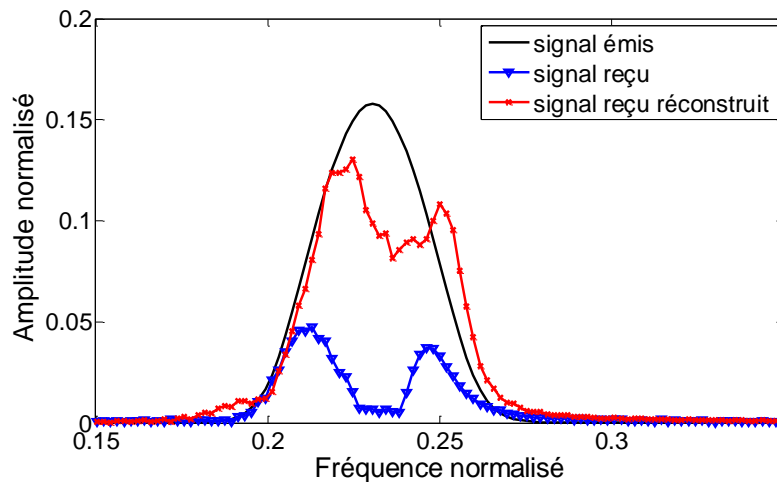


Figure B.7. Le spectre du signal émis, du signal reçu et du signal après la reconstruction.

Le principe de formation de voie a été validé à travers deux expérimentations et aux analyses des différents écoulements transitoires en utilisant les signaux acoustiques large-bande. Les deux campagnes des tests expérimentaux ont été réalisées au Centre d'Etudes et de Recherche de Grenoble (CERG) ainsi que à l'Institut de Recherche en Energie de Bucarest.

Les expérimentations au CERG se sont déroulées sur une boucle d'essais capable de reproduire des essais de débitmètrie à ultrason (en mode intrusif et non intrusif) sur une conduite de faible diamètre et de produire des fortes variations des vitesses d'écoulement (de 1 m/s à 11.5 m/s). Les essais concernés ont eu deux objectifs :

- étudier l'effet « flow blow » dans le contexte des vitesses d'écoulement élevées ;
- tester les algorithmes de filtrage adapté et de formation de voie en termes de performances d'estimation des vitesses d'écoulement dans une plage de variation relativement large.

Concernant le fonctionnement du filtrage adapté simple, on constate que l'erreur diminue dans la partie inférieure de la plage de mesure (de 3 m/sec à environ 9 m/sec). Cette constatation est également valable dans le cas du filtrage adapté + la formation de voie et elle s'explique par le fait que la mesure de différence de temps de transit est mieux estimée lorsque la vitesse d'écoulement augmente. Lorsque la vitesse d'écoulement passe dans la phase supérieure, dans le cas du traitement par filtrage adapté, on constate une dégradation des résultats qui se traduit par une augmentation de l'erreur d'estimation de la vitesse d'écoulement.

Cette tendance n'est plus visible dans le cas de la méthode de filtrage adapté et la formation de voie, l'erreur continue à diminuer toujours en raison de l'estimation plus précise de la différence de temps de transit (Figure B.8). Ce résultat montre clairement l'intérêt pour l'adaptation de voie qui permet de garantir des bonnes performances de mesure de vitesses d'écoulement malgré les limites des systèmes de transducteurs provoquant l'effet «flow blow»).

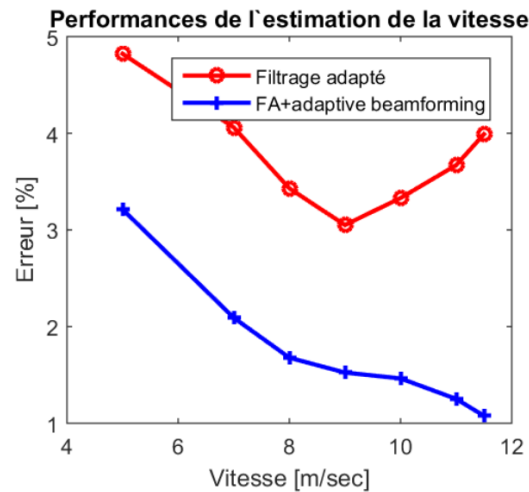


Figure B.8. La variation de l'erreur pour l'estimation de la vitesse d'écoulement en utilisant le filtrage adapté et la technique basée sur la formation de voie.

L'objectif de la séance d'expérimentation, déroulé en aout 2015, à l'Institut de Recherche en Energie de Bucarest, est de réaliser des mesures des champs des vitesses dans deux cas – profil symétrique et asymétrique (Figure B.9). Nous avons utilisé trois cordes de mesures acoustiques et nous avons obtenu de très bons résultats de mesure de profil de vitesse, par rapport aux méthodes de référence. L'implémentation de la formation de voie permet la d'adapter électroniquement la réception du signal, pour une estimation robuste du profil des vitesses dans différents régimes de l'écoulement.

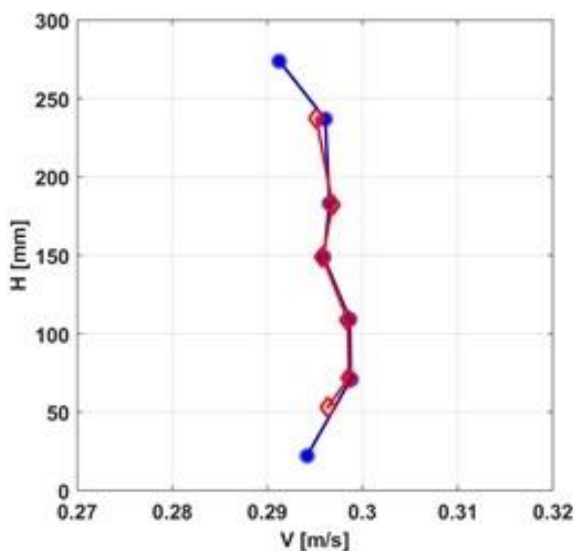


Figure B.9.a Profil des vitesses symétrique mesuré avec le tube Pitot (la courbe bleu) et estimé avec les cordes acoustiques (la courbe rouge)

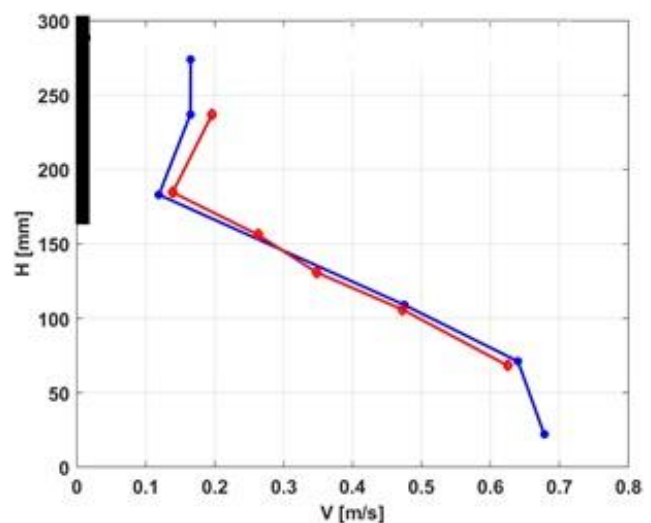


Figure B.9.b Profil des vitesses asymétrique mesuré avec le tube Pitot (la courbe bleu) et estimé avec les cordes acoustiques (la courbe rouge)

Les conclusions et les perspectives de ces travaux se retrouvent dans le dernier chapitre. Elle portent essentiellement sur le développement des futures méthodes d'analyse de signal dans un contexte d'écoulement diphasique en exploitant conjointement l'information temporelle ainsi que l'effet Doppler distribué dans la colonne d'écoulement. Dans ce contexte, l'analyse en digrammes de phase semble une excellente piste qui sera sûrement développée dans les travaux futurs.

La liste complète des publications

1. Murgan I, Ciocan G, Bunea F, Digulescu A, Ioana C, Candel I, Vasile G, Anghel A, *Flow velocity profiling using acoustic time of flight flow metering based on wide band signals and adaptive beam-forming techniques*, 28th IAHR symposium on Hydraulic Machinery and Systems, July 2016, Grenoble, France. IOP Conference Series: Earth and Environmental Science, 49, 2016, <[10.1088/1755-1315/49/6/062003](https://doi.org/10.1088/1755-1315/49/6/062003)>
2. Murgan I, Ioana C, Candel I, Anghel A, Ballester JL, Reeb B, Combes G, *(A new time of flight) Acoustic flow meter using wide band signals and adaptive beamforming techniques*, 28th IAHR symposium on Hydraulic Machinery and Systems, July 2016, Grenoble, France. 2016, <[10.1088/1755-1315/49/6/062002](https://doi.org/10.1088/1755-1315/49/6/062002)>
3. Murgan I, Digulescu A, Candel I, Ioana C, *Compensation of position offset of acoustic transducers using compressive sensing concept*, OCEANS 2016 MTS/IEEE Monterey, September 2016, Monterey, United States, pp.1-4, 2016, <[10.1109/OCEANS.2016.7761083](https://doi.org/10.1109/OCEANS.2016.7761083)>
4. Murgan I, Bunea B, Ciocan G, *Experimental PIV and LIF characterization of a bubble column flow*, Flow Measurement and Instrumentation, Volume 54, April 2017, Pages 224–235, <[10.1016/j.flowmeasinst.2017.02.004](https://doi.org/10.1016/j.flowmeasinst.2017.02.004)>
5. Murgan I, Vasile G, Ioana C, Barre S, Lora-Ronco T, *Hydraulic turbine vortex detection and visualization using strain gauge sensor*, Vol.1, No5, October 2017, IEEE Sensors Letters.
6. Digulescu A, Murgan I, Ioana C, Candel I, Serbanescu A, *Applications of Transient Signal Analysis Using the Concept of Recurrence Plot Analysis*, Recurrence Plots and Their Quantifications: Expanding Horizons, 180, pp.19-38, 2016, 978-3-319-29921-1. <[10.1007/978-3-319-29922-8_2](https://doi.org/10.1007/978-3-319-29922-8_2)>
7. Digulescu A, Murgan I, Candel I, Ioana C, Bunea A, Ciocan G, *Cavitating vortex characterization based on acoustic signal detection*, 28th IAHR Symposium on Hydraulic Machinery and Systems, July 2016, Grenoble, France. 49, pp.82009 - 82009, 2016, <[10.1088/1755-1315/49/8/082009](https://doi.org/10.1088/1755-1315/49/8/082009)>
8. Digulescu A, Murgan I, Ioana C, Candel I, Serbanescu A, *On the use of phase diagram domain properties for the Instantaneous Frequency Law tracking*, The 7th Recurrence Plot Symposium 2017.

Bibliography

- [Ant84] I. Anton, *Cavitatia*, Ed. Academiei Romane, vol. 1, 1984 (in Romanian).
- [AS64] M. Abramowitz, I. Stegun, *Handbook of mathematical functions with formulas, graphs and mathematical tables*, 1964, pp. 302.
- [BA98] B. Barshan, B. Ayrulu, "Performance comparison of four time-of-flight estimation methods for sonar signals", *Electronics Letters* 34(16):1616-1617, 1998.
- [BBL07] J. Bresson, R. Barriol, J. P. Longuemard, "Antenne acoustique multiéléments à focalisation. Modélisation du champ acoustique", *Revue de Physique Appliquée*, Tome 22, N° 10, 2007.
- [BIO15] C. Bernard, C. Ioana, I. Orovic, S. Stankovic, "Analysis of underwater signals with nonlinear time-frequency structures using warping-based compressive sensing algorithm", *IEEE Oceans Conference*, October 2015.
- [Bra07] R.G. Baraniuk, *Compressive Sensing*, IEEE Signal Processing Magazine, vol. 24, pp.118-121, 2007.
- [But06] E. Butikov, "Precession and nutation of a gyroscope", *IOP Publishing Ltd European Journal of Physics*, Volume 27, Number 5, 2006.
- [CBD14] I. Candel, F. Bunea, G. Dunca, D. Bucur, C. Ioana, B. Reeb, G. Ciocan, "Detection of cavitation vortex in hydraulic turbines using acoustic techniques", *27th IAHR Symposium on Hydraulic Machinery and Systems*, Montréal, September 22 - 26, 2014.
- [Che87] N.P. Cheremisinoff, *Practical Statistics for Engineers and Scientists*, Technomic Publishing Company, Pennsylvania, ISBN 87762-505-0, 1987, pp. 61-63.
- [DPC14] A. Digulescu, T. Petrut, I. Candel, F. Bunea, G. Dunca, D. Bucur, C. Ioana, A. Serbanescu, "On the vortex parameter estimation using wide band signals in active acoustic systems", *IEEE Oceans Conference*, Taipei, 2014.
- [FM85] J. P. Franc, J. M. Michel, "Attached cavitation and the boundary layer: Experimental and numerical treatment", *Journal of Fluid Mechanics*, vol. 154, pp. 63-90, 1985.
- [Fra05] J. P. Franc, *Fundamentals of cavitation*, Springer Netherlands, 2005, vol 76, pp. 265.

- [GP14] D. O. Guaraglia, J. L. Pousa, *Introduction to Modern Instrumentation for Hydraulics and Environmental Sciences*, pp. 51, October 2014, ISBN 978-3-11-040172-1.
- [Gra95] R. A. Granger, *Fluid Mechanics*, Dover Publications INC., New York, 1995.
- [HLNZ08] F. Hongqing, C. Long, D.Nkosinathi, S. Zuyi, “Basic modeling and simulation tool for analysis of hydraulic transients in hydroelectric power plants”, *IEEE Trans. on Energy Conversion*, 2008.
- [ICA08] M. S. Iliescu, G. D. Ciocan, F. Avellan, “Analysis of the Cavitating Draft Tube Vortex in a Francis Turbine Using Particle Image Velocimetry Measurements in Two-Phase Flow”, *Journal of Fluids Engineering*, vol. 130, Issue 2, 2008.
- [IGSM10] C. Ioana, C. Gervaise, Y. Stéphan, J. I. Mars, ”Analysis of underwater mammal vocalisations using time-frequency-phase tracker”, *Applied Acoustics*, 71(11):1070-1080, November 2010.
- [Ili07] M. Iliescu, Analysis of large scale phenomena in turbine draft tubes, Ph. D. dissertation, EPFL Lausanne, Switzerland, 2007.
- [Ili07] M. Iliescu, Analysis of large scale phenomena in turbine draft tubes, Ph. D. dissertation, EPFL Lausanne, Switzerland, 2007.
- [IQS06] C. Ioana, A. Quinquis, Y. Stephan, ”Feature Extraction from Underwater Signals using Time-Frequency Warping Operators”, *IEEE Journal of Oceanic Engineering*, vol. 31, no. 3, pp. 628–646, Jul. 2006.
- [JAS13] B. Jokanovic, M. Amin, S. Stankovic, ”Instantaneous frequency and time-frequency signature estimation using compressive sensing”, *SPIE Defense, Security and Sensing*, Baltimore, Maryland, United States, 2013.
- [JIQ06] A. Jarrot, C. Ioana, and A. Quinquis, ”An Extension of the Class Of Unitary Time Warping Projectors To Discrete Time Sequences”, *IEEE International Conference on Acoustics, Speech, and Signal Processing*, volume 3, pages 412-415, 2006.
- [JW92] J. Jeong and W. Williams, “Time-varying filtering and signal synthesis”, *Time-Frequency Signal Analysis: Methods and Applications*, B. Boashash, Ed., Wiley Press, 1992, ch. 17, pp. 389-405.
- [KT97] D.N. Konidaris, J.A. Tegopoulos, “Investigation of oscillatory problems of hydraulic generating units equipped with Francis turbines”, *IEEE Trans. on Energy Conversion*, 1997.
- [LL76] L.D. Landau and E. M. Lifschitz, *Mechanics*, New York Pergamon 1976, pp. 113.
- [LSB11] J. Lerga, V. Sucic and B. Boashash, ”An Efficient Algorithm for Instantaneous Frequency Estimation of Nonstationary Multicomponent Signals in Low SNR”, *EURASIP J. on Adv. In Signal Processing*, SP/725189, Jan 2011.

- [Mai03] R. J. Miller, *Phased Array Antenna Handbook*, 2nd edition, Artech House, 2003.
- [Mill96] R. W. Miller, *Flow Measurement Engineering Handbook*, New York, McGraw-Hill, 1996.
- [MBC17] I. A. Murgan, F. Bunea, G. Ciocan, “Experimental PIV and LIF characterization of a bubble column flow”, *Flow measurement and Instrumentation*, Volume 54, April 2017, Pages 224-235.
- [MCBD16] I. A. Murgan, G. Ciocan, F. Bunea, A. Digulescu, C. Ioana, I. Candel, G. Vasile, A. Anghel, “Flow velocity profiling using acoustic time of flight flow metering based on wide band signals and adaptive beam-forming techniques”, *28th IAHR symposium on Hydraulic Machinery and Systems*, Grenoble, France. IOP Conference Series: Earth and Environmental Science, 49, 2016.
- [MDCI16] I. A. Murgan, A. Digulescu, I. Candel, C. Ioana, “Compensation of position offset of acoustic transducers using compressive sensing concept”, *OCEANS 2016 MTS/IEEE Monterey*, United States, pp.1-4, 2016.
- [MIC16] I. A. Murgan, C. Ioana, I. Candel, A. Anghel, J.L. Ballester, B. Reeb, G. Combes, “(A new time of flight) Acoustic flow meter using wide band signals and adaptive beamforming techniques”, *28th IAHR symposium on Hydraulic Machinery and Systems*, Grenoble, France. IOP Conference Series: Earth and Environmental Science, 49, 2016.
- [MIK05] D.G. Manolakis, V.K. Ingle, S.M. Kogon, *Statistical and Adaptive Signal Processing*, Artech House, 2005.
- [MVI17] I. A. Murgan, G. Vasile, C. Ioana, S. Barre, T. Lora-Ronco, “Hydraulic turbine vortex detection and visualization using strain gauge sensor”, Vol.1, No5, October 2017, *IEEE Sensors Letters*.
- [OSS14] I. Orovic, S. Stankovic, and L. Stankovic, “Compressive sensing based separation of LFM signals”, *Proceedings ELMAR-2014. IEEE*, pp. 1–4. 2014.
- [PB10] P. Flandrin, P. Borgnat, ”Time-Frequency Energy Distributions Meet Compressed Sensing”, *IEEE Trans. SP* vol. 58, no. 6, pp. 2974–2982, 2010.
- [Rou04] G.F. Round, *Incompressible flow turbomachines: design, selection, applications and theory*, Elsevier, Amsterdam, 2004, pp. 55-102.
- [RVL15] M. Le Roux, G. Vasile, T. Lora-Ronco, “Analyse de signaux issus de capteurs extensométriques de poussée hydraulique”, Internship report, <https://doi.org/10.13140/RG.2.2.26709.01768>.
- [RWW07] M. Ragel, C. Willert, S. Wereley, J. Kompenhans, *Particle Image Velocimetry: a practical guide*, 2nd edition, Springer 2007.
- [SAF09] P. Schmitt, F. Abda, S. Fischer, A. Pallares, *Utilisation de l’effet Doppler dans la mesure par ultrasons pulses de profils de vitesses*, La Houille Blanche/n° 3-2009.

- [San02] M. L. Sanderson, “Guidelines for the use of Ultrasonic Non-invasive Metering Techniques”, *Flow Measurement and Instrumentation* 13, 2002, pp. 125-142.
- [SDT13] L. Stankovic, M. Dorovic, T. Thayaparan, *Time-Frequency Signal Analysis with Applications*, Artech House 2013.
- [SGA06] R. Susan-Resiga, G. Ciocan, I. Anton, F. Avellan, “Analysis of the swirling flow downstream a Francis turbine runner”, *Journal of Fluids Engineering*, Vol. 128, pp. 177-189, 2006.
- [SOS12] S. Stankovic, I. Orovic, E. Sejdic, *Compressive Sensing, Multimedia Signals and Systems*, Springer 2012.
- [SOS13] L. Stankovic, I. Orovic, S. Stankovic, and M. Amin, “Compressive Sensing Based Separation of Nonstationary and Stationary Signals Overlapping in Time-Frequency”, *IEEE Transactions on Signal Processing* vol. 61, no. 18, pp. 4562–4572, Sep. 2013.
- [Tak95] Y. Takeda, “Velocity profile measurement by ultrasonic Doppler method”, *Experimental Thermal and Fluid Science, Elsevier Science*, 1995.
- [TMY03] J. Takeuchi, R. Miraghaie, K. Yuki, S. Satake, T. Kunugi, N. B. Morley, “Turbulent velocity profile measurement in curcular pipe flow using particle image velocimetry technique”, *20th IEEE/NPSS Symposium on Fusion Engineering*, 2003.
- [Tro95] C. Tropea, “Laser Doppler anemometry: recent developments and future challenges”, *Measurement Science and Technologie*, vol. 6, pp. 605-619.
- [Tuv16] UK National Measurement System, “An Introduction to Non-invasive Ultrasonic Flow Metering”, http://www.tuvnel.com/x90lbm/An_Introduction_to_Non-Invasive_Ultrasonic_Flow_Metering.pdf, Accessed: 2017-05-15.
- [Ven73] H. Ventsel, *Théorie des probabilités*, Editions de Moscou, 1973, pp. 251-253.
- [WCS03] T. M. Walski, D. V Chase, D. A. Savic, Grayman, W. Beckwith, S. Koelle, *Advanced water distribution modelling and management*, First edition, 2003.
- [Web99] J. G. Webster, *The Measurement, Instrumentation and Sensors Handbook*, IEEE Press, 1999.

Résumé — L'objectif de cette thèse est proposer des méthodes de traitement des signaux ultrasonores pour améliorer le calcul des vitesses d'écoulements transitoires à l'intérieur des conduites en mode non intrusif et en conditions complexes de mesure. Par conditions complexes nous entendons des fortes et, respectivement, des basses vitesses d'écoulement ainsi que des mesures en contexte d'un écoulement transitoire ou turbulent. Classiquement, la vitesse de l'écoulement d'un fluide peut être estimée, de manière non intrusive, avec des ultrasons par le biais des débitmètres à temps de transit. Les débitmètres à temps de transit conventionnels sont basés sur l'émission alternée des pulses acoustiques mono-fréquentielles (donc, à bande étroite) et le calcul de la différence absolue entre les temps de vol dans le sens de l'écoulement (direct) et le sens opposé (inverse). La vitesse du fluide (et le débit), ou plutôt la précision de ces grandeurs, reposent principalement sur l'estimation de cette différence. La partie sensible de cette technique est le choix du seuil (en admettant que le signal reçu n'est pas affecté par d'autres phénomènes comme des échos parasites, atténuation excessive ou des effets Doppler) déterminé principalement de façon empirique: au-dessus de 50% ou 80% de la valeur maximale attendue du signal. Des techniques pour automatiser et réduire l'erreur de mesure sont tout à fait envisageables et qui assurent une précision acceptable dans des conditions de mesure presque idéales. Néanmoins, hormis les cas des figures ayant des conditions de mesure idéalisées, il existe plusieurs scénarii où les techniques actuelles sont déficientes: le désalignement des capteurs, une vitesse d'écoulement trop forte qui conduit à l'effet «flow blow», les écoulements bi-phasiques et/ou la présence de l'effet Doppler. Ces constats, présentés dans le deuxième chapitre du manuscrit, nous ont conduit à envisager, dans le cadre de cette thèse, des axes de recherche qui ont pour objectif commun de fournir les outils de traitement du signal capables de lever les verrous opérationnels. Ainsi, les principes de traitement du signal envisagés pour répondre à cet objectif sont: le principe des signaux à large bande qui confère au système de traitement du signal une résolution plus fine et une meilleure robustesse aux perturbations; le concept de compressive sensing afin de reconstruire les échantillons perdus suite aux interférences au point de réception; le principe de formation de voie et le principe des multi-cordes qui permet d'évaluer le profil de vitesse dans une section de la conduite. L'ensemble de ces axes de recherche ont été classé, dans deux chapitres, selon la configuration des capteurs utilisée: la configuration mono-élément et la configuration multiélément. Les conclusions et les perspectives de ces travaux sont discutés à la fin du manuscrit.

Abstract — The purpose of this thesis is to propose ultrasonic signal processing methods in order to improve the transitory flow velocity non-intrusive detection through pipes, in complex measurement conditions. By complex measurement conditions, we refer to high or very low flow rates and also to transitory or turbulent flows. Usually, the flow velocity can be non-intrusive estimated, using ultrasonic flow meters based on transit time estimation. Conventional transit time flowmeters are based on the alternating emission of single-frequency acoustic pulses (ie, narrow-band acoustic pulses) and the calculation of the absolute difference between flight times in the direction of flow (direct) and in the opposite direction (reverse). The fluid velocity (and the flow rate), or rather the precision of estimation of these quantities, rest mainly on the estimation of this difference. The sensitive part of this technique is the choice of the threshold (assuming that the received signal is not affected by other phenomena such as echoes, excessive attenuation or Doppler effects) determined mainly empirically: above 50% or 80% of the maximum expected value of the signal. Techniques for reducing measurement errors are quite conceivable and provide acceptable accuracy under almost ideal measurement conditions. However, apart from the case with idealized measurement conditions, there are several scenarios where current techniques are deficient: sensor misalignment, excessive flow velocity which leads to the “flow blow” effect, two-phase flow and / or the presence of the Doppler effect. These facts, presented in the second chapter of the manuscript, led us to consider, within the framework of this thesis, research axes whose common objective are to provide the signal processing tools capable of lifting the operational locks. Thus, the signal processing principles considered to meet this objective are: the principle of wide-band signals which gives the signal processing system a finer resolution and better robustness to disturbances; the concept of compressive sensing in order to reconstruct the missing samples due to interference at the reception point; the principle of beamforming and the principle of multi-paths which makes it possible to evaluate the velocity profile in a pipe section. All of these research axes have been classified in two chapters, depending on the configuration of the sensors used: the single-path configuration and the multi-path configuration. The conclusions and perspectives of this work are discussed at the end of the manuscript.